IVANE JAVAKHISHVILI TBILISI STATE UNIVERSITY

ILIA VEKUA INSTITUTE OF APPLIED MATHEMATICS

GEORGIAN ACADEMY OF NATURAL SCIENCES

TBILISI INTERNATIONAL CENTRE OF

MATHEMATICS AND INFORMATICS

L E C T U R E   N O T E S

of

TICMI

Volume 18, 2017

V.Yu. Belashov, E.S. Belashova, O.A. Kharshiladze

NONLINEAR WAVE STRUCTURES OF THE SOLITON AND VORTEX TYPES IN COMPLEX CONTINUOUS MEDIA: THEORY, SIMULATION, APPLICATIONS

Tbilisi

LECTURE NOTES OF TICMI

Lecture Notes of TICMI publishes peer-reviewed texts of courses given at Advanced Courses and Workshops organized by TICMI (Tbilisi International Center of Mathematics and Informatics). The advanced courses cover the entire field of mathematics (especially of its applications to mechanics and natural sciences) and from informatics which are of interest to postgraduate and PhD students and young scientists.

Contents

Abstract. This edition of the Lecture Notes of TICMI is devoted to the problems of study of nonlinear wave structures of the soliton and vortex types in complex continuous media including theory and simulation of these processes and also some applications of the results in real physical media such as space plasma and plasma of the ionosphere and magnetosphere of the Earth.

The results obtained in the collaborative works of the Kazan Federal University, Russia and I. Vekua Institute of Applied Mathematics, I. Javakhishvili Tbilisi State University, Georgia are presented. Some of them were discussed on special session of the VIII Annual Meeting of the Georgian Mechanical Union dedicated to the 110th Birthday Anniversary of Ilia Vekua on September 27-29, 2017, Tbilisi, Georgia.

This edition consists of two parts devoted to the nonlinear wave structures and vortical structures in complex continuous media, respectively. In the first part the theory of the Belashov-Karpman (BK) system for its two partial cases describing by the two- and three-dimensional (2D and 3D) generalized Kadomtsev-Petviashvili (GKP) equation and the 3D derivative nonlinear Schrödinger (3-DNLS) equation, including the problem of stability of multidimensional solutions of these equations, and the problem of classification of the solutions of the GKP-class equations on the basis of methods of qualitative and asymptotic analysis is considered. Special Section is devoted to consideration of applications of the theory to the problems of the dynamics of nonlinear ion-acoustic waves in a unmagnetized plasma in view of relativistic effects, evolution of 3D nonlinear fast magnetosonic (FMS) and Alfvén waves in the magnetized plasma of the ionosphere and magnetosphere, and also to the problem of study on 2D internal-gravity waves and travelling ionospheric disturbances at heights of the ionosphere *F*-region.

In the second part of this book the results of analysis and numerical simulation of evolution and interaction of the *N*-vortex structures of various configuration and different vorticities in the continuum including atmosphere, hydrosphere and plasma on the basis of modified contour dynamic (CD) method are presented. In particular, some of the results on 2D and 3D simulation of such vortical objects and phenomena as the atmospheric synoptic vortices of cyclonic types and tornado, hydrodynamic 4-vortex interaction and also interaction in the systems of a type of "hydrodynamic vortex – dust particles" are presented. The applications of undertaken approach to the problems of such plasma systems as streams of charged particles in a uniform magnetic field and plasma clouds in the ionosphere are also considered in special Section.

In both parts of the book it is shown that the results presented here have obvious applications in studies of the dynamics of the nonlinear wave structures of the soliton and vortex types in atmosphere, hydrosphere and plasma.

V.Yu. Belashov
Institute of Physics,
Kazan Federal University,
18 Kremlyovskaya Str., Kazan 420008, Russia

 E.S. Belashova
Institute for Computer Technologies and Information Protection,
Kazan National Research Technical University named after A.N. Tupolev – KAI,
55 Bol'shaya Krasnaya Str., Kazan 420015, Russia

O.A. Kharshiladze
Ivane Javakhishvili Tbilisi State University,
M. Nodia Institute of Geophysics,
1 Aleksidze Str., 0160 Tbilisi, Georgia

*Corresponding Author. Email: oleg.kharshiladze@gmail.com

Preface

This edition of the Lecture Notes of TICMI is devoted to the problems of study of nonlinear wave structures of the soliton and vortex types in complex continuous media including theory and simulation of these processes and also some applications of the results in real physical media such as space plasma and plasma of the ionosphere and magnetosphere of the Earth.

We present here the results obtained in our works in collaboration with the Kazan Federal University, Russia and I. Vekua Institute of Applied Mathematics, I. Javakhishvili Tbilisi State University, Georgia. Some of them were discussed on special session of the VIII Annual Meeting of the Georgian Mechanical Union dedicated to the 110th Birthday Anniversary of Ilia Vekua on September 27-29, 2017, Tbilisi, Georgia.

This edition consists of two parts devoted to the nonlinear wave structures and vortical structures in complex continuous media, respectively.

In the first part we consider the theory of the Belashov-Karpman (BK) system for its two partial cases described by the two- and three-dimensional (2D and 3D) generalized Kadomtsev-Petviashvili (GKP) equation and the 3D derivative nonlinear Schrödinger (3-DNLS) equation, including the problem of stability of multidimensional solutions of these equations, and the problem of classification of the solutions of the GKP-class equations on the basis of methods of qualitative and asymptotic analysis. Section 1.4 is devoted to consideration of applications of the theory to the problems of the dynamics of nonlinear ion-acoustic waves in an unmagnetized plasma in view of relativistic effects, evolution of 3D nonlinear fast magnetosonic (FMS) and Alfvén waves in the magnetized plasma of the ionosphere and magnetosphere, and also to the problem of study on 2D internal-gravity waves and travelling ionospheric disturbances at heights of the ionosphere *F*-region.

In the second part of this book the results of analysis and numerical simulation on the basis of modified contour dynamic (CD) method (Sect. 2.3) of evolution and interaction of the *N*-vortex structures of various configuration and different vorticities in the continuum including atmosphere, hydrosphere and plasma are presented. In particular, in Sect. 2.5 we present some of our results on 2D and 3D simulation of such vortical objects and phenomena as the atmospheric synoptic vortices of cyclonic types and tornado, hydrodynamic 4-vortex interaction and also interaction in the systems of a type of "hydrodynamic vortex – dust particles". The applications of undertaken approach to the problems of such plasma systems as streams of charged particles in a uniform magnetic field and plasma clouds in the ionosphere are also considered in Sect. 2.5.

In both parts of the book it is shown that the results presented here have obvious applications in studies of the dynamics of the nonlinear wave structures of the soliton and vortex types in atmosphere, hydrosphere and plasma.

It is our pleasure to thank George Jaiani for his stimulating interest to the topic in our results, and especially Natalia Chinchaladze for her initiation of this edition, fruitful consultations and help in the edition preparation.

<div align="right">Authors</div>

1. NONLINEAR WAVE STRUCTURES OF THE SOLITON TYPE IN COMPLEX CONTINUOUS MEDIA

1.1. Basic equations. The BK system. The GKP and the 3-DNLS equations

In this Section, we derive the generalized Kadomtsev-Petviashvili (GKP) equation by introducing into classic KP equation the higher order dispersion correction, the terms describing dissipation of the viscous type, as well as an instability and stochastic fluctuations of the wave field. We then reduce this equation to a simplified form, allowing its subsequent analysis (Sect. 1.1.1). Furthermore, in Sect. 1.1.2, we derive the three-dimensional (3D) derivative nonlinear Schrödinger (3-DNLS) equation from the full set of the plasma one-fluid magnetohydrodynamic (MHD) equations, and then, using the scale transforms, reduce it to a dimensionless form convenient for further analysis. Also, a generalization of 3-DNLS equation in the presence of dissipation in a medium is considered. Finally, in Sect. 1.1.3, we write the Belashov-Karpman (BK) system which includes both cases, namely: GKP and 3-DNLS equations.

1.1.1 Generalized KP Equation

In [27], [40] we derived the KdV equation from the full set of the hydrodynamic equations:

$$\partial_t \mathbf{v} + (\mathbf{v}\nabla)\mathbf{v} + (c^2/\rho)\nabla\rho = 0,$$
$$\partial_t \rho + \nabla(\rho\mathbf{v}) = 0, \tag{1.1.1}$$

$$\partial_t \Phi + \tfrac{1}{2}(\nabla\Phi)^2 + \frac{c^2(\rho-\rho_0)}{2\rho} + \frac{c^2 z}{\rho} = 0, \tag{1.1.2}$$

$$\Delta\Phi = 0 \tag{1.1.3}$$

($\rho_0 = \text{const}$) with the boundary conditions:

$$\begin{cases} \partial_t \eta + \partial_x \eta \ \partial_x \Phi + \partial_y \eta \ \partial_y \Phi - \partial_z \Phi = 0, \\ \partial_t \Phi + \tfrac{1}{2}(\nabla\Phi)^2 + (c^2/\rho)\eta = 0, \\ z = \eta(x,y,t), \\ \partial_z \Phi\big|_{z=-\rho_0} = 0. \end{cases} \tag{1.1.4}$$

Here eqs. (1.1.1) are the equation of motion and the continuity equation for the generalized velocity and density, eqs. (1.1.2) and (1.1.3) are the equation of motion for potential and the Laplace equation, respectively.

In dependence on physical sense of functions and variables eqs. (1.1.1)-(1.1.4) describe different physical systems, for example:

- the surface waves in the water, in this case: $\rho \equiv H$ is the depth and , $c(\rho)$ is the phase velocity of the waves; $c(\rho) = c_0 = \sqrt{gH}$ for small-amplitude waves;

- the ion-acoustic (IA) waves in a collisionless plasma: ρ is the plasma (gas) density and $c(\rho)$ is the phase velocity of the ion sound; $c(\rho) = c_0 = c_s = \sqrt{T_e/m}$ for the long-wavelength linear waves, where T_e is the electron temperature in energy units (Boltzmann constant equals unity), and m_i is the ion mass;

- the magnetosonic (MS) waves in a magnetized plasma: $\rho \equiv H$ is (the strength of) the external magnetic field and $c(\rho) = c(H) = v_A = H / \sqrt{4\pi nm}$ is the Alfvén velocity, in this case usually the plasma density $nm \approx n_i m_i$ where n_i is the ion density.

For the surface waves in shallow water, **v** is the hydrodynamic velocity in the wave (the "mass" velocity); for the IA waves it is the ion velocity, for the MS waves $\mathbf{v} \equiv \mathbf{h} = \mathbf{H}_\sim / \mathbf{H}_0$ is the wave magnetic field normalized to the external magnetic field.

Further, in [27],[40] we generalized this type of derivation for the systems described by the classic two-dimensional (2D) and 3D KP equations:

$$\partial_t u + \alpha u \partial_x u + \beta \partial_x^3 u = \kappa \int_{-\infty}^{x} \Delta_\perp u \, dx, \qquad (1.1.5)$$

where $\Delta_\perp = \partial_y^2 + \partial_z^2$ and $\Delta_\perp = \partial_y^2$ for 3D and 2D cases, respectively.

However, as is known [15], for some cases the coefficient at the third-order derivative in the KP-class equations can be negligible or even exactly equal to zero (this takes place, for example, for the gravity-capillary wavesin shallow water when $H^2 \to 3\sigma/\rho g$, and for the FMS waves propagating at the angles close to $\theta \to \mathrm{arctg} \sqrt{m_i / m_e}$ with respect to an external magnetic field **B**, see [27]. Nevertheless, this does not mean total disappearance of the effects of the medium's dispersion: the equilibrium between the nonlinear and dispersive processes in this case can still be recovered by invoking higher order terms in the expansion of the full dispersion equation in the powers of the wave number k. As a result, for equations of the KP class dispersive correction terms proportional to the fifth derivative $\gamma \partial_x^5 u$ appear in the left-hand side of (1.1.5), often playing the decisive role in the dynamics of multidimensional solitons (see, for example, [61],[62] and Sects. 1.4.2 and 1.4.4).

When dissipation cannot be neglected, eq. (1.1.5) should be supplemented by the corresponding term. Since we consider here the hydrodynamic approximation when, for example, for waves in a plasma $\omega \sim \tau^{-1} << (4\pi n_0 e^2 / m_e)^{1/2}$, we are limited in our study with the effects of dissipative processes of the so-called viscous type (assuming that the Landau damping can be neglected) on the structure and evolution of nonlinear waves and solitons. In this case, for the ion plasma oscillations when the wave frequency (and the characteristic times of the processes) is significantly less than the electron plasma frequency, $\omega << \omega_{0e}$, the dissipative effects associated with the processes of relaxation in the medium lead to the imaginary term of the type $-i\nu k_x^2$ in the dispersion equation

$$\omega \approx c_0 k_x \left(1 + k_\perp^2 / 2k_x^2 + \delta^2 k_x^2\right),$$

and the KP equation takes the form

$$\partial_x \left(\partial_t u + \alpha u \partial_x u - \nu \partial_x^2 u + \beta \partial_x^3 u + \gamma \partial_x^5 u\right) = \kappa \Delta_\perp u,$$
$$\kappa = -c_0 / 2 \qquad (1.1.6)$$

and we call it the generalized KP equation or the GKP equation. It has the same degree of universality, as the standard KdV and KP equations in the sense that it is valid always when the dispersion law is given by

$$\omega \approx c_0 k_x \left[1 + k_\perp^2 / 2k_x^2 - i\nu k_x / c_0 + \left(-\beta k_x^2 + \gamma k_x^4\right)/ c_0\right]. \qquad (1.1.7)$$

The 2D and 3D eq. (1.1.6) has wide applications in the physics of nonlinear dispersive waves, and we will show it in Sect. 1.4.

For convenience of further analysis when $\delta = 0$, we transform eq. (1.1.6) using changes $x \to -sx$, $y \to -s\kappa^{1/2}y$, $z \to -s\kappa^{1/2}z$, $t \to st$, $u \to -(6/\alpha)u$, $s = |\gamma|^{1/4}$. Thus the basic equation in this case can be written as

$$\partial_x\left(\partial_t u + 6u\partial_x u - \mu\partial_x^2 u - \varepsilon\partial_x^3 u - \lambda\partial_x^5 u\right) = \Delta_\perp u, \tag{1.1.8}$$

where $\mu = \nu s^{-1}$, $\varepsilon = \beta s^{-2}$, $\lambda = \mathrm{sgn}(\gamma)$. In Sect. 1.2, we study analytical approaches to the problem of stability of multidimensional solitons and nonlinear wave packets described by equations of the GKP class in the form (1.1.8). In Sect. 1.3 we investigate the classes of possible solutions and their asymptotics employing the methods of qualitative analysis (usually used in the theory of dynamic systems) as well as the asymptotic analysis (when $|x| \to \infty$) of the structure of the solutions.

1.1.2. The 3-DNLS equation

In [27],[40] we introduced the derivative nonlinear Schrödinger (DNLS) equation, omitting its detailed derivation, and considered it as an integrability condition for two linear differential equations. Since we investigate multidimensional systems (and would like to emphasize the physics of phenomena described by this equation more clearly) here, we present a brief derivation of the three-dimensional DNLS (3-DNLS) equation.

Here, we write the full set of the one-fluid MHD equations assuming that $k_\perp^2 << k_x^2$ (in this case we can change $\nabla \to \hat{\mathbf{x}}\partial_x$ in the MHD equations [34]):

$$\left(\partial_t + v_x\partial_x\right)\mathbf{v}_\perp = v_A^2\partial_x\mathbf{h}, \tag{1.1.9}$$

$$\left(\partial_t + v_x\partial_x\right)v_x = -\left(v_A^2/2\right)\partial_x\mathbf{h}^2, \tag{1.1.10}$$

$$\partial_t\mathbf{h} = \partial_x\left(\mathbf{v}_\perp - v_x\mathbf{h}\right), \tag{1.1.11}$$

$$\partial_t\rho + \partial_x\left(v_x\rho\right) = 0, \tag{1.1.12}$$

where $\mathbf{h} = \mathbf{B}_\perp / B_0$ is the dimensionless perturbation of the perpendicular magnetic field. Following [27], consider dependence of all functions in these equations on t and x in the form $f = f(x - v_A t, t)$, where the first argument is due to nonlinear effects. Since perturbations of the density ρ and the x-component of the velocity v_x are also stipulated by the presence of the nonlinearity of the medium, it is possible to approximate $\partial_t \cong -v_A\partial_x$.

Thus, integrating (1.1.12) and taking into account that $\lim_{|x|\to\infty} \rho = \rho_0$, we find

$$\rho = \rho_0\left(1 + v_x/v_A\right). \tag{1.1.13}$$

Furthermore, by neglecting the small term on the order of v_x^2 on the left-hand side of (1.1.10), and applying the same assumptions as above, we obtain from (1.1.10)

$$v_x = \left(v_A/2\right)\mathbf{h}^2. \tag{1.1.14}$$

According to relation (1.1.14), the plasma is pushed away by the wave field in the direction of the wave propagation thus forming the "Alfvén wind" with the effect of the ponderomotive force [27]. Substituting relations (1.1.13) and (1.1.14) into (1.1.9) and (1.1.10), taking into account the parabolic equation for the magnetic field B (see, e.g.,

[86],[21]), and retaining the dispersion effects, we find that the equation for the dimensionless perpendicular magnetic field $h = h_y + ih_z$ is given by

$$\partial_x\left[(2/\omega_{0i})\partial_t h + r_A\partial_x\left(|h|^2 h\right) + ir_A^2\partial_x^2 h\right] = -\left(r_A/2\right)\nabla_\perp^2 h, \qquad (1.1.15)$$

where $r_A = v_A/\omega_{0i}$. Eq. (1.1.15) describes the left-circularly polarized wave mode; for the right-circularly polarized mode we have the "minus" sign in front of the dispersion term. It is possible to incorporate the sign of the nonlinearity by the factor $s = \pm 1$ in front of the nonlinear term. Thus after introducing $\sigma = -r_A/2$, converting to the dimensionless variables $t \to \omega_{Hi}t/2$, $x \to x/r_A$, $\mathbf{r}_\perp \to \mathbf{r}_\perp\sqrt{2}/r_A$, $r_A = v_A/\omega_{Hi}$ and integrating in x, we find that the 3-DNLS equation in the reference frame moving in the positive direction of the x-axis with the Alfvén velocity can be written as

$$\partial_t h + s\partial_x\left(|h|^2 h\right) - i\lambda\partial_x^2 h = \sigma\int_{-\infty}^x \Delta_\perp h\, dx, \qquad (1.1.16)$$

where the upper(lower) sign of the factor $\lambda = \pm 1$ corresponds to the right(left)-circularly polarized wave mode, respectively.

When the dissipation effects cannot be neglected, (1.1.16) should be supplemented by the proper term. Taking into account the hydrodynamic approximation considered in this Section (when $\omega \ll \omega_{0e}$) it is thus sufficient to limit the study (of the influence of dissipation on the structure and evolution of nonlinear waves) to only processes of the "viscous" type [15] (e.g., taking place in a plasma for the ion oscillations), with the inverse times being much less than the electron plasma frequency, i.e., $\tau^{-1} \ll (4\pi n_0 e^2/m_e)^{1/2}$ (in this case, for $T_e \gg T_i$ the Landau damping is small). Thus, dissipative effects associated with such type of relaxation process lead to appearance of the imaginary term $-i\nu k_x^2$ in the dispersion equation. Accordingly, the Burgers-type term $\nu\partial_x^2 u$ has to be included into the left-hand side of (1.1.16). In this case, the coefficient

$$\nu = (\rho_0/2\rho)\left(c_\infty^2 - c_0^2\right)\tau\int_0^\infty \xi\varphi(\xi)d\xi$$

defines the logarithmic damping rate and, as it is shown in [27], is the characteristic rate of the relaxation damping of the "sound" wave. Here, c_∞ and c_0 are the velocities of the high- and low-frequency "sound" mode and φ is the function defining the relaxation process. Thus the 3-DNLS equation generalized by the viscous type dissipative term can be written as

$$\partial_t h + s\partial_x\left(|h|^2 h\right) - i\lambda\partial_x^2 h - \nu\partial_x^2 h = \sigma\int_{-\infty}^x \Delta_\perp h\, dx. \qquad (1.1.17)$$

For this equation, taking into account $\sigma = -c_0/2, c_0 = v_A$, and (formally) $\beta k_x = \lambda, \gamma = 0, s = c_0$, the dispersion relation has the following form

$$\omega \approx v_A k_x\left[1 + k_\perp^2/2k_x^2 - i\nu k_x/v_A - \lambda k_x/v_A\right]. \qquad (1.1.18)$$

We note here that the 3D eq. (1.1.17) (as well as the GKP equation (1.1.6) is not completely integrable and for its solution it is necessary to use numerical methods developed in [27],[40],[34]. It is also necessary to take into account, that even for the 1D equation (1-DNLS equation), the solutions cannot always be obtained analytically in the closed form, since the use of the known inverse scattering transform (IST) procedure requires rather strong limits on the initial and boundary conditions (first of all, on the

localization of the potential $h(x, t)$ at any time moment and $h(x,0) \to 0$ when $|x| \to 0$ [27]. Thus development of numerical codes for the integration of the DNLS-type equations is an important and actual issue, and we use them for numerical modeling of the dynamics of the Alfvén waves in Sect. 1.4.3.

1.1.3. The BK system

In [28] we introduced the system describing the dynamics of a wide class of multidimensional nonlinear wave processes (known now as the Belashov-Karpman (BK) system):

$$\partial_t u + \text{A}(t,u)u = f, \qquad f = \kappa \int_{-\infty}^{x} \Delta_\perp u dx, \qquad \Delta_\perp = \partial_y^2 + \partial_z^2 \qquad (1.1.19)$$

which with the operator

$$\text{A}(t,u) = \alpha u \partial_x - \partial_x^2 (\nu - \beta \partial_x - \gamma \partial_x^3) \qquad (1.1.20)$$

turns into the GKP equation and in case when $\beta \equiv 4\pi nT / B^2 \ll 1$ for $\omega < \omega_B = eB / Mc$ (here M is the ion mass), $k\lambda_D \ll 1$ describes propagation of the fast magnetosonic (FMS) waves in the magnetized plasma with $k_x^2 \gg k_\perp^2$, $v_x \ll c_A$ near the cone of $\theta = \arctan(M / m)^{1/2}$ where M is the ion mass [13]. In this case function u has a sense the dimensionless amplitude of the magnetic field of the wave, $h = B_\sim / B$, the coefficients at the terms describing nonlinearity, dissipation and dispersion effects, respectively, are defined by values of plasma parameters and angle between magnetic field and wave vector, $\theta = (\mathbf{B}, \mathbf{k})$. In the opposite case, when the operator

$$\text{A}(t,u) = 3s |p|^2 u^2 \partial_x - \partial_x^2 (i\lambda + \nu) \qquad (1.1.21)$$

in eq. (1.1.19) turns into the 3-DNLS equation and in case when $\beta > 1$ describes the dynamics of the finite-amplitude Alfvén waves propagating near-to-parallel to $\mathbf{B}$ for $u = h = (B_y + iB_z) / 2B |1 - \beta|$, $\mathbf{h} = \mathbf{B}_\perp / B_0$ where $p = (1 + ie)$, and e is "an eccentricity" of the polarization ellipse of the Alfvén wave [34]. The upper and lower signs of $\lambda = \pm 1$ correspond to the right and left circularly polarized wave, respectively; sign of nonlinearity is accounted by the coefficient $s = \text{sgn}(1 - p) = \pm 1$ in the nonlinear term: $\kappa = -r_A / 2$, $r_A = v_A / \omega_{0i}$.

In the next Sections we will consider both cases for the BK system including the GKP equation (1.1.19), (1.1.20) and the 3-DNLS equation (1.1.19), (1.1.21).

1.2. Problem of stability of multidimensional solutions of the GKP and 3-DNLS equations

In this Section the problem of stability of the multidimensional solutions of the BK class equations describing the nonlinear waves which are formed on the low-frequency branch of oscillations in plasma for cases when $\beta \equiv 4\pi nT / B^2 \ll 1$ and $\beta > 1$ is studied. In first case, for $\omega < \omega_B = eB / Mc, k\lambda_D \ll 1$ the FMS waves are excited, and their dynamics under conditions $k_x^2 \gg k_\perp^2$, $v_x \ll c_A$ near the cone of $\theta = \arctan(M / m)^{1/2}$, is described by the equation of the BK class known as the GKP equation for the magnetic field $h = B_\sim / B$ with due account of the high order dispersive correction defined by values of plasma parameters and angle $\theta = (\mathbf{B}, \mathbf{k})$. In another case,

the dynamics of the finite-amplitude Alfvén waves propagating near-to-parallel to **B** is described by the equation of the same class known as the 3-DNLS equation for $h = (B_y + iB_z)/2B\,|1-\beta|$. To study the stability of multidimensional solutions in both cases the method of investigation of the Hamiltonian bounding with deformation conserving momentum by solving the variation problem is used. As a result, we have obtained the conditions of existence of the 2D and 3D soliton solutions in the BK system for cases of the GKP and 3-DNLS equation (i.e. for the FMS and Alfvén waves, respectively) in dependence on the equations' coefficients, i.e. on the parameters of both plasma and wave.

1.2.1. Introduction. Basic equations

In this Section we study the stability of the multidimensional solitons forming on the low-frequency branch of oscillations in a plasma for cases $\beta \equiv 4\pi nT/B^2 << 1$ and $\beta > 1$. These oscillations are described by the Belashov-Karpman (BK) class of eqs. (1.1.19)

$$\partial_t u + \mathrm{A}(t,u)u = f \qquad (1.2.1)$$

when operator $\mathrm{A}(t,\,u)$ takes the form (1.1.20) and form (1.1.21), respectively. As we have noted in Sect. 1.1.3, in the first case the system (1.1.19) when $\omega < \omega_B = eB/Mc$, $k\lambda_D << 1$ is the generalized Kadomtsev-Petviashvili (GKP) equation

$$\partial_x\left(\partial_t u + \alpha u \partial_x u - \nu\partial_x^2 u + \beta\partial_x^3 u + \gamma\partial_x^5 u \right) = \kappa\Delta_\perp u, \qquad (1.2.2)$$

$\kappa = -c_0/2$, which is valid when the dispersion relation has form (1.1.7) and describes propagation of the FMS waves with $k_x^2 >> k_\perp^2$, $v_x << c_A$ in magnetized plasma for the dimensionless amplitude of the magnetic field of the wave, $h = B_\sim/B$ [13]. In the second case we have the 3-dimensional derivative nonlinear Schrödinger (3-DNLS) equation

$$\partial_t h + s\partial_x\left(|h|^2 h\right) - i\lambda\partial_x^2 h - \nu\partial_x^2 h = \sigma\int_{-\infty}^{x}\Delta_\perp h dx,$$
$$\sigma = -r_A/2, \quad r_A = v_A/\omega_{Hi} \qquad (1.2.3)$$

where $s = \pm 1$, $\lambda = \pm 1$ with dissipative factor

$$\nu = (\rho_0/2\rho)\left(c_\infty^2 - c_0^2\right)\tau\int_0^\infty \xi\varphi(\xi)d\xi.$$

Equation (1.2.3) is valid when the dispersion relation has form (1.1.18) and describes propagation of the finite-amplitude Alfvén waves near-to-parallel to magnetic field **B** for the dimensionless function $u = h = (B_y + iB_z)/2B\,|1-\beta|$ [31].

The sets of eqs. (1.1.19), (1.1.20) [or eq. (1.2.2)] and (1.1.19), (1.1.21) [or eq. 1.2.3)] are not completely integrable ones, and a problem of existence of multidimensional stable soliton solutions requires especial investigation. Let us consider the problem of stability of possible multidimensional solutions for two particular cases of the BK system mentioned above which correspond two branches of oscillations in space plasma. Let us assume that dissipation is absent in the medium, i.e. $\nu=0$ in eqs. (1.2.2) and (1.2.3). At first, for the whole diapason of the dispersion coefficients' change we will give the estimations and formulate the sufficient conditions of stability of the

GKP equation solutions in the two-dimensional (2D) and three-dimensional (3D) geometry on the basis of transformational properties of the Hamiltonian. Further, we will consider the same problem for the 3-DNLS equation in the 3D geometry.

1.2.2. Case of the GKP equation

To study the solutions stability, performing the coordinate transformation (see Sect. 1.1.1), rewrite eq. (1.2.2) with $\nu=0$ in form

$$\partial_x\left(\partial_t u + 6u\partial_x u - \varepsilon\partial_x^3 u - \lambda\partial_x^5 u\right)=\Delta_\perp u, \qquad (1.2.4)$$

where $\varepsilon = \beta\,|\,\gamma\,|^{-1/2}$, $\lambda = \mathrm{sgn}\,\gamma$. Note that (1.2.4) is now the Hamiltonian equation. Rewriting it into the form

$$\partial_t u = \partial_x(\delta\mathrm{H}/\delta u) = -\int_{-\infty}^{\infty}\delta'(x - x')(\delta\,\mathrm{H}/\delta u)dx', \qquad (1.2.5)$$

with the Hamiltonian

$$\mathrm{H} = \int\left[-\frac{\varepsilon}{2}\left(\partial_x u\right)^2 + \frac{\lambda}{2}\left(\partial_x^2 u\right)^2 + \frac{1}{2}\left(\nabla_\perp\partial_x v\right)^2 - u^3\right]d\mathbf{r} \qquad (1.2.6)$$

and $\partial_x^2 v = u$, we obtain the Hamiltonian equation where the continuum of values, $u \in \mathsf{M}$, plays the role of the point coordinates in the phase space M, the matrix $\omega(x,x') = \delta'(x - x')$ is skew-symmetric and, because of the inversibility of the operator ∂_x on the decreasing functions for $|x| \to \infty$, is a non-degenerate one on u. Thus the Hamiltonian structure can be represented by the Poisson bracket [27]

$$\{S,R\} = \int_{-\infty}^{\infty}(\delta S/\delta u)\partial_x(\delta R/\delta u)dx, \quad S,R \in \mathsf{M},$$

with $S;R \in \mathsf{M}$, which satisfies the Jacobi's identity since ω does not depend on the point u in the space M.

The problem of the stability of the soliton-like solutions of (1.2.5) was studied before in [11] on the basis of an analysis of transformational properties of the Hamiltonian (1.2.6) in the 2D and 3D geometry ($\partial_z = 0$ and $\partial_{yz} \neq 0$, respectively) for $\lambda = \pm 1$, $\varepsilon_{<}^{>}0$ (corresponding to different types of the medium).

The stationary solutions of eq. (1.2.4) are defined from the variation problem,

$$\delta(\mathrm{H} + \nu P_x) = 0 \qquad (1.2.7)$$

where $P_x = \frac{1}{2}\int u^2 d\mathbf{r}$ is the momentum projection onto the x axis, ν is a Lagrange's factor, which illustrates the fact that all finite solutions of eq. (1.2.4) are the stationary points of the Hamiltonian for fixed P_x.

Consider now the problem of stability. In a dynamic system, according to Lyapunov's theorem, the stationary points corresponding to the maximum or minimum of the Hamiltonian H are absolutely stable. If an extremum is local then the locally stable solutions are possible. The unstable states correspond to the monotonous dependence of H on its variables, i.e., those cases when the stationary point is the saddle point. According to that, all we need is to prove that the Hamiltonian H is limited from below for the fixed P_x.

Similar to what was done for the classic KP equation in [70], we consider the scale transformations in the real vector space R,

$$u(x, \mathbf{r}_\perp) \rightarrow \zeta^{-1/2} \eta^{(1-d)/2} u(x/\zeta, \mathbf{r}_\perp/\eta) \tag{1.2.8}$$

(where d is the dimension of the problem, and $\zeta, \eta \in \mathsf{R}$) which conserves the momentum P_x. The Hamiltonianas a function of the parameters ζ, η now takes the form

$$\mathrm{H}(\zeta, \eta) = a\zeta^{-2} + b\zeta^2\eta^{-2} - c\zeta^{-1/2}\eta^{(1-d)/2} + e\zeta^{-4}, \tag{1.2.9}$$

where

$$a = -(\varepsilon/2)\int(\partial_x u)^2 d\mathbf{r}, \ b = (1/2)\int(\nabla_\perp \partial_x v)^2 d\mathbf{r}, \ c = \int u^3 d\mathbf{r},$$

$$e = (\lambda/2)\int(\partial_x^2 u)^2 d\mathbf{r}.$$

The necessary conditions for the existence of Hamiltonian's extremum are given by

$$\partial_\zeta \mathrm{H} = 0 \ \text{and} \ \partial_\eta \mathrm{H} = 0, \tag{1.2.10}$$

The latter enables us to obtain the extremum's coordinates, (ζ_i, η_j), if it exists. Holding the inequalities

$$\begin{vmatrix} \partial_\zeta^2 \mathrm{H}(\zeta_i, \eta_j) & \partial_{\zeta\eta}^2 \mathrm{H}(\zeta_i, \eta_j) \\ \partial_{\eta\zeta}^2 \mathrm{H}(\zeta_i, \eta_j) & \partial_\eta^2 \mathrm{H}(\zeta_i, \eta_j) \end{vmatrix} > 0,$$

$$\partial_\zeta^2 \mathrm{H}(\zeta_i, \eta_j) > 0 \tag{1.2.11}$$

guarantees that the corresponding quadratic form is the positively definite one and therefore these inequalities give the sufficient condition of the existence of the (local) minimum at the point (ζ_i, η_j).

Consider eq. (1.2.2) for $d = 2$, i.e., with $\partial_z = 0$. In this case eqs. (1.2.10) form the following set [11],[27]:

$$G \equiv (c^4/32b)t^4 - (at + 2e)^3 = 0,$$

$$t = \zeta^2, \tag{1.2.12}$$

$$\eta = \left[(4b/c)^2 \zeta^5\right]^{1/3}.$$

Analysis of (1.2.12) shows (see Appendix) that it has one positive root, $t \in \mathsf{R}$, for every quadruple of the functions a, b, c, $e \in \mathsf{R}$ in the case $e > 0$ and any a; two positive roots, $t_{1,2} \in \mathsf{R}$, for $e < 0$ and $a > 0$; and in the case $e < 0$, $a \leq 0$ we have $t \notin \mathsf{R}$.

Inequalities (1.2.11) for $d = 2$, taking into account expressions (1.2.12), lead to

$$G - (C_{11}a^3t^3 + C_{12}a^2et^2 + C_{13}ae^2t + C_{14}e^3) < 0, \tag{1.2.13}$$

$$G - (C_{21}a^3t^3 + C_{22}a^2et^2 + C_{23}ae^2t + C_{24}e^3) < 0, \tag{1.2.14}$$

where $C_{nm} > 0$ are constants. It follows that conditions (1.2.11) are fulfilled on the set $S_t \subset \mathsf{R}$ of solutions of the set (1.2.12) for $e > 0$ and $a \geq 0$, and, consequently, the Hamiltonian $\mathrm{H}(\zeta, \eta)$ is bounded from below. Solving (1.2.13) and (1.2.14) in the R-space for $e > 0$ and $a < 0$, we obtain for $S_t^{(13.1)} \cap S_t^{(13.2)} = A_t \subset \mathsf{R}$ that

$\sup A_t = (3C_{11})^{-1} \times [2C_1 \cos(\varphi_1/3) - C_{12}] a^{-1} e$, and $\inf A_t = 0$ ($t=0$ is not the root of the set (1.2.12) and we therefore discard it). Here,

$$C_1 = (C_{12}^2 - 3C_{11}C_{13})^{1/2} \text{ and } \varphi_1 = \text{Arc} \cos \left\{ (2C_1^3)^{-1} \left[C_{12} (C_{12}^2 - 3C_1^2) - 27C_{11}^2 C_{14} \right] \right\}.$$

Taking into account (A4) (see Appendix; note that $S_t \cap A_t \neq \varnothing$), we conclude that for $e > 0$ and $a < 0$, the sufficient condition of the existence of the local minimum of $H(\zeta, \eta)$ is the relation $S_t \subseteq A_t$, i.e.,

$$(a/c)(b/e)^{1/4} \geq (6C_{11})^{-1} [C_1 \cos(\varphi_1/3) - C_{12}/2]. \tag{1.2.15}$$

Analogously, considering inequalities (1.2.13)-(1.2.14) for the case $e < 0$ and $a > 0$, we obtain

$$\inf B_t^{(1)} = (3C_{21})^{-1} [2C_2 \cosh(\varphi_2/3) - C_{22}] a^{-1} e, \quad \sup B_t^{(1)} = (3C_{11})^{-1} [2C_1 \times$$

$$\times \cos(\varphi_1/3 + 4\pi/3) - C_{12}] a^{-1} e, \inf B_t^{(2)} = (3C_{11})^{-1} [2C_1 \cos(\varphi_1/3 + 2\pi/3) - C_{12}] a^{-1} e,$$

where

$$B_t^{(1)} \cup B_t^{(2)} = S_t^{(13.1)} \cap S_t^{(13.2)} = A_t \subset \mathsf{R}; \, C_2 = (C_{22}^2 - 3C_{21}C_{23})^{1/2};$$

$$\varphi_2 = \text{Ar} \cosh \left\{ (2C_2^3)^{-1} \left[C_{22} (C_{22}^2 - 3C_2^2) - 27C_{21}^2 C_{24} \right] \right\}..$$

Taking into account equalities (A8) we get $B_t^{(1)} \subset S_t \Rightarrow B_t^{(1)} \cap S_t = B_t^{(1)}$, and $B_t^{(2)} \cap S_t = \varnothing$. Then in (A5), by changing $a^4 b/c^4 e \leq -2^4 \cdot 3^{-3} \cdot Q^{-1}$ ($Q > 1$) and using inequalities (A7), we obtain $Q = -2^8 \cdot 3^{-3} (T+2)/T^2$ ($T = \inf B_t^{(1)} a e^{-1}$). This corresponds to the sufficient condition of the existence of the local minimum of the Hamiltonian $H(\zeta, \eta)$, namely $\inf S_t = \inf B_t^{(1)}$, which can now be rewritten as

$$a^4 b/c^4 e \leq 2^{-4} T^2 /(T+2). \tag{1.2.16}$$

Fig. 1.2.1 shows the change of the Hamiltonian $H(\zeta, \eta)$ for the test values of the integrals $a; b; c$, and e for $d = 2$, $\lambda = \pm 1$, $\varepsilon \gtrless 0$.

Consider now eq. (1.2.5) for $d=3$ ($\partial_{yz} \neq 0$). In this case, for every quadruple $a; b; c; e \in \mathsf{R}$, with $a \neq 0$, we immediately obtain from (1.2.10)

$$\zeta_i = (16ab)^{-1} \left(3c^2 \pm \sqrt{9c^4 - 512ab^2 e} \right),$$

$$\eta_j = (2b/c)\zeta_i^{5/2}, \tag{1.2.17}$$

$$i = 1, 2; \quad j = 1, 2, 3, 4.$$

We note here that $(\zeta_i, \eta_j) \notin \mathsf{R}$ for $\zeta_i < 0$, and therefore we consider below only the roots $\zeta_i > 0$ (we map out equality $\zeta_i = 0$, taking into account $e \neq 0$, otherwise (1.2.5) degenerates into the standard KP equation).

Inequalities (1.2.11) taking into account (1.2.17) are now given by

$$a\zeta^2 - (c^2/2b)\zeta + 10e/3 > 0, \tag{1.2.18}$$

$$a\zeta^2 + (c^2/48b)\zeta + 10e/3 > 0. \tag{1.2.19}$$
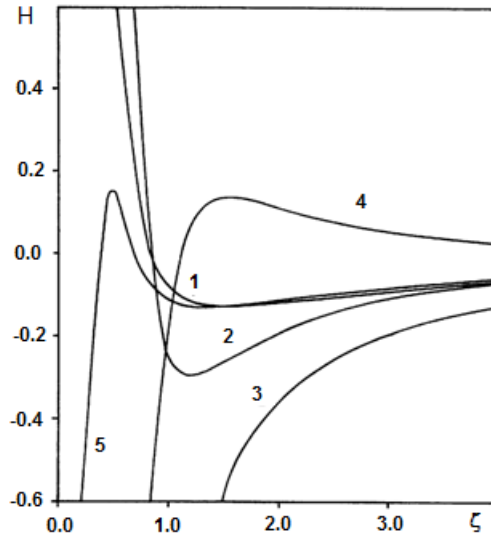
Figure 1.2.1. Change of the Hamiltonian $H(\zeta,\eta)$ in the 2D case ($d=2$) along lines $\eta=\left[(4b/c)^2\zeta^5\right]^{1/3}$ for the test values of the integrals: $1-a=0.5,\ b=0.5,\ c=1,\ e=0.02$; $2-a=-0.5,\ b=0.5,\ c=0.5,\ e=0.5$; $3-a=-0.5,\ b=0.5,\ c=1,\ e=-0.02$.

In the case $e>0$ and $a>0$, the condition $\zeta_i\in R$, i.e.,

$$c^4\geq(512/9)ab^2e \qquad (1.2.20)$$

gives $\zeta_{1,2}>0$. Elementary analysis then shows that $S_{\zeta_1}^{(16)}\cap S_{\zeta_1}^{(17.1)}=\varnothing$ and, if strict inequality (1.2.20) holds $S_{\zeta_2}^{(16)}\subset S_{\zeta_2}^{(17)}$. Thus, for the existence of the local minimum of $H(\zeta,\eta)$ for $e>0$ and $a>0$, it is sufficient to have

$$ab^2e/c^4<9/512. \qquad (1.2.21)$$

When $e>0$ and $a<0$, for each quadruple of a, b, c, $e\in R$ we have from the equality of (1.2.13) $\zeta_1<0$ and, therefore, $S_{\eta_{1,2}}^{(16)}\cap R=\varnothing$. For $S_{\zeta_2}^{(16)}$, elementary analysis of inequalities (1.2.18)-(1.2.19) gives us $S_{\zeta_2}^{(16)}\subset S_{\zeta_2}^{(17)}$. Thus for any $e>0$ and $a<0$ the function $H(\zeta,\eta)$ is limited from below.

Analogous consideration in the case $e<0$ shows that for $a<0$, when condition (1.2.20) is satisfied for every quadruple $a,b,c,e\in R$, we have $\zeta_{1,2}<0$ and, therefore, $S_{\eta_{1,2,3,4}}^{(16)}\cap R=\varnothing$; for $a>0$ we have $\zeta_2<0\Rightarrow S_{\eta_{3,4}}^{(16)}\cap R=\varnothing,\ \zeta_1>0$ but $S_{\zeta_1}^{(16)}\cap S_{\zeta_1}^{(17.1)}=\varnothing$.

For $a=0$ and $e\gtrless 0$ (i.e., $e\neq 0$), instead of (1.2.17) we have

$$\zeta_i=16be/3c^2,\quad \eta_j=(2b/c)\zeta_i^{5/2},$$
$$i=1,\quad j=1,2$$

for every triplet of functions $b,c,e\in R$. For $e<0$ it immediately follows that $S_{\eta_j}\cap R=\varnothing$. For $e>0$, it is not difficult to show that $S_\zeta\subset S_\zeta^{(14)}$.

Fig. 1.2.2 shows the change of the Hamiltonian $H(\zeta,\eta)$ for the test values of the integrals a, b, c, e for $d=3$, $\lambda=\pm1$, $\varepsilon\gtrless 0$.

To sum up the above results, we conclude the following. In the 2D case the Hamiltonian (1.2.6) of eq.(1.2.5) is limited from below at the fixed projection of the
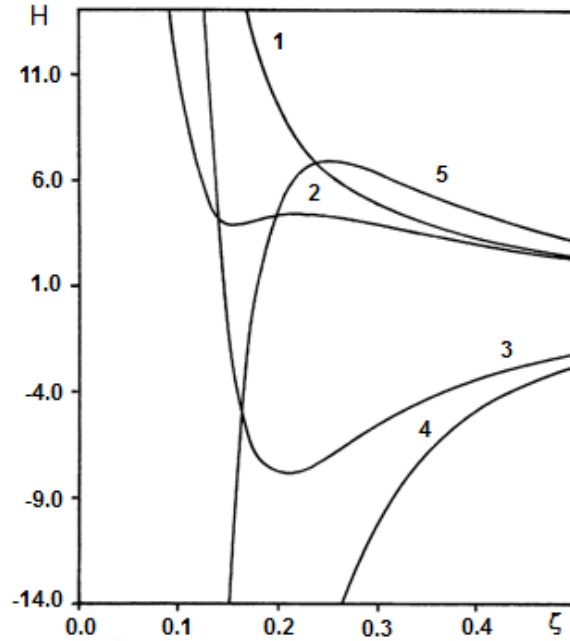
Figure 1.2.2. Change of the Hamiltonian H(ζ, η) for $d=3$ along

the lines $\eta = (2b/c)\zeta^{5/2}$ for the test values of the integrals:
1 $-a=1$, $b=1$, $c=1$, $e=0.025$; 2 $-a=1$, $b=1$, $c=1$,
$e=0.017$; 3 $-a=-0.5$, $b=1$, $c=0.5$, $e=0.02$; 4 $-a=-0.5$,
$b=1$, $c=0.5$, $e=-0.02$; 5 $-a=1$, $b=1$, $c=0.5$, $e=-0.02$.

momentum P_x for the integral values $e>0$ and $a \geq 0$ (i.e. when $\lambda=1$, $\varepsilon \leq 0$ in expression (1.2.6)) and has the local minima for $e>0$ and $a<0$ ($\lambda=1$, $\varepsilon>0$) and $e<0$ and $a>0$ ($\lambda=-1$, $\varepsilon<0$) when the conditions (1.2.15) and (1.2.16), respectively, are satisfied.

In the 3D case H has a local minimum for $e>0$ and $a \geq 0$ [i.e. when $\lambda=1$, $\varepsilon \leq 0$ in (1.2.6)] if condition (1.2.21) is satisfied, and it is limited from below for $e>0$ and $a<0$ ($\lambda=1$, $\varepsilon>0$). Note that the class of scale transformations (8) of course does not include all possible deformations of the Hamiltonian H but the estimations obtained above justify that it is limited for the cases considered when, according to Lyapunov's theorem, absolutely and locally stable soliton solutions should exist. Analysis of the boundedness of H on the numerical solutions of (1.2.4) for $d=2$ and $d=3$ obtained in [61],[62],[15] was presented in [27] and it has confirmed the results presented above.

This is a noteworthy fact that the GKP equation accounting, unlike the usual KP equation, the next order dispersive correction has the stable 3D solutions.

1.2.3. Case of the 3-DNLS equation

Consider now a case of the 3-DNLS equation in the BK system, i.e. eqs. (1.1.19), (1.1.21), using the same approach as in the previous Section for the GKP equation (see also [19]). We rewrite 3-DNLS equation (1.2.3) by performing the formal change $u \rightarrow h$ into the Hamiltonian form

$$\partial_t h = \partial_x (\delta H / \delta h), \qquad (1.2.22)$$

with the Hamiltonian [29]

$$H = \int_{-\infty}^{\infty} \left[\frac{1}{2}|h|^4 + \lambda shh^* \partial_x \varphi + \frac{1}{2}\kappa (\nabla_\perp \partial_x w)^2 \right] d\mathbf{r},$$

(1.2.23)

$$\partial_x^2 w = h, \ \varphi = \arg(h)$$

which has a sense of energy of the system, and solve the variation problem (1.2.7) where $P_x = \frac{1}{2}\int |h|^2 d\mathbf{r}$ is the momentum projection onto the x axis, that illustrates the fact that all finite solutions of eq. (1.2.22) are the stationary points of the Hamiltonian for fixed P_x. It is needed now to prove the Hamiltonian's boundedness (from below) for fixed P_x. Consider the scale transformation $h(x,\mathbf{r}_\perp) \to \zeta^{-1/2}\eta^{-1}h(x/\zeta, \mathbf{r}_\perp/\eta)$ ($\zeta, \eta \in \mathbb{C}$) conserving P_x, in complex vector space $\mathbb{C}$. The Hamiltonian as a function of ζ, η is given by

$$H(\zeta,\eta) = a\zeta^{-1}\eta^{-2} + b\zeta^{-1} + c\zeta^2\eta^{-2},$$

(1.2.24)

where $a = (1/2)\int |h|^4 d\mathbf{r}, \ b = \lambda s\int hh^*\partial_x\varphi d\mathbf{r}, \ c = (\sigma/2)\int (\nabla_\perp \partial_x w)^2 d\mathbf{r}$.

The necessary conditions for the existence of the extremum (1.2.10) immediately allows us to obtain the extremum's coordinates

$$\zeta = -a/c,$$

$$\eta = \left\{ -(a/b)\left[1 + (a^2/c^2) \right] \right\},$$

(1.2.25)

where $b < 0$ if $\eta \in \mathbb{R} \subset \mathbb{C}$ because $a > 0, c > 0$ by definition, and $b > 0$ if $\eta \in \mathbb{C}$. The sufficient conditions for the existence of the local minimum of H at the point (ζ_i, η_i) are given by inequalities (1.2.11) and we therefore obtain for $b < 0$

$$a/c < d = \left(2\sqrt{2}\right)^{-1}\sqrt{13 + \sqrt{185}}.$$

(1.2.26)

Thus it follows from (1.2.11) and (1.2.24)-(1.2.26) that the Hamiltonian H of eq. (1.2.22) is limited from below, i.e.

$$H > -3bd/(1 + 2d^2),$$

(1.2.27)

where $b < 0$ if condition (1.2.26) holds. In this case the 3D solutions of 3-DNLS equation are stable. The solutions are unstable in the opposite case, $ac^{-1} \geq d, b < 0$. Condition $b < 0$ corresponds to the right circularly polarized wave with $\beta = 4\pi nT/B^2 > 1$, i.e. when $\lambda = 1, \ s = -1$ in eq. (1.2.3), and to the left circularly polarized wave when $\lambda = -1, \ s = 1$. It is necessary to note that the sign change $\lambda = 1 \to -1, s = -1 \to 1$ is equivalent to the change $t \to -t, \kappa \to -\kappa$ and for negative κ the Hamiltonian becomes negative in the area "occupied" by the 3D wave weakly limited in the $\mathbf{k}_\perp$-direction; in this case condition (1.2.27) is not satisfied. The change of the sign of b to positive [when $\lambda = 1, s = 1$ or $\lambda = -1, s = -1$ in eq. (1.2.3)] is equivalent to the analytical extension of solution from real values of y, z to the pure imaginary ones: $y \to -iy, z \to -iz$ and, therefore, equivalent to the change of sign of κ in the basic equations. In this case instead of inequality (1.2.27) the opposite inequality will take place. From the physical point of view this means that if the opposite inequality is satisfied, the right polarized wave with the positive nonlinearity and the left polarized wave with the negative nonlinearity are stable. Note that in the particular case $\kappa = 0$ in eqs. (1.2.1), (1.2.2) (1D approximation), instead of inequality (1.2.27) and the

opposite one, it is easy to obtain the conditions $\mathrm{H} > 0$ and $\mathrm{H} < 0$, respectively, that is completely in agreement with the results obtained in [46] for the 1-DNLS equation.

Thus the analysis of the transformation properties of the Hamiltonian of the 3-DNLS equation allows us to determine the ranges of the respective coefficients as well as H which has the sense of the energy of the system, corresponding to the stable and unstable 3D solutions. So, we have proved the possibility of existence in the 3-DNLS model of absolutely stable 3D solutions.

1.2.4. Conclusion

So, we have investigated analytically the problem of stability of multidimensional solitons and nonlinear wave packets in the framework of model of the BK class of equations. Under the assumption of negligible dissipative effects, these solutions coincide with those of the GKP class equations in the form (1.1.19), (1.1.20) with $\nu = 0$ and the 3-DNLS equation (1.1.19), (1.1.21). In the first Section we have presented analytical estimates and formulate the sufficient conditions for the stability of solutions of GKP equation in the 2D and 3D cases, based on the transformational properties of the system's Hamiltonian for the whole range of the dispersive coefficients. Then an analogous problem for the 3-DNLS equation in the 3D geometry has been studied. Despite the fact that the considered classes of the Hamiltonian's deformations for both equations do not include all possible deformations of H, the obtained results clearly demonstrate the stability of the solutions if some (found and formulated) conditions are satisfied and can at least be considered as the necessary conditions of the stability of the multidimensional solutions.

The application of our analysis to the problem of the FMS waves beam's propagation in magnetized plasma enables us to prove [35], for example, that the 3D beam propagating at θ angle to magnetic field doesn't focuse and becomes stationary and stable in the cone of $\theta < \arctan (M / m)^{1/2}$ when the inequality

$$(m / M - \cot^2 \theta)^2 [\cot^4 \theta (1 + \cot^2 \theta)]^{-1} > 4 / 3$$

is satisfied. Let us note also that the obtained results give us the possibility to interpret correctly some our numerical and theoretical results on the dynamics of the internal gravity waves' solitons, induced by the pulse-type sources, which propagate at heights of the ionosphere *F* region [32] from the point of view of such solitons stability.

Note also that our analytical results presented above are well confirmed by the results of our numerical experiments on the study of structure and stability of multidimensional solitons in the model of the 3-DNLS equations [27],[29],[31]. So, we have obtained that for a solitary wave propagating in a plasma, on a level with wave spreading and wave collapse (in other terminology, self-contraction), the formation of the 3D solitons can be observed. These results are well applicable and useful in studies of dynamics of the Alfvén waves propagating in space plasma.

1.2.5. Appendix

Performing the transform $t \to t' + 8a^3 b / c^4$ in eq. (1.2.12), we obtain the reduced equation

$$t'^4 + pt'^2 + qt' + r = 0. \qquad (A1)$$

The cubic resolvent kernel $z^3 + 2pz^2 + (p^2 - 4r)z - q^2 = 0$, using the change $z \to x - 2p/3$, can be reduced to the equation

$$x^3 + p'x + q' = 0, \qquad (A2)$$

where $p' = 2^{10} b e^3 / c^4$; $q' = -2^{14} a^2 b^2 e^4 / c^8$, with the discriminant

$$D = 2^{26} b^3 c^{-12} e^8 \left(2^4 3^{-3} e + a^4 b c^{-4}\right).$$ (A3)

In the case $e > 0$ and, $a \gtrless 0$ we have $D > 0$, therefore eq. (A2) as well as the resolvent kernel in the real vector space R for each quadruple of the values of functions a, b, c, $e \in \mathsf{R}$ have one root. Thus, using Descartes' rule of signs, we can conclude that (1.2.12) for $e > 0$ and $a \gtrless 0$ has one positive root $t \in \mathsf{R}$ (note that $t \leq 0$ does not satisfy (1.2.12), in this case $\zeta \notin \mathsf{R}$). It follows from the analysis of eq. (1.2.12) that in the space R for $S_t \subset \mathsf{R}$ the equalities

$$\inf_{a>0} S_t = \sup_{a<0} S_t = 4\left(be^3\right)^{1/4} / c, \quad \inf_{a<0} S_t = 0.$$ (A4)

take place.

Consider now the case when $e < 0$, $a \gtrless 0$. It follows from eq. (1.2.12) that for $a \leq 0$ this equation foes not have roots $t > 0$ in the space R, therefore, we limit ourselves by an analysis of (1.2.12) for $a > 0$. When

$$F = a^4 b / c^4 e < -2^4 3^{-3}$$ (A5)

we have $D > 0$ from (A3). It then follows that (A2) and the resolvent kernel in the space R for each quadruple of the functions a, b, c, $e \in \mathsf{R}$ have one root, and eq. (1.2.12), taking into account the rule of signs, has two positive roots $t_{1,2} \in \mathsf{R}$.

Let us estimate boundaries of the set $S_t \subset \mathsf{R}$. With the two changes $t \to t + h$ and $t \to -t + h$ in (1.2.12), we obtain, respectively, the sets

$$c^4 > 8 i a^{4-i} b h^{-i} \left(ah + 2e\right)^{i-1},$$ (A6)

$$(-1)^i c^4 > (-1)^i 8 i a^{4-i} b h^{-i} \left(ah + 2e\right)^{i-1},$$ (A7)

$$i = 1, 2, 3, 4.$$

Solving inequalities (A6) and (A7) with the condition (A5), we obtain

$$\sup S_t = 2^5 \cdot 3^{-3} \left[\sqrt{10} \cos\left(\psi_1 / 3 + 2\pi/3\right) - 4\right] a^{-1} e,$$

$$\psi_1 = \text{Arc}\cos\left[-11/\left(2^5 \cdot 5\sqrt{10}\right)\right],$$

$$\inf S_t = \min\left\{\max\left(h'_1, h'_2\right), \ 2^4 3^{-3}\left(\sqrt{10} - 8\right) a^{-1} e\right\},$$ (A8)

$$h'_1 = 8\left[\sqrt{-2FF'} \cos\left(\psi_2/3\right) + F\right] a^{-1} e,$$

$$h'_2 = 8\left[\sqrt{-2FF'} \cos\left(\psi_2/3 + 4\pi/3\right) + F\right] a^{-1} e,$$

$$\psi_2 = \text{Arc}\cos\left\{\left(2^7 F^2 + 3 \cdot 2^3 F + 3\right)/\left(2^3 F' \sqrt{-2FF'}\right)\right\},$$

$$FF' = 1 - 2F.$$

If condition (A5) is not satisfied, we have $D \leq 0$. In this case, a simple analysis shows that (A2) and the resolvent kernel for each quadruple of the functions $a, b, c, e \in \mathsf{R}$

($e < 0$, $a > 0$) have one positive and two negative roots. Therefore, eqs. (A1) and (1.2.12) in the real vector space R have no roots.

1.3.   Qualitative analysis and asymptotics of solutions of the GKP-class equations

In this Section we study the dynamical systems associated with the generalized Kadomtsev-Petviashvili (GKP) equation and consider the structure of possible multidimensional solutions and their asymptotics. We also present some considerations on constructing the phase portraits of the systems in the 8-dimensional phase space for the GKP equation on the basis of the results of qualitative analysis of the generalized equations of the KdV-class.

1.3.1. Basic equations

Consider the generalized Kadomtsev-Petviashvili (GKP) equation (or so-called Belashov-Karpman (BK) [61],[62],[15] equation without the terms describing the dissipation and instability)[1]:

$$\partial_\eta \left(\partial_t u + \alpha u \partial_\eta u + \beta \partial_\eta^3 u + \gamma \partial_\eta^5 u \right) = \kappa \Delta_\perp u \qquad (1.3.1)$$

$$\Delta_\perp = \partial_{\zeta_1}^2 + \partial_{\zeta_2}^2,$$

where ζ_1 and ζ_2 are the transverse coordinates. At $\gamma = 0$ eq. (1.3.1) is the classic Kadomtsev-Petviashvili (KP) equation which is the completely integrable Hamiltonian system and has in case $\Delta_\perp = \partial_{\zeta_1}^2$ the solutions in form of the 1D (for $\beta\kappa < 0$) or 2D (for $\beta\kappa > 0$) solitons (see [27],[59]). The structure and the dynamics of the solutions of the non-integrable analytically GKP model (1.3.1) with $\beta, \gamma = \mathrm{const}$ has been investigated in detail in [61],[62] where it was shown that in dependence on the signs of coefficients β, γ and κ the 2D and 3D soliton type solutions with the monotonous or oscillatory asymptotics can take place. In [16] the asymptotes of the 1D analogue of eq. (1.3.1) with $\beta, \gamma = \mathrm{const}$ were studied, and the sufficiently complete classification of its 1D solutions in the phase space was constructed.

Note, that if the dispersion in medium is variable, introducing the high order dispersive correction (term with γ) into the KP equation has a principal role. Thus, for example, in the problems of the propagation of the 2D gravity and gravity-capillar waves on the surface of "shallow" water [15] when β is defined respectively as $\beta = c_0 H^2 / 6$ and $\beta = (c_0 / 6)\left[H^2 - 3\sigma / \rho g \right]$ where H is the depth, ρ is the density, and σ is the coefficient of surface tension of fluid, the depth can be variable, $H = H(t, x, y)$, and in this case β also becomes the function of the coordinates and time. Similar situation takes place on studying the evolution of the 3D fast magneto-sonic (FMS) waves in a magnetized plasma in case of the inhomogeneous and/or non-stationary plasma and magnetic field [13],[35] when β is a function of the Alfvén velocity $v_\mathrm{A} = f\left[B(t, \mathbf{r}), n(t, \mathbf{r}) \right]$ and angle $\theta = (\mathbf{k}^\wedge \mathbf{B})$: $\beta = v_A (c^2 / 2\omega_{0i}^2)(\cot^2 \theta - m / M)$. In these cases the situations, when $\beta \to 0$ or even becomes equal zero are possible, that, however, does not mean that the dispersion in medium is completely absent, simply it is necessary to keep the next order dispersive term in the Taylor expansion of a full dispersion equation with respect to *k*, at this, a balance between nonlinearity and dispersion, defining the existence of the soliton, will be conserved, and the term

---

[1] The role of these terms was considered in detail in [15],[27].

proportional to the fifth derivative will appear in the KP equation. Therefore, if the dispersion can vary in medium, it is necessary to consider the BK equation in form (1.3.1), namely the GKP equation.

So, our purpose is the generalization of the results obtained in [16] to the multidimensional cases when β or/and γ are not constants (the dispersion is variable) with due account of the results presented in [15],[27].

To avoid unnecessary cumbersome expressions, consider eq. (1.3.1) in the 2D form assuming that $\Delta_\perp = \partial^2_{\zeta_1}$. Further generalization of the technique used (as well as the results obtained) to the full 3D case $\Delta_\perp = \partial^2_{\zeta_1} + \partial^2_{\zeta_2}$ is rather trivial, as we demonstrate below. Assume that $\zeta_1 \equiv \zeta$ and, for clarity, $\alpha = 6$ (the latter can be easily obtained by the scale transform $u \to (6/\alpha)u$ in the GKP equation).

Now, let us introduce the new variables: $\bar{\eta} = \eta + \zeta$, $\bar{\zeta} = \eta - \zeta$. Applying first $\bar{\eta}$ and then $\bar{\zeta}$ to (1.3.1) we obtain the pair of one-dimensional equations:

$$\partial_{\bar{\eta}}\left(\partial_t u + 6u\partial_{\bar{\eta}}u + \beta\partial^3_{\bar{\eta}}u + \gamma\partial^5_{\bar{\eta}}u\right) = \kappa\partial^2_{\bar{\eta}}u,$$
$$\partial_{\bar{\zeta}}\left(\partial_t u + 6u\partial_{\bar{\zeta}}u + \beta\partial^3_{\bar{\zeta}}u + \gamma\partial^5_{\bar{\zeta}}u\right) = \kappa\partial^2_{\bar{\zeta}}u \tag{1.3.2}$$

written in the reference frame with the axes $\bar{\eta}$ and $-\bar{\zeta}$ rotated through an angle $+45°$ relative to the axes η and ζ. Representation (1.3.2) means in fact that the starting eq. (1.3.1) admits two types of 1D solutions, $u(\bar{\eta}, t)$ and $u(\bar{\zeta}, t)$, satisfying the first and the second equations of the set (1.3.2), respectively. It is necessary, however, to bear in mind that the "one-dimensionality" of these solutions nevertheless implicity assumes the linear dependence of each of the new variables $\bar{\eta}$ and $\bar{\zeta}$ on both coordinates, η and ζ. Integrating eqs. (1.3.2) over $\bar{\eta}$ and $-\bar{\zeta}$, respectively, we obtain equiform generalized KdV equations

$$\partial_t u + (-\kappa + 6u)\partial_{\bar{\eta}}u + \beta\partial^3_{\bar{\eta}}u + \gamma\partial^5_{\bar{\eta}}u = 0,$$
$$\partial_t u + (-\kappa + 6u)\partial_{\bar{\zeta}}u + \beta\partial^3_{\bar{\zeta}}u + \gamma\partial^5_{\bar{\zeta}}u = 0 \tag{1.3.3}$$

coupled with each other by the way of the change of the coordinates made above. Now, transferring to the coordinates moving along the corresponding axis with the velocity $-\kappa$, i.e. applying the change $\eta' = \bar{\eta} + \kappa t$, $\zeta' = \bar{\zeta} + \kappa t$ in eqs. (1.3.3) and omitting "primes" for simplicity, we write eqs. (1.3.3) in the standard form:

$$\partial_t u + 6u\partial_\eta u + \beta\partial^3_\eta u + \gamma\partial^5_\eta u = 0,$$
$$\partial_t u + 6u\partial_\zeta u + \beta\partial^3_\zeta u + \gamma\partial^5_\zeta u = 0. \tag{1.3.4}$$

So, we can now conduct the analysis for only one generalized equation of the set (1.3.3), and then, making the inverse change of the variables, extend the results to the 2D solutions $u(\eta, \zeta, t)$ of the GKP equation (1.3.1) with $\Delta_\perp = \partial^2_\zeta$.

1.3.2. Qualitative analysis for 1D equation

Taking into account the more general case we extend the class of eqs. (1.3.4) by introducing the arbitrary positive exponent p of the nonlinear term:

$$\partial_t u + 6u^p\partial_\eta u + \beta\partial^3_\eta u + \gamma\partial^5_\eta u = 0. \tag{1.3.5}$$

Equation (1.3.5) for $\gamma = 0$ is the usual KdV equation when $p=1$, and it is the modified

KdV (MKdV) equation when $p=2$. The asymptotics of (1.3.5) with $p=1$ were first investigated in [61],[63] where it was shown that depending on the signs of the coefficients β and γ the soliton type solutions with monotonous or oscillating asymptotics can take place. But note, that eq. (1.3.5) with $\gamma \neq 0$ and $p \geq 1$ is not exactly integrable (i.e., the known analytical methods such as the IST method, are not applicable to this equation). In [16] eq. (1.3.5) was investigated by the methods of the both asymptotic and qualitative analysis, and, as a result, the sufficiently full classification of its solutions was constructed. In this Section we mainly follow the ideas and technique of [16].

Note, that from the physical point of view, the cases when in eq. (1.3.5) $p=1,2$ are the most interesting, and applications for $p>2$ are presently unknown. However, since equations of the family (1.3.5) with an arbitrary integer $p>0$ demonstrate, to a considerable extent, similar mathematical properties, we use here a general approach elucidating, apart from other, the dependence of the characteristics of the solutions on the nonlinearity exponent.

Performing transformation $\xi = x - Vt$ and integrating (1.3.5) in ξ we obtain

$$-Vu + \frac{6}{p+1}u^{p+1} + \beta\partial_\xi^2 u + \gamma\partial_\xi^4 u = 0. \tag{1.3.6}$$

Assuming without loss of generality that $\gamma > 0$ and $\beta = \pm 1$, after the change $u=Vw$, $\xi \to |V|^{-1/4}\xi$ we convert (1.3.6) to

$$\mathrm{sgn}(V)\gamma\partial_\xi^4 w + \mathrm{sgn}(V)\beta|V|^{-1/2}\partial_\xi^2 w - w + \frac{6s}{p+1}|V|^{p-1}w^{p+1} = 0 \tag{1.3.7}$$

where

$$s = \begin{cases} \mathrm{sgn}(V) & \text{for even } p \\ 1 & \text{for odd } p. \end{cases}$$

Depending on sign of V in (1.3.7) the following two cases can be considered:

a) $V>0$:

$$\gamma\partial_\xi^4 w + |V|^{-1/2}\beta\partial_\xi^2 w - w + \frac{6s}{p+1}|V|^{p-1}w^{p+1} = 0; \tag{1.3.8a}$$

b) $V<0$:

$$-\gamma\partial_\xi^4 w - |V|^{-1/2}\beta\partial_\xi^2 w - w + \frac{6s}{p+1}|V|^{p-1}w^{p+1} = 0. \tag{1.3.8b}$$

However, as one can see from (1.3.5), the velocity of the wave, V, depends on the equation's coefficients and it is restricted by:

$$V \begin{cases} < V_{\min}^{ph} = -1/4\gamma, & \beta = 1; \\ > V_{\max}^{ph} = -1/4\gamma, & \beta = -1. \end{cases} \tag{1.3.9.1} \tag{1.3.9.2}$$

The right-hand sides of inequalities (1.3.9) correspond to results obtained in [61] and comparing these relations with expressions (1.3.8a) and (1.3.8b) leads to contradictions in the cases $\beta = 1$ and $\beta = -1$, $V > 0$, respectively. Therefore, below we will limited by the consideration of cases (a) with $\beta = -1$ and (b) with $\beta = 1$ and $\beta = -1$, $-1/4\gamma < V < 0$.

Qualitative analysis and asymptotes of the solutions. First, we note that every equation of the set (1.3.8) is equivalent to the set of the first order ordinary differential equations
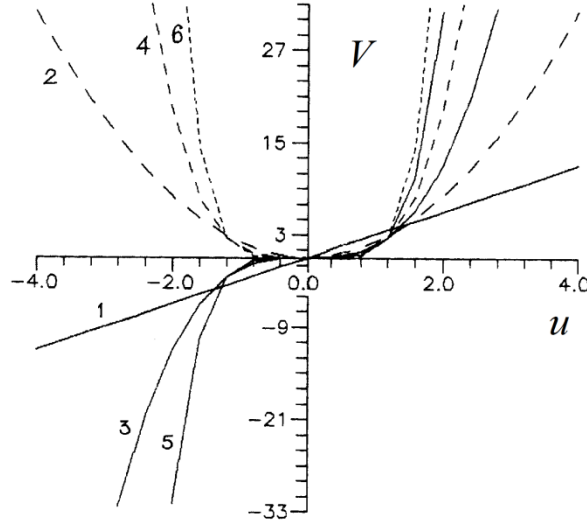
Figure 1.3.1. Dependence $V = f(u)$ for eq. (1.3.6) for different values of p. Numbers of curves corresponds $p = 1, 2, ..., 6.$

$$
\begin{cases}
x_1 = \dot{w}, \qquad x_2 = \dot{x}_1, \qquad x_3 = \dot{x}_2, \\
\begin{pmatrix} + \\ - \\ - \end{pmatrix} \gamma \dot{x}_3 = \begin{pmatrix} + \\ + \\ - \end{pmatrix} C^2 x_2 + w - \dfrac{6sC^{4(1-p)}}{p+1} w^{p+1},
\end{cases}
\tag{1.3.10}
$$

where the dots stand for the ξ-derivatives, and the signs in the brackets correspond to three cases mentioned above; furthermore, $C = |V|^{-1/4}$. Solutions of eqs. (1.3.10) are stable if there exist the singular trajectories of the imaging point in the phase space(w, x_1, x_2, x_3) of the set (1.3.10). Each trajectory of its kind is related to the state of equilibrium near the maximum of the soliton-like solution and at the boundaries $|\xi| = \infty$. Assuming as the boundary conditions that

$$
w = \partial_\xi^n w = 0, \quad n = 1, 2, 3 \text{ at } |\xi| \to \infty,
\tag{1.3.11}
$$

we can find from (1.3.10) the number as well as the coordinates of the singular points:

$$
w_1 = 0, \quad w_j = \sqrt[p]{\dfrac{p+1}{6sC^{4(1-p)}}},
\tag{1.3.12}
$$

where the points $w_1 = 0$ and w_j correspond, respectively, to $|\xi| = \infty$ and the bending points of the function $u(\xi)$; $j = 2$ for the odd and $j = 2, 3$ for the even p, in the last case $w_2 = -w_3$. Considering only real roots of (1.3.12) we immediately conclude (using Sturm's theorem) that for the odd p there are two singular points, and for any even p there are three singular points. The distance between the singular points defines the amplitude of the soliton-like solution of (1.3.6). Besides, the value of the nonlinearity exponent p defines a character of dependence $V = f(u)$: for $p > 1$ this dependence becomes nonlinear (Fig. 1.3.1) unlike the known linear one for $p = 1$ (e.g., in the case of the KdV equation). As one can see in Fig. 1.3.1, for the even p the solutions of eq. (1.3.6) can have the positive as well as negative polarity ($u \gtrless 0$) for any sign of V.

To investigate the types of the singular points, it is necessary to linearize the set (1.3.10) in the neighborhood of every point. Using Taylor's formula, we obtain from eqs. (1.3.10) [16]:

1) for the singular point $w_1{=}0$, that corresponds to $u_1{=}0$ in (1.3.6), taking into account the conditions (1.3.11),

$$\begin{cases} x_1 = \dot{w}, \quad x_2 = \dot{x}_1, \quad x_3 = \dot{x}_2, \\ \binom{+}{-}\gamma\dot{x}_3 = \binom{+}{+}_{-} C^2 x_2 + w; \end{cases}$$

(1.3.13.1)

2) for the singular point w_j, that corresponds to $u_j = \sqrt[p]{(p+1)V/6s}$ in (1.3.6),

$$\begin{cases} x_1 = \dot{w}, \quad x_2 = \dot{x}_1, \quad x_3 = \dot{x}_2, \\ \binom{+}{-}\gamma\dot{x}_3 = \binom{+}{+}_{-} C^2\beta x_2 - pw \, . \end{cases}$$

(1.3.13.2)

Since the sets (1.3.13) are essentially four-dimensional, we investigate them by expanding the corresponding canonical systems into the subsystems [27]. In this case, it is possible to consider the phase portraits of the linear sets (1.3.13) as projections of the singular points and trajectories onto two planes. For the singular point $w_1{=}0$ we obtain that the eigenvalues of the matrices of subsets of set (1.3.13.1) (see [27]) corresponding to the phase planes P1(w, x_1) and P2(x_2, x_3) are defined by

$$\lambda_{1,2}^{(\text{P1,P2})} = \pm(2\gamma)^{-1/2}\left[\binom{+}{-}C^2 \pm \sqrt{C^4\binom{+}{-}4\gamma}\,\right]^{1/2}.$$

(1.3.14)

In the case (a) with $\beta = -1$, λ_1, λ_2 are real on the phase plane P1 and pure imaginary on the phase plane P2, besides, $\lambda_1 = -\lambda_2$ on both planes. In the case (b) with $\beta = 1$, taking into account the conditions (1.3.9), the characteristic roots λ_1 and λ_2 are complex with positive and negative real part on the planes P1 and P2, respectively, and $\lambda_1 = \lambda_2^*$. In the case (b) with $\beta = -1$, taking into account condition (1.3.9.2), all four roots are real and $\lambda_1 = -\lambda_2$ on both planes. Therefore, the singular points $w_1{=}0$ of three types exist in the phase space, namely: the "saddle–center" point, the "stable focus–unstable focus" point, and the "saddle–saddle" point in the cases mentioned above, respectively.

Considering by analogy the matrix of subsets corresponding to set (1.3.13.2) we obtain eigenvalues for the singular points w_j defined by (1.3.12) in three cases considered for the subsets corresponding to the projections to the phase spaces P1(w, x_1) and P2(x_2, x_3) [16]:

$$\lambda_{1,2}^{(\text{P1,P2})} = \pm(2\gamma)^{-1/2}\left[\binom{+}{-}C^2 \pm \sqrt{C^4\binom{-}{+}4\gamma p}\,\right]^{1/2}.$$

(1.3.15)

One can see from (1.3.15) that the character of the singular point depends on the nonlinearity exponent p defining the wave velocity $V = 6s(p+1)^{-1}u^p$. Nevertheless, conditions (1.3.9) remain valid in these cases as well.

Analysis of (1.3.15) enables to conclude the following. The eigenvalues λ_1 and λ_2 are complex (moreover $\lambda_1 = \lambda_2^*$) with the positive real parts on the plane P1 and the negative ones on the plane P2 in case (a) ($\beta = -1$) taking into account the condition (1.3.9.1). In case (b) with $\beta = -1$ λ_1 and λ_2 are real on the plane P1 and pure imaginary on the plane P2, and $\lambda_1 = -\lambda_2$ in the both cases. In the case (b) with $\beta = 1$

the situation is analogous to that of the case (b) with $\beta = -1$. Therefore, only singular points w_j of the type "stable focus–unstable focus" take place in the phase space in the
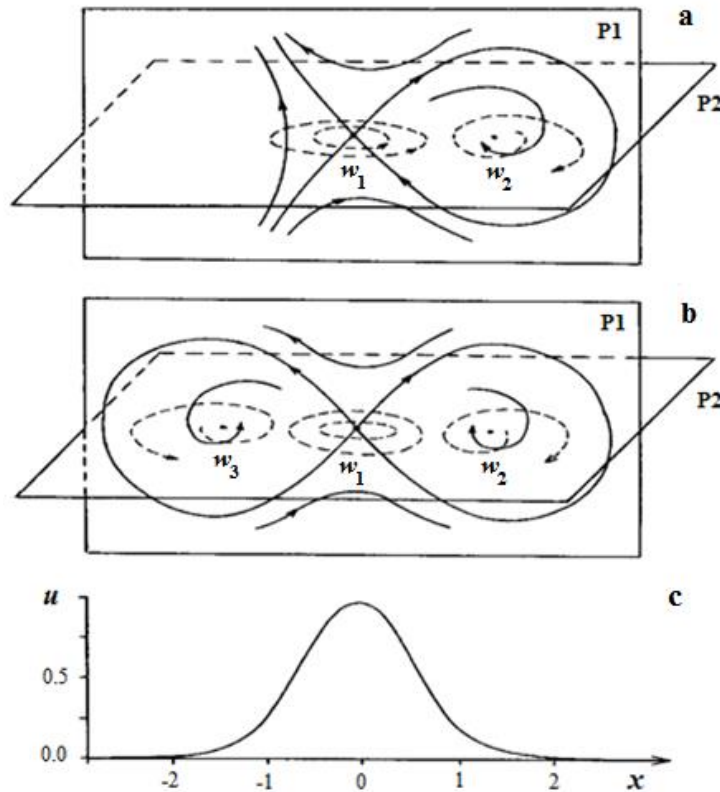

Figure 1.3.2. The phase portraits of the solutions of (1.3.10a) with $\beta=1$ for $p=1$ (a) and $p=2$ (b) (solid and broken lines correspond to the phase trajectories respectively in the planes P1 and P2) and numerical solution of eq.(1.3.5) with $\gamma=1$, $\beta=-1$ for $p=1$.

case (a), and of the type "saddle–center" take place in the case (b) for both signs of β.

To study the global phase portraits including singular trajectories corresponding to the stable solutions of eqs. (1.3.10), in [27],[16] the Bendixon and Dulac criterions have been used, and also the first and the second Lyapunov quantities have been calculated. Omitting here cumbersome mathematical calculations, we note that in all three cases considered the closed trajectories have place in the phase space. At this, formulae (1.3.14) and (1.3.15) enable us to obtain such parameters of the curves as their directions and, consequently, the angles with respect to the coordinate axes on both planes, and, therefore, to construct the global phase portraits.

The examples of such phase portraits for the cases (a) and (b) for $p=1$, 2 are shown in Fig. 1.3.2,a,b and Fig. 1.3.3,a,b.

Using the values of the characteristic roots λ_1 and λ_2 (1.3.14) for singular points $w_1=0$, taking into account the conditions (1.3.9) and (1.3.11) we obtain the asymptotics of the solutions of eq. (1.3.5) for considered cases [27], namely:
1) for the cases (a) and (b) with $\beta = -1$

$$w = A_1 \exp\left\{ (2\gamma)^{-1/2} \left[C^2 + \sqrt{C^4 \pm 4\gamma} \right]^{1/2} \xi \right\} \qquad (1.3.16.1)$$

(the upper/lower sign corresponds to the cases (a)/(b), respectively);
2) for the case (b) with $\beta = 1$

$$w = A_2 \exp\left[\left(2C^{-1}\gamma^{1/2}\right)^{-1}\left(2C^{-2}\gamma^{1/2}-1\right)^{1/2}\xi\right]\cos\left[\left(2C^{-1}\gamma^{1/2}\right)^{-1}\left(2C^{-2}\gamma^{1/2}+1\right)^{1/2}\xi+\Theta\right], \quad (1.3.16.2)$$

where A_1, A_2 and Θ are arbitrary constants. As we can see from (1.3.16), in the solutions of (1.3.5) in dependence of the signs of V and β the solitons with both monotonous and oscillating asymptotics can take place. At this, the phase portraits shown in Fig. 1.3.2,a,b correspond to the solitons with monotonous asymptotics, and the phase portraits shown in Fig. 1.3.3,a,b correspond to solitons with oscillating asymptotics. Figs. 1.3.2,c and 1.3.3,c show the results of numerical integration of eq. (1.3.5) for the initial condition $u = u_0 \exp(-x^2/l^2)$, that corresponds to the results of the asymptotic analysis.

1.3.3. Generalization of the results to the GKP-class equations

Making the inverse change of the variables, extend the obtained results to the 2D
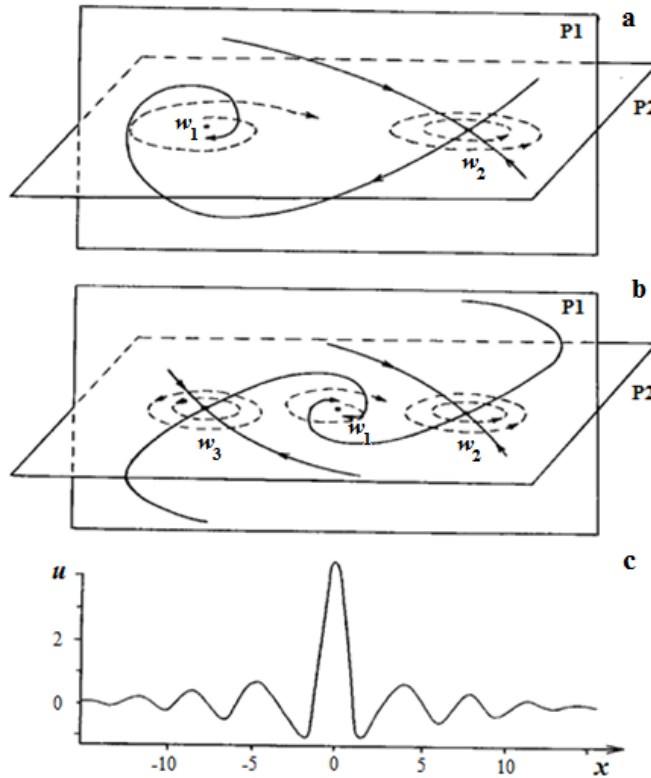
Figure 1.3.3. Phase portraits of the solutions of (1.3.10b) with
$\beta=1$ for the same values of parameters as in Fig. 1.3.2,a,b –
respectively the positions (a), (b), and numerical solution of
(1.3.5) with $\gamma=1$, $\beta=3.16$, $p=1$ (c).

solutions $u(\eta,\zeta,t)$ of the GKP equation (1.3.1) with $\Delta_\perp = \partial_\zeta^2$. The asymptotics of the solutions are defined by relations [15],[27]:

a) for the cases $V > 0$, $\beta = -1$ and $V < 0$, $\beta = -1$ (the upper and lower signs, respectively):

$$w = A_1 \exp\left\{(2\gamma)^{-1/2}\left[C^2 + \sqrt{C^4 \pm 4\gamma}\right]^{1/2}\chi\right\}, \quad (1.3.17)$$

b) for the case $V < 0$, $\beta = 1$:

$$w = A_2 \exp\left\{\left(2C^{-1}\gamma^{-1/2}\right)^{-1}\left(2C^{-2}\gamma^{1/2} - 1\right)^{1/2}\chi\right\} \times \cos\left\{\left(2C^{-1}\gamma^{-1/2}\right)^{-1}\left(2C^{-2}\gamma^{1/2} + 1\right)\chi + \Theta\right\} \quad (1.3.18)$$

Where A_1, A_2 and Θ are the arbitrary constants, $C = |V|^{-1/4}$, and $\chi = \left(\eta \pm \zeta + (\kappa - V)t\right)$ (here the signs "plus" and "minus" relate to the first and second equations of the set (1.3.2), respectively). As we can see from (1.3.17), (1.3.18)[2], solitons with monotonous as well as oscillating asymptotics can take a place depending on the signs of V and β as the solutions $u(\eta, \zeta, t)$ of eq. (1.3.1). (Note, that for $\beta = 0$ and any $\gamma > 0$ solutions of eqs. (1.3.2) have the form $w = (A_1 + A_2 C^{-1}\chi)\exp(\gamma^{-1/4}C^{-1}\chi)$ and, consequently, also describe a soliton with monotonous asymptotics [15],[27].) Fig. 1.3.4 shows the results of numerical integration of eq. (1.3.1) with the initial condition

$$u = u_0 \exp\left(-x^2/l_1^2 - y^2/l_2^2\right),$$
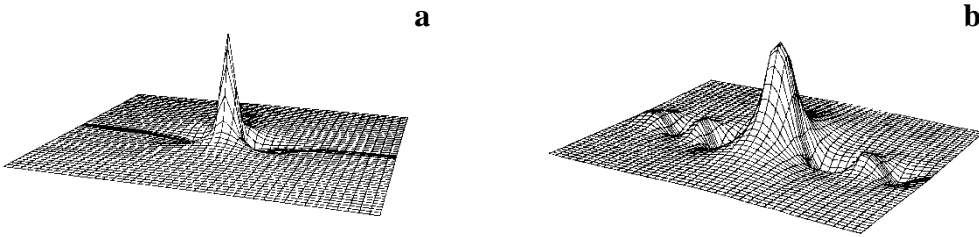
that confirms the results of our asymptotic analysis.

a   **b**

Figure 1.3.4. General view of a 2D soliton of eq. (1.3.1) with $\Delta_\perp = \partial_\zeta^2$ for $p = 1$:
(a) $\gamma = 1$, $\beta = -0.8$ ($t = 0.2$); (b) $\gamma = 1$, $\beta = 3.16$ ($t = 0.5$).

As to the proper transform of the phase portraits of the system and "bind" them for the 2D equation, owing to the phase space is 8-dimensional in this case, we can employ the results obtained in [16] coupling the characteristics of every singular point of each equation of the set (1.3.2) in the 8-dimensional phase space, at this the type of the singularities in the 4-dimensional subspaces (see [27]) under the inverse transform of the coordinates, $\eta = (\bar\eta + \bar\zeta)/2$ and $\zeta = (\bar\eta - \bar\zeta)/2$, is not changed, and only parameters of the phase portraits that correspond to solutions of the same class change (leading to the respective changes such parameters as the amplitude, the fronts steepness, frequency of the oscillations etc.).

1.3.4. Concluding remarks

To conclude, we note that for the BK equation we considered only the particular cases when it is possible to neglect the effects of dissipation and different types of instability here. For other cases when it is necessary to account dissipation and instabilities, more complex wave structures resulting from the simultaneous presence of all the effects discussed, for example, in [27] can be observed. Indeed, results obtained numerically in [14],[64],[38], demonstrate that in general BK model [27] with $\gamma = 0$ in the presence of the Gaussian random fluctuations of the wave field (for harmonic initial conditions and initial conditions in the form of a solitary pulse) stable wave structures of the soliton-like type can be formed too, with the time evolution. Furthermore, stable soliton structures can be formed also for $\gamma \neq 0$. An analytical study of such cases is

---

[2] Other correlations of signs of V and β are not realized (see [15],[27]).

highly complicated, however, although the approach considered above can be used for them as well. Note also that the results presented here for the GKP equation can be very useful when studying solutions and interpreting the multidimensional phase portraits of more complicated multidimensional model equations (see, for example, [15],[27],[38],[31],[32]).

1.4. Applications

We consider here some applications of the theory for real complex continuous media on the basis of the equations of the BK system.

In Sect. 1.4.1 the structure and dynamics of ion-acoustic waves in an unmagnetized plasma, including the case of weakly relativistic collisional plasma (when it is necessary to take into account the high energy particle flows which are observed in the magnetospheric plasma), are studied analytically and numerically on the basis of a model of the Kadomtsev-Petviashvili (KP) equation. We show that, if the velocity of plasma particles approaches the speed of light, the relativistic effects start to strongly influence on the wave characteristics, such as its phase velocity, amplitude, and characteristic wavelength, with the propagation of the two dimensional solitary ion-acoustic wave. These our results can be used in the study of nonlinear wave processes in the magnetosphere and in laser and astrophysical plasma.

In Sect. 1.4.2, on the basis of the model of the three-dimensional (3D) generalized Kadomtsev-Petviashvili (GKP) equation for the magnetic field $h = B_{\backsim}/B$ the formation, stability, and dynamics of 3D soliton-like structures, such as the beams of fast magnetosonic (FMS) waves generated in ionospheric and magnetospheric plasma at a low-frequency branch of oscillations when $\beta = 4\pi nT/B^2 << 1$ and $\beta > 1$, are studied. The study takes into account the highest dispersion correction determined by values of the plasma parameters and the angle $\theta = (\mathbf{k}^{\wedge}\mathbf{B})$ which plays a key role in the FMS beam propagation at those angles to the magnetic field that are close to $\pi/2$. The stability of multidimensional solutions is studied by an investigation of the Hamiltonian boundness under its deformations on the basis of solving of the corresponding variational problem. The evolution and dynamics of the 3D FMS wave beam are studied by the numerical integration of equations with the use of specially developed methods. The results can be interpreted in terms of the self-focusing phenomenon, as the formation of a stationary beam and the scattering and self-focusing of the solitary beam of FMS waves. These cases were studied with a detailed investigation of all evolutionary stages of the 3D FMS wave beams in the ionospheric and magnetospheric plasma.

The nonlinear dynamics of the 3D solitary Alfvén waves propagating nearly parallel to the external magnetic field in plasma of ionosphere and magnetosphere, which are described by the model of the 3-DNLS equation, is studied analytically and numerically in Sect. 1.4.3. Under the assumption of negligible dissipative effects the analytical estimates and the sufficient conditions for the stability of 3D solutions of the 3-DNLS equation are obtained, based on the transformational properties of the system's Hamiltonian for the whole range of the equation coefficients. On the basis of asymptotic analysis the solutions asymptotics are presented. To study the evolution of the 3D Alfven solitary waves including propagation of the Alfven waves' beams in a magnetized plasma the equation are integrated numerically using the simulation codes specially developed. The results show that the 3-DNLS equation in the non-dissipative case can have the stable 3D solutions in the form of the 3D Alfvén solitons, and also on a level with them the 3D solutions collapsing or dispersing with time. In terms of the self-focusing phenomenon the results obtained can be interpreted as the formation of the

stationary Alfvén wave beam propagating nearly parallel to the magnetic field, or Alfvén wave beam spreading, or the self-focusing of the Alfvén wave beam. The influence of the dissipation in the medium on structure and character of evolution of 3D Alfvén waves is studied.

The dynamics of the 2D solitary nonlinear internal gravity waves (IGW), as well as traveling ionospheric disturbances (TID) of the electron density excited by them at heights of the ionosphere *F*-region, for conditions close to those of the *F*-layer assuming that the source of initial perturbation has the pulse character is studied in Sect. 1.4.4 analytically and numerically. On a level with general case the rather interesting applications when the sharp gradients of the ionospheric parameters are the functions of space coordinates and time, namely the IGW and TID dynamics in the frontal regions of the solar terminator and solar eclipse are considered. The results obtained describe the dynamical structure, evolution and transformation of the IGW and TID at heights of the ionosphere *F*-layer including its strongly heterogeneous regions.

1.4.1. Nonlinear Ion-Acoustic Waves in a Plasma in View of Relativistic Effects

Despite the essential progress taking place in this field in recent years ([27],[75], [76], and numerous references in these works), the study of nonlinear wave processes in real media with dispersion still remains actual. In particular, this concerns the dynamics of fluctuations in cases in which high energy particle flows in the medium (magnetosphere, compact astrophysical systems, e.g., white dwarfs, laser plasma [51], [91]) take place, essentially changing such parameters of propagating wave structures as their phase velocity, amplitude, and characteristic length. A rather large number of works is devoted to investigations of such relativistic effects (e.g., [42], [50], [76], [83], [90], [92]); however, practically all of them consider only a one-dimensional (1D) approach. In particular, in [75], [76] and in earlier works by Washimi and Taniuti [100] and Das and Paul [45], the relativistic effects for the ionacoustic branch of oscillations were investigated in a 1D plasma. The studies by Nejon [81] and Taniuti and Wei [93] are perhaps exceptions: however, only some extreme cases were studied in these papers.

The purpose of our investigation is to study the relativistic effects in the dynamics of ion-acoustic multidimensional nonlinear wave structures in electron-ionic plasma, which is especially important in astrophysical applications and in magnetosphere physics. To solve this problem, in principle, we could start from the general set of hydrodynamic equations for the relativistic case (e.g., [48]); however, since we are interested in the effects which are displayed at relativistic velocities in comparison with the nonrelativistic case, it would be more logical to consider first the nonrelativistic approach and, further, introducing the relativistic factor (by analogy with [81]) to consider its influence on the time-space characteristics of multidimensional nonlinear ion-acoustic wave. We shall undertake this approach further.

In the absence of the magnetic field and for a negligible ion temperature, the equations of motion and continuity for ions take the form [15]

$$\frac{\partial v}{\partial t} + (v\nabla)v = -\frac{e}{M}\nabla\varphi, \quad \frac{\partial n_i}{\partial t} + div(n_i v) = 0, \tag{1.4.1}$$

where M is the mass of an ion and φ is the electric potential. Comparison with the equations in generalized variables for an ideal gas in neglect a dissipation

$$\frac{\partial v}{\partial t} + (v\nabla)v + \frac{c^2}{\rho}\nabla\rho = 0, \quad \frac{\partial \rho}{\partial t} + \nabla(\rho v) = 0,$$

where ρ and $c = c(\rho)$ have the sense of a generalized "density" and velocity of "sound," respectively, at density ρ in neglect a dispersion [60], shows that in this case the ion density n_i and ion-acoustic velocity $c_s = (T_e/M)^{1/2}$ play the role of ρ and c; the dispersion "length" is defined by $\delta^2 = D^2/2 = T_e/8\pi e^2 n_0$, where n_0 is the unperturbed electron density. The electrons in the ion-acoustic wave are Boltzmann distributed

$$n_e = n_0 \exp(e\varphi/T_e). \tag{1.4.2}$$

The ion and electron densities are related to the electric potential φ via Poisson's equation

$$\Delta\varphi = 4\pi e(n_e - n_i). \tag{1.4.3}$$

The dispersion equation for the set (1.4.1)–(1.4.3) is written as [44]

$$\omega^2 = c_s^2 k^2/(1 + D^2 k^2). \tag{1.4.4}$$

Following further to the techniques developed in [27] and proceeding from the presented reasons, let us consider the basic equation describing the dynamics of the ion-acoustic waves in an unmagnetized collisional plasma and discuss its possible solutions; after that, introducing the relativistic factor, let us consider the effects related to particles moving with the velocities, which are rather close to the speed of light.

Let us consider the wave packet propagating in the direction close to the x axis. We assume that the wave numbers of its harmonics are small satisfying the inequalities

$$kD \ll 1, \quad k_x^2 \gg k_\perp^2, \quad v' \ll c_s, \tag{1.4.5}$$

where v' is the x component of ion velocity. It is well known that the weakly dispersive (see the first inequality of (1.4.5)) ion-acoustic wave steepens in the direction of its propagation; therefore, at some time moment, the second inequality of (1.4.5) "switches on." Conditions (1.4.5) enable us to reduce the dispersion relation (1.4.4) to the form

$$\omega \approx c_s k_x (1 + k_\perp^2/2k_x^2 - \delta^2 k_x^2);$$

therefore, limiting ourselves in the nonlinear expansion by the terms quadratic in the wave amplitude and considering the solution in the form of a propagating wave $u = u(t, x - c_s t, r_\perp)$, and applying the procedure described in [27], we obtain the nonlinear equation

$$\frac{\partial}{\partial x}\left(\frac{\partial v}{\partial t} + c_s \frac{\partial v}{\partial x} - c_s \delta^2 \frac{\partial^3 v}{\partial x^3} + v v_x\right) = \pm \frac{c_s}{2} \Delta_\perp v, \tag{1.4.6}$$

which, after homothetic transformation and in the reference frame moving along the x axis with the velocity c_s coincides with the Kadomtsev-Petviashvili (KP) equation in its standard form [17]:

$$\partial_t u + \alpha u \partial_x u + \beta \partial_x^3 u = \kappa \int_{-\infty}^x \Delta_\perp u \, dx, \quad \Delta_\perp = \partial_y^2 + \partial_z^2, \tag{1.4.7}$$

where $\kappa = 1$ is related to the positive dispersion, $\kappa = -1$ corresponds to the negative dispersion, respectively, and the factors at the equation terms for the case of ion sound are [60]

$$\alpha = \frac{3}{2} c_s/n_i, \quad \kappa = c_s/2, \quad \beta = c_s D^2/2, _s = \sqrt{T_e/M}, \quad D^2 = T/4\pi n_0 e^2.$$

Generally speaking, the sign in the right-hand side of (1.4.6) for the ion-acoustic wave is positive, such that the dispersion is negative, $\kappa = -1$ in (1.4.7). However, there are cases for other modes when the dispersion is positive, i.e., there is a "minus" sign in the right-hand side of (1.4.6). The term $c_s \partial_x v$ describes the wave propagation along the x

axis with the "sound" velocity, and other terms responsible for dispersion, nonlinearity, and diffraction describe slow changes of the acoustic field on the background of the wave motion with the velocity c_s. Such acoustic waves are mainly characteristic for isotropic media (e.g., an unmagnetized plasma), but sometimes it can be observed in anisotropic media as well. Thus, if the characteristic frequency of the ion-acoustic wave packet significantly exceeds the ion-cyclotron frequency in a magnetized plasma, ω_{Hi}, the plasma anisotropy can be neglected and therefore (1.4.6) can be reduced to the KP equation (1.4.7) [44]. In the opposite case, when $\omega \ll \omega_{Hi}$, the anisotropy cannot be neglected. In this case the additional term $\omega_{Hi}[i, v]$ (i is the dimensionless vector of the x axis) appears in the right-hand side of the equation of motion (1.4.1), and the sign of the second term in the dispersion equation changes to minus. In this case we also have the equation of the KP class but with the right-hand side of the form $\mu \Delta_\perp \partial_x u$ [102]. The upper sign in this equality, as in eq. (1.4.6), corresponds to the case of negative dispersion, and the lower sign corresponds to the positive one.
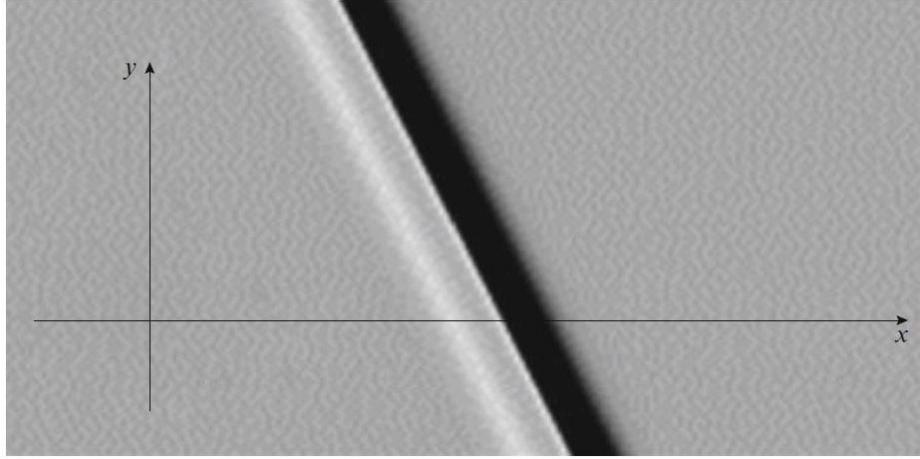

Figure 1.4.1. General view of 2D solution of the KP equation (1.4.7) at $\alpha = 6$, $\beta = 1$.

In [17], the isotropic case of (1.4.7) for the ion-acoustic waves in an unmagnetized plasma was considered. Further, the results were generalized for a wider spectrum of nonlinear systems in [27]. Using the approaches proposed in these works, a numerical simulation based on specially developed high-accuracy methods [12], [27] was conducted for the initial condition in the form of a solitary pulse of form $u(0, x, y) = u_0 \exp[-(x/l_x + y/l_y)^2/L^2]$ with periodic boundary conditions. The figure shows an example of the numerical results obtained for the two-dimensional (2D) $(\Delta_\perp = \partial_y^2)$ eq. (1.4.7).

We can see that, as a result of the evolution of the 2D acoustic perturbation $u(0, x, y)$ in an isotropic plasma, a 1D soliton of the KP equation is formed. The form of the soliton corresponds to that obtained analytically for the negative dispersion in [59] by the Krylov-Bogolyubov method and in [104] by the inverse scattering transform (IST) method. It was shown in our numerical simulation that the soliton velocity and the first three integrals of the 2D KP equation for sufficiently large t are conserved within the limits of the accuracy of the numerical simulation:

$$\partial_t J_1 = \partial_t \iint u\, dx\, dy = 0 + O(\tau^2, h_{x,y}^4), \quad \partial_t J_2 = \partial_t \iint u^2 dx\, dy = 0 + O(\tau^2, h_{x,y}^4),$$

$$\partial_t J_3 = \partial_t \iint \left[\frac{1}{2}(\partial_x u)^2 - \frac{1}{2}\kappa \left(\int_{-\infty}^x \partial_y u\, dx \right)^2 - u^3 \right] dx\, dy = 0 + O(\tau^2, h_{x,y}^4),$$

where τ and $h_{x,y}$ are the steps on the time and space grids, respectively (the last two integrals have a sense of momentum and energy of medium described by the KP equation). This confirms our earlier results [15] and the existence of a 2D ion-acoustic soliton in such a physical system. Let us now consider the problem of the influence of relativistic effects on the evolution of the ion-acoustic wave.

As we already demonstrated, the ion-acoustic waves in a plasma can be described by the KP equation (1.4.7). However, if the velocity of plasma particles approaches the speed of light, the relativistic effects start to influence strongly the wave characteristics (such as its phase velocity, amplitude, and the characteristic wavelength) in the propagation of the 2D solitary ion-acoustic wave.

For the 2D ion-acoustic solitary waves in a weakly relativistic collisional plasma, the KP equation in form (1.4.7) can be obtained when the relativistic factor u/c is taken into account [81] by the reduced perturbation method [93]. We can rewrite it in the following form:

$$\frac{\partial \Phi_1}{\partial \tau} + \alpha(\theta_1)\Phi_1 \frac{\partial \Phi_1}{\partial \xi} + \frac{1}{2}\beta(\theta_1)\frac{\partial^3 \Phi_1}{\partial \xi^3} = -\frac{1}{2}\int_{-\infty}^{\xi} \frac{\partial^2 \Phi_1}{\partial \eta^2} d\xi, \qquad (1.4.8)$$

where $\Phi_1 = \theta_1^{1/2} u_1$ is a small perturbation of the electrostatic potential $\Phi = \varepsilon\Phi_1 + \varepsilon^2\Phi_2 + \cdots$, ε is the small expansion parameter; and u_1 is the perturbation of the plasma particle velocity $(u = u_0 + \varepsilon u_1 + \varepsilon^2 u_2 + \cdots)$,

$$\alpha(\theta_1) = \beta(\theta_1)\left(1 - \frac{\theta_2}{\theta_1^{3/2}}\right), \qquad \beta(\theta_1) = \theta_1^{-1/2},$$

$$\theta_1 = 1 + \frac{3}{2}\left(\frac{u_0}{c}\right)^2, \quad \theta_2 = \frac{3}{2}\frac{u_0}{2c^2}. \tag{1.4.9}$$

Equation (1.4.8) is written in the reference frame moving along the x-axis: $\xi = \varepsilon^{1/2}(x - \lambda t)$, $\eta = \varepsilon y$, $\tau = \varepsilon^{3/2} t$, where λ is the phase velocity. Note that the coefficient at nonlinear term $\alpha > 0$, since $\theta_1 \gg \theta_2$. In this case we can obtain the stationary solution as propagating in the system solitary wave. Introducing the new variable $\zeta = k_x \xi + k_y \eta - \omega\tau$ and substituting it into (1.4.8), let us write the solution in the form of a 2D wave

$$\Phi_1 = \Phi_0 \operatorname{sech}^2\left\{ \frac{1}{W}\left(\xi + \frac{k_y}{k_x}\eta - \frac{\omega}{k_x}\tau \right) \right\}, \qquad (1.4.10)$$

where the amplitude Φ_0 and the characteristic size W are defined by the expressions

$$\Phi_0 = \frac{3\delta}{\alpha(\theta_1)}, \qquad W = \left[\frac{2\beta(\theta_1)}{\delta} \right]^{1/2}, \qquad (1.4.11)$$

and $\delta = \omega/k_x - \frac{1}{2}(k_y/k_x)^2$, and the boundary conditions are $\Phi_1 \to 0$, $\partial_\zeta^n \Phi_1 \to 0$ for $n = 1,2$ and $|\zeta| \to \infty$. The dispersion law for these waves is given by

$$\omega = k_x[2\beta(\theta_1)k_x^2 + k_y^2/2k_x^2].$$

We see from (1.4.9) that the factors at the nonlinear term, as well at the dispersion term, are defined by the relativistic factor θ_1; eq. (1.4.11) shows the dependence of the amplitude and the characteristic length of the 2D ion-acoustic soliton of the KP equation on the weakly relativistic effects. Comparison of the results following from (1.4.9)-(1.4.11) with those for the three extreme cases considered by Kadomtsev and

Table 1.1. Comparison of the obtained results with the results for three extreme cases

Parameter	Obtained results	Results of Kadomtsev and Petviashvili [59], Nejon [81], Washimi and Taniuti [100]; and Das and Paul [45].		
		$u_0/c = 0$, $\eta \neq 0$	$u_0/c = 0$, $\eta = 0$	$u_0/c \neq 0$, $\eta = 0$
λ	$u_0 + \vartheta_1^{-1/2}$	1	1	$u_0 + \vartheta_1^{-1/2}$
α	$\vartheta_1^{-1/2}(1 - \vartheta_2/\vartheta_1^{3/2})$	1	1	$\vartheta_1^{-1/2}(1 - \vartheta_2/\vartheta_1^{3/2})$
β	$\vartheta_1^{-1/2}$	1	1	$\vartheta_1^{-1/2}$
Φ_0	$3\delta\vartheta_1^{1/2}(1 - \vartheta_2/\vartheta_1^{3/2})$	3δ	$3s$	$3s\vartheta_1^{1/2}(1 - \vartheta_2/\vartheta_1^{3/2})$
W	$\vartheta_1^{-1/4}(2/\delta)^{1/2}$	$(2/\delta)^{1/2}$	$(2/s)^{1/2}$	$\vartheta_1^{-1/4}(2/s)^{1/2}$

Petviashvili [59], Nejon [81], Washimi and Taniuti [100], and Das and Paul [45] is given in the table. Here

$$s = (\omega/k) \cong v_0 + \theta_1^{-1/2}\left(1 - \frac{1}{2}k^2\right),$$

where v_0 is the velocity of the ion flow (if $v_0 \sim 0$ and the relativistic effects are ignored, we have $s \cong 1 - \frac{1}{2}k^2$). One can see that the obtained results include all three extreme cases too, but they are essentially more general, because they describe the influence of the relativistic effects on such parameters as the amplitude, characteristic size, and the phase velocity of the 2D solitary wave, which, in its turn, are defined by the dependencies of the factors at the nonlinear term, as well at the dispersion term of the KP equation: $\alpha(\theta_1)$ and $\beta(\theta_1)$, respectively, on the particles' velocity u.

One can also see that the dependencies of the amplitude and characteristic size of the wave on relativistic factor essentially differ for the 2D and 1D cases (compare the second and the last column in the table): in the expressions for Φ_0 and W, we have the parameters δ and s, respectively.

Thus, in this paper on the basis of a model of the KP equation, the structure and dynamics of ionacoustic waves in an unmagnetized plasma, including the case of collisional weakly relativistic plasma, when the high energy particle flows should be taken into account, were studied analytically and numerically. In particular, when the kinetic energy of ions $Mu_0^2/2$ at $u_0/c \cong 0.1$ reaches values $\cong 4.7$ MeV, the 2D weakly relativistic ion-acoustic solitary waves will describe the motion of high energy protons with a velocity that is significant in comparison with the speed of light, that is observed in the magnetospheric plasma (trapping region, outer radiation belt, plasma sheet) [99]. We showed that, if the velocity of plasma particles approaches the tenth shares of the speed of light (for example, in the region of the maximum of the outer radiation belt on

L-shell $L = 3.1$ [69], the relativistic effects start to influence strongly the wave characteristics, such as its phase velocity, amplitude, and the characteristic wavelength, at propagation of the 2D solitary ion-acoustic wave. Let us also note that, besides the physics of nonlinear processes in the magnetosphere, the study of the relativistic nonlinear waves has also applications in such physical systems as laser plasma [91] and astrophysics [42], [9], [51], [90].

1.4.2. Nonlinear 3D Beams of FMS Waves Propagating in the Ionosphere and Magnetosphere

The objective of this Section is to study the formation, structure, stability, and dynamics of multidimensional (two-dimensional (2D) and three-dimensional (3D)) soliton-like structures generated at a low-frequency branch of oscillations in the ionospheric and magnetospheric plasma when $\beta = 4\pi nT/B^2 \ll 1$ and $\beta > 1$. These processes are described by the following equation [29]:

$$\partial_t u + A(t,u)u = f, \quad f = \kappa \int_{-\infty}^{x} \Delta_\perp u\, dx, \quad \Delta_\perp = \partial_y^2 + \partial_z^2, \tag{1.4.12}$$

which corresponds to the dispersion law in the limiting case of long waves [60]:

$$\omega_{1,2} = \frac{v_A k}{2\sqrt{1 + k^2 c^2/\omega_{pe}^2}} \left\{ \left[(1 + \cos\theta)^2 + \frac{k^2 c^2}{\omega_{pi}^2} \frac{\cos^2\theta}{1 + k^2 c^2/\omega_{pe}^2} \right]^{1/2} \right.$$

$$\left. \pm \left[(1 - \cos\theta)^2 + \frac{k^2 c^2}{\omega_{pi}^2} \frac{\cos^2\theta}{1 + k^2 c^2/\omega_{pe}^2} \right]^{1/2} \right\}$$

($\omega_{pe} = (4\pi n_e e^2/m)^{1/2}$ and $\omega_{pi} = (4\pi n_i e^2/M)^{1/2}$ are the electronic and ionic plasma frequencies, respectively, $v_A = B^2/4\pi n_i M$ is the Alfvén velocity, M is the ionic mass, θ is the angle between the direction of wave vector and magnetic field **B**) and, depending on differential operator A describes waves propagating longitudinally and transversely relative to the external magnetic field. The case in which the lower sign (Alfven mode) is implemented in the dispersion relation was studied in detail in [31], here we are interested in the case with a plus sign, when the operator A has the form

$$A(t,u) = \alpha u \partial_x - \partial_x^2 (\nu - \gamma_1 \partial_x - \gamma_2 \partial_x^3), \tag{1.4.13}$$

and eq. (1.4.12) represents the generalized Kadomtsev-Petviashvili (KP) equation (Belashov-Karpman (BK) equation [62], [27]), and in case when $\beta = 4\pi nT/B^2 \ll 1$ at $\omega < \omega_{Bi} = eB/Mc$ (where ω_{Bi} is an ion-cyclotron frequency);, $|\mathbf{k}|r_D \ll 1$, describes the propagation of fast magnetosonic (FMS) waves in a magnetized plasma at $k_x^2 \gg \mathbf{k}_\perp^2$, $v_x \ll v_A$, near the cone of angles relative to the magnetic field **B** (which is assumed to be homogeneous) $\theta = \arctan(M/m)^{1/2}$ [13]. In this case, function u has the meaning of a dimensionless amplitude of the magnetic field of the wave, $h = B_\sim/B$ while the coefficients of terms describing nonlinear, dissipative, and dispersive effects are determined by the plasma parameters and the angle $\theta = (\mathbf{B}, \mathbf{k})$.

Equations (1.4.12) and (1.4.13) can not be analytically integrated. Therefore, in order to study the stability of multidimensional solutions, we will use the approach developed in [11] and investigate the Hamiltonian boundness for eqs. (1.4.12) and (1.4.13) upon its deformations, which conserve the system momentum, by solving the corresponding variational problem. We will also carry out an asymptotic analysis of

multidimensional solutions in an analytical investigation of this system. The equations were integrated numerically with specially developed methods and codes described in detail in [27] in order to study the evolution of 3D solutions, including the propagation of a 3D beam of FMS waves in the magnetized plasma. These problems will be considered below for the set of eqs. (1.4.12) and (1.4.13).

The problem of the stability of solitary wave solutions for KP and BK models remains highly relevant and is widely discussed in many literature sources related to the soliton theory (for example, [27], [73], [84], [49]). As for the BK dissipation-free equation, it has already been solved analytically [11]; herein, in the investigation of the stability of (1.4.12) and (1.4.13) solutions with $v = 0$, we will follow the method developed in the above-mentioned paper in the context of the problem under discussion. Let us make a transformation of coordinates and rewrite eqs. (1.4.12) and (1.4.13) with $v = 0$ in a Hamiltonian form:

$$\partial_t u = \partial_x (\delta H / \delta u), \tag{1.4.14}$$

where

$$H = \int \left[-\frac{\varepsilon}{2}(\partial_x u)^2 + \frac{\lambda}{2}(\partial_x^2 u)^2 + \frac{1}{2}(\nabla_\perp \partial_x v)^2 - u^3 \right] dr, \tag{1.4.15}$$

$\partial_x^2 v = u$, $\varepsilon = \gamma_1 |\gamma_2|^{-1/2}$, and $\lambda = \text{sgn}\gamma_2$. Stationary solutions of eq. (1.4.14) are obtained from the variational problem $\delta(H + vP_x) = 0$ ($P_x = \frac{1}{2}\int u^2 dr$ is a projection of system momentum on the x-axis, v has the meaning of a Lagrange factor), illustrating the fact that all finite solutions of eq. (1.4.14) are stationary points of Hamiltonian (1.4.15) under a fixed P_x. In accordance with Lyapunov's theorem, the stationary points of a dynamic system which realized the Hamiltonian maximum or minimum are absolutely stable; if the extremum is local, then locally stable solutions are possible. Unstable states correspond to the Hamiltonian monotonic dependence on its variables, i.e., the case in which the stationary point is a saddle one. Hence, it is necessary to prove the Hamiltonian boundness (from below) at a fixed P_x. Let us consider scale transformations in a real vector space R [29] $u(x, r_\perp) \to \zeta^{-1/2}\eta^{(1-d)/2}u(x/\zeta, r_\perp/\eta)$ (where d is a problem dimension, and ζ, $\eta \in R$) that conserve the momentum projection P_x. Hamiltonian (as a function of ζ, η parameters) will take the form

$$H(\zeta, \eta) = a\zeta^{-2} + b\zeta^2\eta^{-2} - c\zeta^{-1/2}\eta^{(1-d)/2} + e\zeta^{-4}, \tag{1.4.16}$$

where $a = -(\varepsilon/2)\int(\partial_x u)^2 dr$, $b = (1/2)\int(\nabla_\perp \partial_x v)^2 dr$, $c = \int u^3 dr$, and $e = (\lambda/2)\int(\partial_x^2 u)^2 dr$. The necessary conditions of extremum existence are defined by the following set of equations: $\partial_\zeta H = 0$, $\partial_\eta H = 0$, while sufficient conditions for the Hamiltonian minimum are provided by a set of inequalities

$$\begin{vmatrix} \partial_\zeta^2 H(\zeta_i, \eta_j) & \partial_{\zeta\eta}^2 H(\zeta_i, \eta_j) \\ \partial_{\eta\zeta}^2 H(\zeta_i, \eta_j) & \partial_\eta^2 H(\zeta_i, \eta_j) \end{vmatrix} > 0, \quad \partial_\zeta^2 H(\zeta_i, \eta_j) > 0.$$

The joint solution of these equations and inequalities yields the following results (Fig. 1.4.2). In the 3D case (d=3 in the equations), 3D solutions are absolutely stable at $\lambda = 1$, $\varepsilon > 0$. For $\lambda = 1$, $\varepsilon \leq 0$ the locally stable solutions can be observed, when the condition $ab^2e/c^4 < 9/512$ is satisfied for the integral Hamiltonian coefficients (1.4.16). Hence, we easily proved the possible existence of absolutely and locally stable solutions in the

BK model and found the stability conditions for the 3D soliton solutions. It should be noted that the BK equation takes into account the dispersion correction of the next order, in contrast to the usual KP equation, and has stable 3D solutions, in contrast to the KP model [71]. The used approach, when applied to the problem of FMS wave beam propagation in the magnetized plasma (see the following Section), makes it possible to prove, for instance, that a 3D beam propagating at an angle of θ to the magnetic field is not focused; it becomes stationary and stable in the cone of angles $\theta < \arctan(M/m)^{1/2}$ when the following condition is valid [30]:

$$(m/M - \cot^2\theta)^2[\cot^4\theta(1+\cot^2\theta)]^{-1} > 4/3.$$

As follows from the asymptotic analysis of possible solutions of eqs. (1.4.12) and (1.4.13), the asymptotics of solutions at $\gamma_2 > 0$ and $\gamma_1 = \pm 1$ in terms of $w = u(x, |\mathbf{r}_\perp|, t)/V$ are defined as follows:

(a) when the velocity of wave propagation along the x-axis is $V > 0$ and $\gamma_1 = -1$ and when $V < 0$, $\gamma_1 = -1$ (upper and lower signs, respectively):

$$w = A_l \exp\{(2\gamma_2)^{-1/2}[C^2 + \sqrt{C^4 \pm 4\gamma_2}]^{1/2}\chi\}; \tag{1.4.17}$$

(b) when $V < 0$, $\gamma_1 = 1$:

$$w = A_2 \exp\{(2C^{-1}\gamma_2^{-1/2})^{-1}(2C^{-2}\gamma_2^{1/2}-1)^{1/2}\chi\}$$
$$\times \cos\{(2C^{-1}\gamma_2^{-1/2})^{-1}(2C^{-2}\gamma_2^{1/2}+1)\chi + \Theta\}. \tag{1.4.18}$$

where A_1, A_2 and Θ are arbitrary constants, and $C = |V|^{-1/4}$ and $\chi = x + |\mathbf{r}_\perp| + (\kappa - V)t$.

As follows from eqs. (1.4.17) and (1.4.18), eqs. (1.4.12) and (1.4.13) with $\nu = 0$, depending on the V and γ_1 signs, can have soliton solutions $u(x, |\mathbf{r}_\perp|, t)$ with both monotonous and oscillating asymptotics. It should also be noted that the solutions at $\gamma_1 = 0$ and $\gamma_2 > 0$ have the form of $w = (A_1 + A_2\chi/C)\exp(\chi/\gamma_2^{1/4}C)$ and consequently also represent solitons with monotonous asymptotics [62].

It should be recalled that FMS waves can propagate in magnetized plasma at $\beta = 4\pi nT/B^2 \ll 1$ in the frequency region of $\omega < \omega_{Bi} = eB/Mc$, while in equations (1.4.12)-(1.4.16), from the physical point of view, function u is a dimensionless amplitude of magnetic field of the wave: $h = B_\sim/B$. The dispersion law at $|\mathbf{k}|r_D \ll 1$, $k_x^2 \gg k_\perp^2$, and $v_x \ll v_A$ will have the following form:

$$\omega \approx v_A k_x (1 + k_\perp^2/k_x^2 + \chi(\theta)D^2 k_x^2), \tag{1.4.19}$$

where $\mathbf{k}_\perp$ is a transversal (relative to the wave propagation direction) component of the wave vector, v_x is an x-component of ionic velocity, D is a dispersion length, and θ is the angle between wave vector component k_x, and the external magnetic field $\mathbf{B}$. It should be also recalled that the term "low dispersion" means that the primary nonlinear process is a threewave interaction of low-amplitude waves; the low nonlinearity condition is based on the small angle between the interacting waves. At a relatively high ionic temperature, $\beta > m/M$, the dispersion length in (1.4.19) is defined by the following equation [13]:

$$\chi(\theta)D^2 = \frac{c^2}{2\omega_{pi}^2}\cot^2\theta - \frac{1}{2}\rho_i^2\left(3 - \frac{11}{4}\sin^2\theta\right) \tag{1.4.20}$$

where $\rho_i = v_{Ti}/\omega_{Bi}$ is an ionic Larmor radius. Under this process the plasma is quasineutral, because $\omega = \omega_{pi} = (4\pi n_i e^2/M)^{1/2}$. According to (1.4.20), the dispersion is positive (phase velocity grows with growth in $|\mathbf{k}|$), except for angle regions near $\theta = 0$ and $\theta = \pi/2$. With propagation that is almost transversal relative to the magnetic field $\mathbf{B}$, when $|\pi/2 - \theta| \le (\beta/4)^{1/2}$ the dispersion is negative and is defined by effects related to
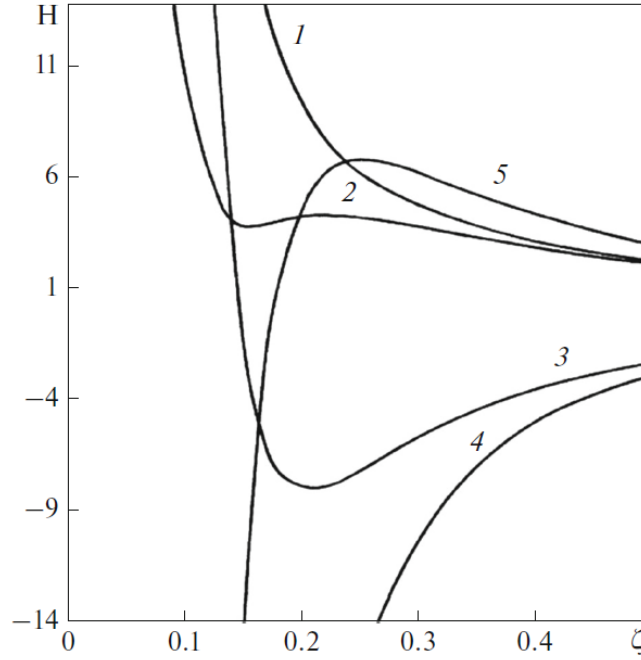

Figure 1.4.2. Changing of $H(\zeta, \eta)$ at $d = 3$ for different values of integral coefficients along the lines of $\eta = (2b/c)\xi^{5/2}$ at: (*1*) $a = 1.0$, $b = 1.0$, $c = 1.0$, $e = 0.025$; (*2*) $a = 1.0$, $b = 1.0$, $c = 1.0$, $e = 0.017$; (*3*) $a = -0.5$, $b = 1.0$, $c = 0.5$, $e = 0.02$; (*4*) $a = -0.5$, $b = 1.0$, $c = 0.5$, $e = -0.02$; (*5*) $a = 1.0$, $b = 1.0$, $c = 0.5$, $e = -0.02$.

the finiteness ρ_i. It is known that propagation of the low amplitude FMS wave with a narrow angle distribution can be described by the KP equation ((1.4.12), (1.4.13) at $\nu = \gamma_2 = 0$) [74]. For such angles, when dispersion is positive for low $|\mathbf{k}|$ (at a relatively high ionic temperature), the 3D FMS wave packet in the plasma with $\beta > m/M$ does not form stable stationary solutions and spreads for the angles $|\pi/2 - \theta| < (m/M)^{1/2}$ or collapses outside of this cone [71]. (It should be noted that a similar phenomenon is occasionally termed as wave "self-compression" [97]). The last case, when a relatively intensive FMS wave beam is limited in the $\mathbf{k}_\perp$-direction, can be characterized by the self-focusing phenomenon [30]. This problem was solved for the first time in [74] via the averaging of initial equations and subsequent numerical solution. Yet, relation (1.4.20) will not be valid for the angles $\theta < (kc/\omega_{pi})^{1/2}$, which are characterized by intensive reconstruction of the oscillation dispersion mechanism. At $\beta < m/M$ the dispersion can be defined for any angle θ based from the hydrodynamic equations, and the FMS wave structure will depend in this case on sign of the dispersion coefficient

$$\gamma_1 = -v_A \, \chi(\theta) D^2 = v_A \frac{c^2}{2\omega_{pi}^2} \left(\frac{m}{M} - \cot^2 \theta \right),$$

which is defined by angle θ; in particular: the dispersion is negative for propagation that is almost transversal if $|\pi/2 - \theta| \leq (m/M)^{1/2}$, and it is positive for all other angles. The KP equation can also be used in this case; and for a relatively intensive FMS wave beam, which is limited in the $\mathbf{k}_\perp$-direction, we can expect self-focusing of a beam propagating at such angles θ to the magnetic field, where the dispersion is positive [105].
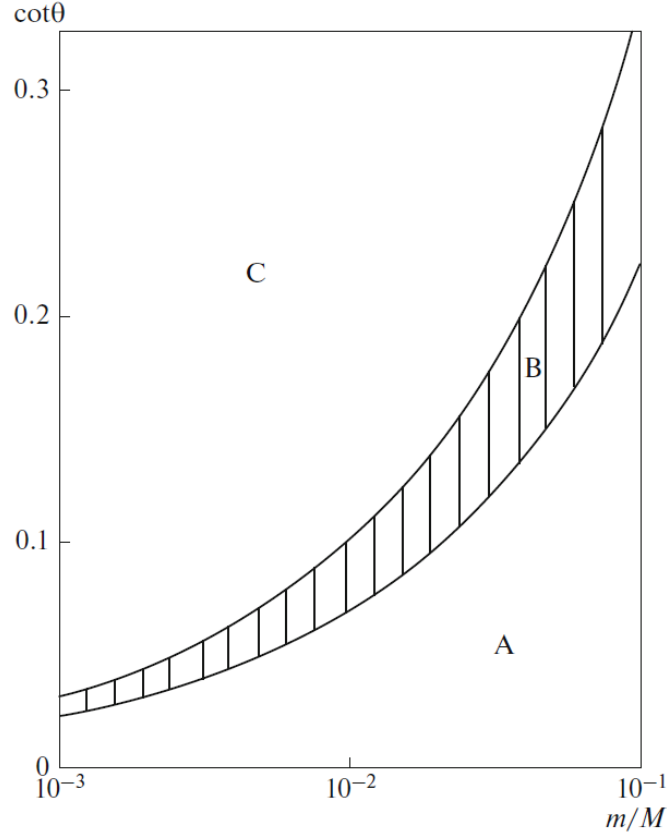

Figure 1.4.3. Dispersion behavior for FMS waves with respect to the angle θ and ratio m/M.

In both cases, $\beta > m/M$ and $\beta < m/M$, it is necessary to take into account the fact that $\gamma_1 \to 0$ near the cone of angles, where dispersion changes the sign. Obviously, this does not mean that the dispersion disappears in this region. It just means that the description based on the KP equation model in its standard form is not correct in this case. Near the $|\pi/2 - \theta| \leq (\beta/4)^{1/2}$, where $\gamma_1 \to 0$ at $\beta > m/M$, the results of [74] should be clarified and even reconsidered. For example, relation (1.4.19) should be supplemented by a dispersion term of the next order, which will play a major role in this case [27]. An analogous situation is possible at $\beta < m/M$ near the cone of angles $\theta = \arctan(M/m)^{1/2}$. In both cases, the dispersion relation takes the form of $\omega \approx v_A k_x \times [1 + k_\perp^2/2k_x^2 + c_0^{-1}(-\gamma_1 k_x^2 + \gamma_2 k_x^4)]$. The dispersion correction of the next order can be obtained by decomposition of the full dispersion equation into the Taylor's series by k [27]. In the case of $\beta < m/M$, which is considered in detail below, we obtain

$$\gamma_2 = v_A \frac{c^4}{8\omega_{pi}^4}[3(\frac{m}{M} - \cot^2\theta)^2 - 4\cot^4\theta(1+\cot^2\theta)].$$

Hence, the dispersion character becomes much more complicated and is now defined by correlation of signs of coefficients γ_1 and γ_2 (Fig. 1.4.3). At $\gamma_1 > 0$, $\gamma_2 < 0$, we observe negative dispersion (region B in Fig. 1.4.3), while the dispersion is "mixed" at $\gamma_{1,2} > 0$ (region A) and $\gamma_{1,2} < 0$ (region C) (the dispersion sign is different for low and high k). In this case, low-amplitude FMS waves with a narrow angle distribution will be described by the BK equation [62]; in the non-dissipative case, it will have the form [29]

$$\partial_x(\partial_t h + \alpha h\partial_x h + \gamma_1\partial_x^3 h + \gamma_2\partial_x^5 h) = -(v_A/2)\Delta_\perp h, \qquad (1.4.21)$$

where $\alpha = (3/2)v_A \sin\theta$. In this case, a nonlinear term $\alpha h\partial_x h$, which is the result of sound velocity renormalization, reflects a low probability of other nonlinear processes caused by vector nonlinearity. In contrast to the KP equations, the solutions of equation (1.4.21) are characterized by a more complicated structure and dynamics, which is related to the ratio of values and signs of the dispersion coefficients γ_1 and γ_2. Hence, it is found in the case of $\beta < m/M$, in contrast to the case, of $\beta > m/M$ (which was considered in [74]), that the 3D beam of FMS waves, which propagates in the plasma at angle θ to the external magnetic field, is not self-focused and becomes stationary and stable in the cone of angles $\theta < \arctan(M/m)^{1/2}$ when the following conditions are satisfied:

$$\left(\frac{m}{M} - \cot^2\theta\right)^2 [\cot^4\theta(1+\cot^2\theta)]^{-1} > 4/3,$$

or, in other words, when $\gamma_{1,2} > 0$ in (1.4.21). This conclusion is confirmed by our analytical (see the previous Section) and numerical [62]) results for 3D solitary wave structures propagating in low dispersive media, where the presence of the highest dispersion correction in BK (as opposed to KP) stops the wave collapse at the initial stage of development of self-focusing instability. This result is of key importance, because, prior to the works of [62], [11]), neither analytical nor numerical studies identified 3D stable wave structures such as 3D solitons. It is the accounting for higher-order dispersion effects that made it possible to found 3D stable soliton solutions in the BK equation model, in contrast to the results obtained for the standard KP equation model [105].

In order to study the dynamics of an FMS wave beam characterized by a narrow angular distribution, we solved the boundary problem (in contrast to [62], in which the Cauchy problem was considered). We numerically integrated the corresponding equation, because the exact analytical solutions of the BK equation, even for the non-dissipative case, are not currently known.

Let us consider the problem of modeling of the FMS wave beam dynamics in the magnetized plasma. It is assumed that there is a 3D FMS beam propagating in the plasma at angle θ to the external magnetic field near the cone of angles $\theta = \arctan(M/m)^{1/2}$. Using the substitutions $x \to -st$, $y \to -s\kappa^{1/2}y$, $z \to -s\kappa^{1/2}z$, $t \to sx$, $h \to -(6/\alpha)h$, $s = |\gamma_2|^{1/4}$, and $\kappa = v_A/2$ we obtain from (1.4.21)

$$\partial_t(\partial_x h + 6h\partial_t h - \varepsilon\partial_t^3 h - \lambda\partial_t^5 h) = \Delta_\perp h, \qquad (1.4.22)$$

where $\varepsilon = \gamma_1 |\gamma_2|^{-1/2}$, $\lambda = \mathrm{sgn}\gamma_2$. Equation (1.4.21) describes the FMS wave beam propagating along the x-axis from the boundary $x = 0$. If it is assumed that $\Delta_\perp = \partial_\rho^2 + (1/\rho)\partial_\rho$, and also $h_0 = h(t,0,\rho) = \cos(mt)\exp(-\rho^2)$, then the boundary condition is defined as the FMS wave beam localized in the (y,z) plane and time-periodic axially symmetric beam of FMS waves.

Equation (1.4.22) with boundary condition h_0 was integrated numerically. The series of performed numerical experiments related to the modeling of FMS beam propagation at its different intensities at the boundary of $x = 0$, h_0 and different angles θ (see above the cases A, B, and C) made it possible to obtain the following results. In region A (corresponding to $\lambda = 1$, $\varepsilon > 0$), as in [27] and [30], the spatial evolution of the FMS wave beam at the initial stage at any h_0 results in beam focusing, which is related to the predominant role of nonlinear processes in this time range. Meanwhile, as in the usual KP equation, we observe (Fig. 1.4.4, curves *1* and *2*) beam compression in a transversal ρ-direction in the course of its propagation along the x-axis, such that its transversal characteristic size $l_\rho(x) \sim l_\rho(0)h(0)/h(x)$ decreases with simultaneous fast growth of the beam intensity in its axis with an increment of $\Gamma = (1/2W)dW/dt \sim 2$ (where $W = \langle h^2\rangle/4\pi$ is a wave energy in the volume unit), which is just slightly dependent on ε. In this case, the characteristic dimensions of the beam, which represents a wave pulse, decrease, its "wings" start lagging behind its central part, and self-focusing instability develops (Fig. 1.4.4, curves 1 and 2; Fig. 1.4.5). This evolution type is also characterized by an increase in P and a decrease (at low $\varepsilon > 0$) in the Hamiltonian H in the system due to a nonlinear term, which grows at this evolution stage much faster than dispersion terms.

Under further growth of t, due to a decrease in a transverse size of wave pulse l_ρ (Fig. 1.4.4), the term, which is proportional to the fifth derivative in the equation (1.4.22), starts playing a predominant role (it is well-seen in the analysis of variations in the integral terms making up the Hamiltonian H). As a result, the "collapse" of the wave pulse wings behind its main part does not lead to a rapid increase in the field
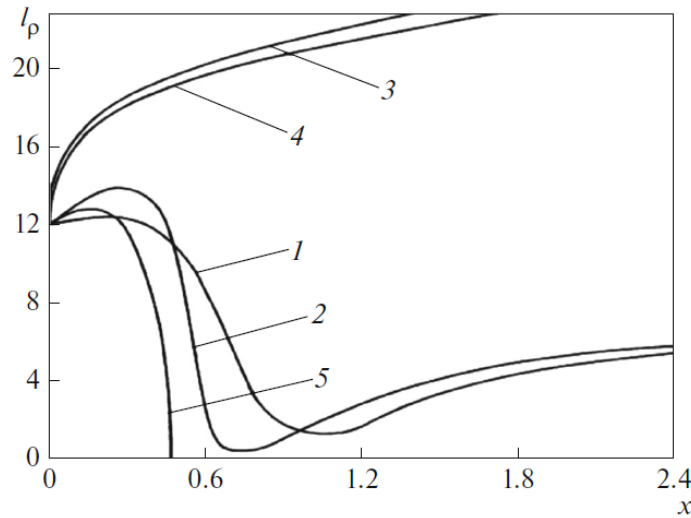

Figure 1.4.4. Changing of a cross-section of the wave beam under its propagation in the x-direction: (*1*) $\lambda = 1$, $\varepsilon = 1.34$; (*2*) $\lambda = 1$, $\varepsilon = 2.24$; (*3*) $\lambda = -1$, $\varepsilon = 1.34$; (*4*) $\lambda = -1$, $\varepsilon = -1.34$; (*5*) $\lambda = 0$, $\varepsilon = -1.34$.

Intensity and singularity formation in the major peak region, which is typical for the standard KP equation model with $\gamma_1/k > 0$ [27]; as a result, a ring region of the elevated field concentration is formed (Fig. 1.4.6). Further evolution of this structure will make it possible to form additional peaks in the x-axis behind the pulse (Fig. 1.4.6). In this case,
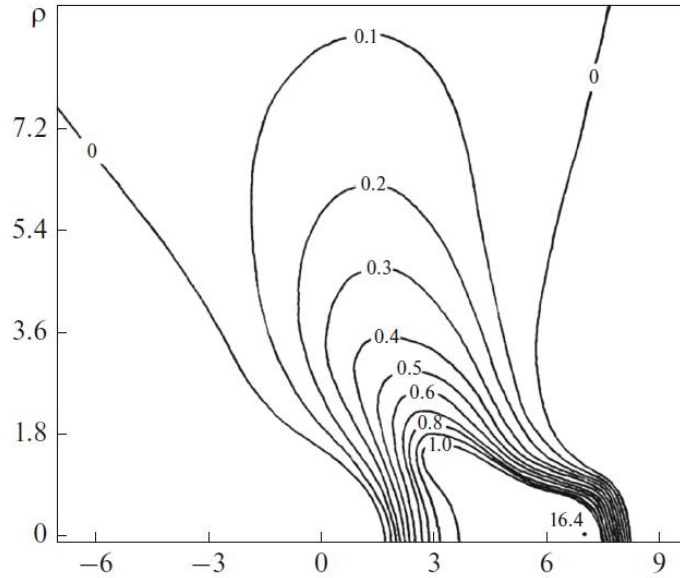

Figure 1.4.5. Solution in the (x, ρ) plane at $\lambda = 1$, $\varepsilon = 0.89$ corresponding to the amplitude maximum stage.

the wave pulse stops being compressed and starts defocusing (Fig. 1.4.4, curves *1* and *2*). This stage is completed by the formation of a stationary wave beam, i.e., by transition into the regime of $h_{\max}(x) = const$ and $l_\rho(x) = const$, which corresponds to the results described in the second Section. The role of the term, which is proportional to the fifth derivative in the eq. (1.4.22), along with the role described above, consists of the appearance of small-scale oscillations forming a regular oscillatory structure of the tail (Fig. 1.4.6).
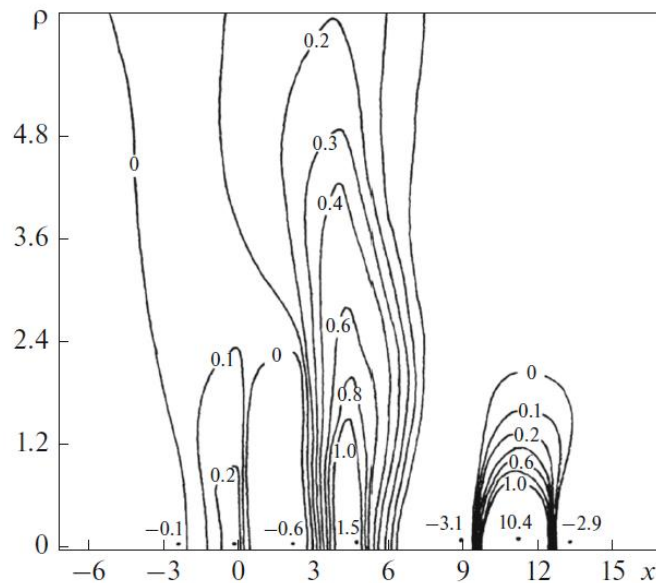

Figure 1.4.6. Solution in the (x, ρ) plane at $\lambda = 1$, $\varepsilon = 0.89$.

In regions B and C (Fig. 1.4.3), which correspond to $\lambda = -1$ and $|\varepsilon| \geq 0$, a sonic wave scatters with propagation along the x-axis at any beam intensity $h(0)$ at the
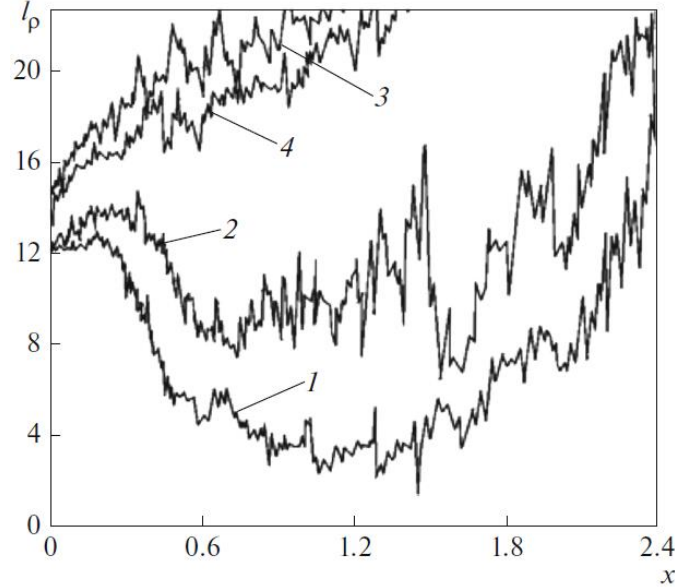

Figure 1.4.7. Variations in a cross section of the beam under its propagation along the x-axis in the plasma with $\eta = \eta(t, x, \rho)$ at a standard deviation of $\sigma = 0.04$ for the same λ and ε values as in Fig. 1.4.4.

boundary (Fig. 1.4.4, curves *3* and *4*), just as in the electromagnetic wave self-action process in the media, where derivatives $\partial^2\omega/\partial k_x^2$ and $\partial^2\omega/\partial k_\perp^2$ have different signs (for example, this phenomenon is characteristic for ion-cyclotron waves, whistlers, etc.) [72].

Fig. 1.4.4 demonstrates that, at $\lambda = 0$, when (1.4.22) transits into the KP equation with a negative dispersion, there are no solutions as a self-focusing beam of FMS waves. Therefore, the self-focusing effect is not observed in the considered model when $\lambda = 0$. According to the test numerical experiments for the model (1.4.22) with $\lambda = 0$, self-focusing is possible only at $\varepsilon < 0$ (Fig. 1.4.4, curve *5*), when the FMS wave beam described by this model does not correspond to any real situation [27].

Hence, according to the study results based on the BK equation model (1.4.22), the self-focusing phenomenon of the FMS beam, which propagates in the plasma at the angles to the magnetic field near the cone of $\theta = \arctan(M/m)^{1/2}$, cannot be observed, in contrast to the standard KP equation model, even if the dispersion for low k is positive. In this case, however, together with the beam scattering, we can observe nonlinear stationary propagation. It should also be noted that eqs. (1.4.21) and (1.4.22) at $|\pi/2 - \theta| \gg (m/M)^{1/2}$ should also be supplemented with terms proportional to mixed derivatives, because $|k_\perp| \geq k_x$, in this case and the dispersion equation acquires terms proportional to $k_x^i |\mathbf{k}_\perp^j|$, where $i, j = 1, 2$, etc.

It should be noted in the conclusion that it is also necessary under the ionospheric and magnetospheric plasma conditions to take into account the effect of stochastic fluctuations of the wave field $h(t, x, r_\perp)$ on wave beam evolution, which should be taken into consideration in basic equations. Hence, eq. (1.4.22) should be supplemented with a term such as $\eta(t, x, \rho)$ and rewritten as follows:

$$\partial_t(\partial_x h + 6h\partial_t h - \varepsilon\partial_t^3 h - \lambda\partial_t^5 h + \eta(t,x,\rho)) = \Delta_\perp h. \qquad (1.4.23)$$

In [14], eq. (1.4.23) at $\lambda = 0$ for the case of low-frequency fluctuations, when $\eta = \eta(t)$, was integrated analytically. The results can be easily applied to (1.4.23) with $\eta = \eta(t)$. The interpretation of results obtained in [14] in terms of this problem is indicative of the fact that even low stochastic fluctuations of the wave field will lead to the decay of the wave pulse upon its propagation, accompanied by the wave transformation into an oscillatory structure. Meanwhile, in the case of $\eta = \eta(t,x,\rho)$, the analytical study of the corresponding process becomes extremely complicated, and [30] carried out numerical integration of eq. (1.4.23) with a stochastic term, which is a function of time and space coordinates. Fig. 1.4.7 demonstrates the results of numerical modeling of the FMS wave beam evolution in a medium with stochastic fluctuations of the wave field in the form of Gaussian noise in the model (1.4.23) with $\eta = \eta(t,x,\rho)$. The obtained results are qualitatively similar to the case of $\eta = \eta(t)$: a decrease in amplitude of the FMS wave beam upon its propagation with the subsequent wave destruction (comparison with Fig. 1.4.4).

In the course of this investigation, we studied analytically and numerically the problem of the stability and dynamics of 3D soliton-like structures, such as a beam of FMS waves, which are formed in a low-frequency branch of oscillations in plasma, for the cases when $\beta \equiv 4\pi nT/B^2 \ll 1$ and $\beta > 1$. The study was based on the model of the 3D BK-equation for the magnetic field $h = B_\sim/B$, upon the assumption of homogeneity of the external magnetic field $\mathbf{B}$, and takes into account the highest dispersion correction determined by the plasma parameters and the angle $\theta = (\mathbf{B}, \mathbf{k})$. According to the results, in contrast to the KP equation model, when the FMS wave beam propagates at the angles to the external magnetic fields near the cone of $\theta = \arctan(M/m)^{1/2}$, the self-focusing phenomenon is not observed, even if dispersion for low k is positive. It is proved that on a level with the magnetic sound scattering the nonlinear stationary beam propagation can be observed; the analytical and numerical methods made it possible to prove the possibility of the formation of stable 3D solitary beams of FMS waves in the course of evolution. It is demonstrated that the presence of stochastic wave field fluctuations in the medium reduces the FMS wave beam amplitude upon propagation, followed by beam destruction.

Our work did not explicitly take into account the possible effects of the external magnetic field inhomogeneity that can take place in the Earth's ionosphere and magnetosphere. For instance, the field inhomogeneity can result in soliton acceleration [89] and other phenomena related to the imbalance between nonlinear and dispersive effects, for example, in soliton deformations and destruction, as happens during the propagation of nonlinear wave structures in the variable dispersion media (see, for example, [27], [40]). The latter can be caused in plasma as heterogeneity of its composition in space, which will lead to spatial dependence of the values such as m/M, n_i and, consequently, $\omega_{pi} = (4\pi n_i e^2/M)^{1/2}$ and also the field $\mathbf{B}$ heterogeneity, and then $v_A = B^2/4\pi n_i M$. In this case, the dispersion coefficients γ_1, γ_2 in the BK equations will also become functions of spatial coordinates. Hence, the heterogeneity effect can be taken into account in our model if we assume that $B = f(r)$, while γ_1, γ_2 and v_A are functions of r in eqs. (1.4.21), (1.4.22). However, such generalization of the BK equation is beyond the scope of the research presented in this paper.

It should be noted in conclusion that the results can be directly applied to nonlinear wave dynamics in the ionospheric and magnetospheric plasma, because, in our opinion, they will contribute to a better understanding of the physics of nonlinear wave processes and may be useful in the interpretation of the results of laboratory and space experiments related to the excitation, evolution, and interaction of FMS wave solitons and of self-action effects, such as wave collapse and wave beam self-focusing.

1.4.3. Nonlinear Alfvén waves propagating in plasma of ionosphere and magnetosphere

We study here stability and dynamics of the multidimensional soliton-like Alfvén structures forming on the low-frequency branch of oscillations in the ionospheric and magnetospheric plasma which are described by equation [28]

$$\partial_t u + A(t,u)u = f, \qquad f = \kappa \int_{-\infty}^x \Delta_\perp u \, dx, \qquad \Delta_\perp = \partial_y^2 + \partial_z^2, \qquad (1.4.24)$$

when for

$$A(t,u) = 3s \, | \, p \, |^2 \, u^2 \partial_x - \partial_x^2 (i\lambda + \nu) \qquad (1.4.25)$$

it falls into 3D derivative nonlinear Schrödinger (3-DNLS) equation class. Derivation of eq. (1.4.24) with differential operator (1.4.25) was presented in detail in [27] with use of the same approach and conditions as in [85],[87],[88]. In the case when $\beta \equiv 4\pi nT / B^2 > 1$ the 3-DNLS equation (1.4.24), (1.4.25) describes dynamics of the finite-amplitude Alfvén waves propagating nearly parallel to homogeneous magnetic field $\mathbf{B}$ for $u = h = (B_y + iB_z)/2B \, | \, 1 - \beta \, |$, $\mathbf{h} = \mathbf{B}_\perp / B_0$ where $p = (1 + ie)$, and e is the "eccentricity" of the polarization ellipse of the Alfvén wave [18], $\nu = \dfrac{\rho_0}{2\rho}(c_\infty^2 - c_0^2)\tau \int_0^\infty \xi \varphi(\xi) d\xi$ defines the logarithmic damping rate, and it is the characteristic rate of the relaxation damping of the "sound" wave [27]. Here ρ is perturbed plasma density $\left(\lim_{|x| \to \infty} \rho = \rho_0 \right)$, c_∞ and c_0 are the velocities of the high and low-frequency "sound" mode (the last one coincides with $c_0 = (T_e / m_i)^{1/2}$) and $\varphi(t, \tau)$ is the function defining the relaxation process. The upper and lower signs of $\lambda = \pm 1$ correspond to the right and left circularly polarized wave, respectively; the sign of nonlinearity is accounted by the factor $s = \mathrm{sgn}(1 - p) = \pm 1$ in the nonlinear term; and $\kappa = -r_A / 2$, $r_A = v_A / \omega_{0i}$.

Equations (1.4.24), (1.4.25) are not completely integrable. Therefore, to study the stability of multidimensional solitons we use the method developed in [19] and investigated the Hamiltonian bounding with its deformation conserving momentum by solving the corresponding variation problem. In the analytical study of this set we use also asymptotic analysis of its multidimensional solutions. To study evolution of 3D solitons including propagation of the Alfven waves' beams in a magnetized plasma the equations were being integrated numerically using the simulation codes specially developed and described in detail in [27].

To study the stability of multidimensional solutions of eqs. (1.4.24), (1.4.25) with $\nu = 0$ we use the same approach as in [19] similar to the one in [35] used for the BK equation. We rewrite 3-DNLS equation (1.4.24), (1.4.25) by performing the formal change $u \to h$ into the Hamiltonian form

$$\partial_t h = \partial_x (\delta H / \delta h), \qquad (1.4.26)$$

where $\delta H/\delta h$ is a variational derivative, with the Hamiltonian [29]

$$H = \int_{-\infty}^{\infty} \left[\tfrac{1}{2}|h|^4 + \lambda s h h^* \partial_x \varphi + \tfrac{1}{2}\kappa \left(\nabla_{\perp} \partial_x w \right)^2 \right] d\mathbf{r}, \quad \partial_x^2 w = h, \; \varphi = \arg(h) \;, \quad (1.4.27)$$

which has a sense of energy of the system, and solve the variation problem, $\delta(H + vP_x)$ $= 0$, where $P_x = \tfrac{1}{2}\int |h|^2 d\mathbf{r}$ is the momentum projection onto the x axis, v is Lagrange's factor, that illustrates the fact that all finite solutions of eq. (1.4.26) are the stationary points of the Hamiltonian for fixed P_x. Conforming with Lyapunov's theorem, the stationary points of a dynamical system realizing maximum or minimum of H are absolutely stable; if the extremum is local then the locally stable solutions are possible. The unstable states correspond to monotonous dependence of H on its variables, i.e. to the case when the stationary point is a saddle point. Thus, it is needed to prove the Hamiltonian's boundedness (from below) for fixed P_x. Consider the scale transformation $h(x, \mathbf{r}_{\perp}) \to \zeta^{-1/2} \eta^{-1} h(x/\zeta, \mathbf{r}_{\perp}/\eta)$ ($\zeta, \eta \in \mathbf{C}$) conserving P_x, in the complex vector space $\mathbf{C}$. The Hamiltonian as a function of ζ, η is given by

$$H(\zeta, \eta) = a\zeta^{-1}\eta^{-2} + b\zeta^{-1} + c\zeta^2\eta^{-2} \;, \qquad (1.4.28)$$

where $a = (1/2)\int |h|^4 d\mathbf{r}, \; b = \lambda s \int h h^* \partial_x \varphi d\mathbf{r}, \; c = (\sigma/2)\int (\nabla_{\perp} \partial_x w)^2 d\mathbf{r}$. The necessary conditions for the existence of the extremum, $\partial_{\zeta} H = 0, \; \partial_{\eta} H = 0$, immediately allows us to obtain the extremum's coordinates

$$\zeta = -a/c, \qquad \eta = \left\{ -(a/b)\left[1 + (a^2/c^2) \right] \right\}, \qquad (1.4.29)$$

where $b < 0$ if $\eta \in \mathbf{R} \subset \mathbf{C}$ because $a > 0, c > 0$ by definition, and $b > 0$ if $\eta \in \mathbf{C}$. The sufficient conditions for the existence of the local minimum of H at the point (ζ_i, η_i) are given by [35]

$$\begin{vmatrix} \partial_{\zeta}^2 H(\zeta_i, \eta_j) & \partial_{\zeta\eta}^2 H(\zeta_i, \eta_j) \\ \partial_{\eta\zeta}^2 H(\zeta_i, \eta_j) & \partial_{\eta}^2 H(\zeta_i, \eta_j) \end{vmatrix} > 0, \qquad \partial_{\zeta}^2 H(\zeta_i, \eta_j) > 0, \qquad (1.4.30)$$

and we therefore obtain for $b < 0$

$$a/c < d = \left(2\sqrt{2} \right)^{-1} \sqrt{13 + \sqrt{185}} \;. \qquad (1.4.31)$$

Thus it follows from (1.4.28)-(1.4.31) that the Hamiltonian H of (1.4.26) is limited from below, i.e.

$$H > -3bd/(1 + 2d^2) \qquad (1.4.32)$$

where $b < 0$ if condition (1.4.31) holds. In this case the 3D solutions of 3-DNLS equation are stable. The solutions are unstable in the opposite case, $ac^{-1} \geq d, b < 0$. Condition $b < 0$ corresponds to the right circularly polarized wave with $\beta = 4\pi n T / B^2 > 1$, i.e. when $\lambda = 1, s = -1$ in eqs. (1.4.24), (1.4.25), and to the left circularly polarized wave when $\lambda = -1, s = 1$. It is necessary to note that the sign change $\lambda = 1 \to -1, s = -1 \to 1$ is equivalent to the change $t \to -t, \kappa \to -\kappa$ and for negative κ the Hamiltonian becomes negative in the area "occupied" by the 3D wave weakly limited in the $\mathbf{k}_{\perp}$-direction; in this case condition (1.4.32) is not satisfied. The change

of the sign of b to positive [when $\lambda = 1$, $s = 1$ or $\lambda = -1$, $s = -1$ in eqs. (1.4.24), (1.4.25)] is equivalent to the analytical extension of solution from real values of y, z to the pure imaginary ones: $y \rightarrow -iy$, $z \rightarrow -iz$ and, therefore, equivalent to the change of sign of κ in the basic equations. In this case instead of inequality (1.4.32) the opposite inequality will take place. From the physical point of view this means that if the opposite inequality is satisfied, the right polarized wave with the positive nonlinearity and the left polarized wave with the negative nonlinearity are stable. Note that in the particular case $\kappa = 0$ in eqs. (1.4.24), (1.4.25) (1D approximation), instead of inequality (1.4.32) and the opposite one, it is easy to obtain the conditions $H > 0$ and $H < 0$, respectively, that is completely in agreement with the results obtained in [46] for the 1-DNLS equation.

Thus the analysis of the transformation properties of the Hamiltonian of the 3-DNLS equation allows us to determine the ranges of the respective coefficients as well as H which has the sense of the energy of the system, corresponding to the stable and unstable 3D solutions. So, we have proved the possibility of existence in the 3-DNLS model of absolutely stable 3D solutions.

Now, following [27] consider the character of the asymptotics of the axially-symmetric solitary pulse solution of the 3-DNLS equation when $\Delta_\perp = \partial_\rho^2 + (1/\rho)\partial_\rho$. In this case eqs. (1.4.24), (1.4.25) can be written in the form of the set

$$\partial_\eta \left[\partial_t h + s\partial_\eta \left(|h|^2 h \right) - i\lambda\partial_\eta^2 h - \nu\partial_\eta^2 h \right] = \kappa \left(\partial_\eta^2 + (1/\rho)\partial_\eta \right) h,$$

$$\partial_\zeta \left[\partial_t h + s\partial_\zeta \left(|h|^2 h \right) - i\lambda\partial_\zeta^2 h - \nu\partial_\zeta^2 h \right] = \kappa \left(\partial_\zeta^2 + (1/\rho)\partial_\zeta \right) h$$

written in the reference frame with the axes $\eta = x + \rho$, $\zeta = \rho - x$ rotated through an angle $\pi/4$ relative to the axes x and ρ. Further obvious transformations give us the set

$$\partial_t h + s\partial_{\eta'} \left(|h|^2 h \right) - i\lambda\partial_{\eta'}^2 h - \nu\partial_{\eta'}^2 h = 0,$$

$$\partial_t h + s\partial_{\zeta'} \left(|h|^2 h \right) - i\lambda\partial_{\zeta'}^2 h - \nu\partial_{\zeta'}^2 h = 0$$

(1.4.33)

written in the coordinates $\eta' = \eta + \kappa t$, $\zeta' = \zeta + \kappa t$, i.e. in the frame moving along the corresponding axis with the velocity $-\kappa$. So, we can conduct the analysis for only one equation of the set (1.4.33) and then, fulfilling the inverse change of the variables, extend the results to the 3D axially-symmetric solutions $h(x,\rho,t)$ of the 3-DNLS equation with $\Delta_\perp = \partial_\rho^2 + (1/\rho)\partial_\rho$.

As it is known from [27],[46], an exact solution of the 1D DNLS equation is given by

$$h(x,t) = (A/2)^{1/2} \left[\exp(-Ax) + i\exp(Ax) \right] \exp(-iA^2 t)\cosh^{-2}(2Ax)$$

(1.4.34)

where A is the amplitude of the wave (see [27] for detail). Now we can apply the inverse change of the variables, $x = (\eta + \zeta)/2$, $\rho = (\eta - \zeta)/2$, and, extending solution (1.4.34) to the 3D case (1.4.24), (1.4.25) with $\Delta_\perp = \partial_\rho^2 + (1/\rho)\partial_\rho$ write at once for $\nu = 0$

$$h(x,\rho,t) = (A/2)^{1/2} \left[\exp(-A\chi) + i\exp(A\chi) \right] \exp(-iA^2 t)\cosh^{-2}(2A\chi)$$

where $\chi = (x \pm \rho + (\kappa - V)t)$, and V is the velocity of the wave propagation relative to

the coordinate axis x or ρ for the first or the second equations of set (1.4.33), respectively.

The dependence of the form of the solution on dissipation in the system as well as the dynamic characteristics of the solution for $\nu > 0$ will be considered in the next Section in detail.

Note, that our analytical results are well confirmed by the results of our numerical experiments on study of structure and stability of multidimensional solitons in the model of the 3-DNLS equations [27],[29]. So, we have obtained that for a single solitons, on a level with wave spreading and wave collapse (in other terminology, self-contraction), the formation of multidimensional 3D solitons can be observed. Let us now consider the nonlinear effects for 3D soliton structures propagating in a magnetized plasma.

For the numerical investigation, we consider the 3-DNLS equation in the integral-differential form (1.4.24), (1.4.25) and integrate it in the axially-symmetric geometry when $\Delta_\perp = \partial_\rho^2 + (1/\rho)\partial_\rho$, $\rho^2 = y^2 + z^2$. The initial conditions are taken in the form of the axially-symmetric solitary pulses of two types:

− soliton-like axially symmetric pulse:

$$h(x, \rho, 0) = h_0(x)\exp\left[i\varphi(x) - \rho^2 / l_\rho^2\right] \qquad (1.4.35)$$

with $h_0(x) = 2\sqrt{2}\delta \sin \vartheta \left[\cosh(4\delta^2 \sin \vartheta x) + \cos \vartheta\right]^{-1/2}$ and

$$\varphi(x) = -2s\delta^2 \cos \vartheta x - (3s/4)\int_{-\infty}^{x} h_0^2(x)dx \ , \ \text{where } 0 < \vartheta < \pi;$$

− modulated plane wave:

$$h(x, \rho, 0) = H_0 \exp\left(2\pi i x / \lambda - x^2 / l_x^2 - \rho^2 / l_\rho^2\right), \qquad (1.4.36)$$

where λ is the wavelength, H_0 is the amplitude, and l_x and l_ρ are the characteristic scales of the Gaussian envelop modulation in the x and ρ-directions. Note that for $\rho=0$, the initial conditions (1.4.33) and (1.4.34) are equivalent to those used for the numerical simulation of the evolution of the 1D Alfvén wave in [46],[47].

To investigate the structure and evolution of the 3D pulses, we have done a number of simulation runs for both signs of the integral parameter b and various initial values of the Hamiltonian by defining various initial values for the pulse amplitude and the widths l_x and l_ρ. Thus, for non-dissipative case, when $\nu = 0$ in eqs. (1.4.24), (1.4.25), we have obtained the following results.

1. For $\lambda=1$, $s = -1$, large $\kappa>0$, and the initial pulse weakly limited in the transverse ρ-direction when the stability condition (1.4.32) is satisfied, the evolution for large t results in formation of the stable 3D (axially-symmetric) solution (Fig. 1.4.8).

2. At the opposite signs of λ and s [that is equivalent to change $t \rightarrow -t$, $\kappa \rightarrow -\kappa$ in eqs. (1.4.24), (1.4.25)] the Hamiltonian (1.4.27) of the 3-DNLS equation becomes negative, and, as it follows from the results of numerical experiments, a 3D Alfvén wave spreads with evolution (Fig. 1.4.9).

3. At $\lambda=1$, $s = -1$ for small $\kappa > 0$ and initial pulse rather strong limited in the ρ-direction the conditions of the existence of the local minimum of H (1.4.30) are not satisfy, and in the numerical experiments one can observe development of the 3D collapsing solutions of the 3-DNLS (Figs. 1.4.10 and 1.4.11). Note, that this effect is typical for all nonlinear systems where the Hamiltonian is unlimited for fixed first integrals (in this case, for the momentum P_x) and the quadratic terms in the expression

for H [the first and third terms in expression (1.4.27)] are positively defined. For example, the same effects have been observed in the systems describing the evolution of the FMS waves [35] and Langmuir waves [103] in a plasma.

The series of the numerical experiments being carried out for $b>0$ when $\lambda = 1$, $s = 1$ and $\lambda = -1$, $s = -1$ in eqs. (1.4.24), (1.4.25) with $v=0$ showed that for these conditions in all cases (for different initial values of the Hamiltonian and the parameters l_x, l_ρ) the initial 3D axially symmetric pulses spread with evolution. That is
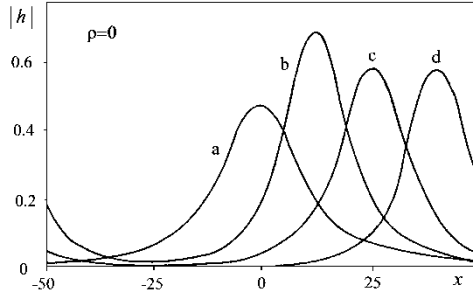

Figure 1.4.8. Evolution of a 3D right circularly polarized nonlinear pulse (1.4.33) for λ=1, s = − 1, κ =1; H > − $3bd/(1+2d^2) > 0$: a) $t=0$, b) $t=25$, c) $t=50$, d) $t=75$.
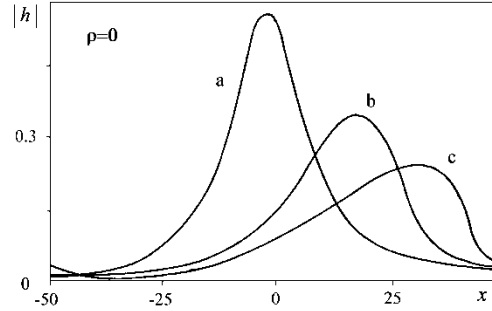
Figure 1.4.9. Evolution of a 3D right circularly polarized nonlinear pulse (1.4.34) for λ=−1, s = 1, κ =1; H > 0: a) $t=0$, b) $t=50$, c) $t=100$.
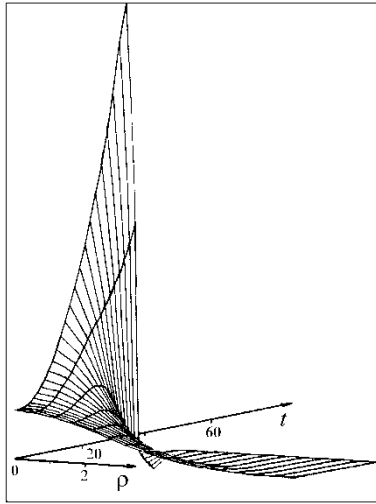

Figure 1.4.10. Dynamics of a 3D right circularly polarized nonlinear pulse (1.4.34) (cross-section by the ρ -plane in the point $h_{\max}$) for λ=1, s = − 1, κ = 0.2; 0<H<− $3bd/(1+2d^2)$.
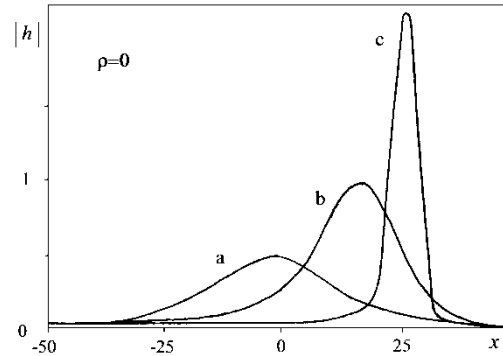
Figure 1.4.11. Evolution of a 3D right circularly polarized nonlinear pulse (1.4.33): a) $t=0$, b) $t=25$, c) $t=30$; the equation coefficients and H are the same as in Fig. 1.4.10.

rather as obvious so far as with such conditions for coefficients the inequality $H < -3bd/(1+2d^2)$ (see Sect. 2) doesn't satisfy and, therefore, the 3D solutions of the 3-DNLS equation are unstable.

But, if we fulfil the transform $h' = -sh^*$ in the 3-DNLS equation, i.e. consider left circularly polarized waves, that the signs in the expression for the Hamiltonian (1.4.27)

change to opposite and for all cases considered above we will observe a mirror opposite picture. Thus, a case $\lambda = -1$, $s = -1$ for big values $\kappa > 0$, and also the cases $\lambda = 1$, $s = 1$ and $\lambda = -1$, $s = -1$ for small values $\kappa > 0$ correspond to the cases (1.4.24), (1.4.25) and (1.4.26), accordingly, with the opposite signs of the Hamiltonian. An example of the dynamics of a 3D left circularly polarized pulse is shown in Fig. 1.4.12.

Summing the above up, conclude that the 3-DNLS equation (1.4.24), (1.4.25) with $\nu=0$ can have the stable 3D solutions in the form of the 3D Alfvén solitons, and also on a level with them the 3D solutions collapsing or dispersing with time. The form of solution is defined by signs of the equation coefficients λ and s, and also by the form of initial condition. The results obtained above can be also interpreted in terms of the self-focusing phenomenon. So, formal change $x \leftrightarrow t$ enables us to do a transition from the Cauchy problem (1.4.24), (1.4.25) and (1.4.33) or (1.4.24), (1.4.25) and (1.4.34) to the boundary-value problem describing the propagation of the 3D Alfvén wave beam localized in the ρ-plane along the x axis from boundary $x = 0$. In this case the results obtained above can be interpreted as: 1) the formation of the stationary Alfvén wave beam propagating along the x axis; 2) Alfvén wave beam spreading; and 3) the self-focusing of the Alfvén wave beam. It is interesting to note that we observe here the dynamics of the Alfvén wave beam propagating in plasma with $\beta > 0$ at near-to-zero angles with respect to the external magnetic field **B,** which is qualitatively similar to the dynamics of the FMS wave beam propagating in plasma with dispersion coefficient $\gamma_1 << 0$ [35] at angle close to $\pi / 2$ with respect to the external magnetic field [74].
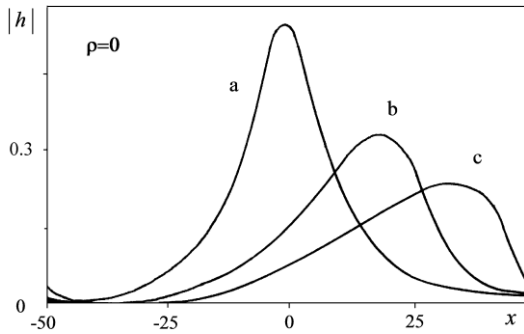

Figure 1.4.12. Evolution of a 3D nonlinear left circularly polarized pulse (1.4.34) for $\lambda = s = \kappa = 1$; $H > 0$: a) $t=0$, b) $t=50$, c) $t=100$.
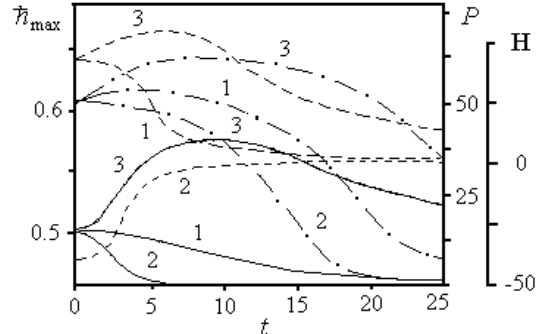
Figure 1.4.13. Change of the amplitude of a 3D axially symmetric Alfvén wave (solid lines), P (chain lines) and H (dashed lines) of the 3-DNLS equation with $\nu = 1$: (1) $\lambda=1$, $s=-1$, $\kappa=1.5$; (2) $\lambda=-1$, $s=1$, $\kappa=1.5$; (3) $\lambda=1$, $s=-1$, $\kappa=0.1$.

The presence of dissipation in a plasma can be caused by many reasons. For example, in [80] it is shown that the dissipation processes of circularly polarized parent Alfvén waves in solar wind plasmas can be observed due to the presence of the beam induced obliquely propagating waves, such as kinetic Alfvén waves (KAW) as a result of the nonlinear wave-wave coupling. Similar effects can be observed at nonlinear interaction of KAW and FMS wave for intermediate β-plasma when $\beta<<1$ [79]. But in the context of our problem we consider here the case when the presence of dissipation in the system [$\nu>0$ in eqs. (1.4.24), (1.4.25)] is caused by the relaxation processes of the viscous type in a medium (the particular physical reason of the energy dissipation depends on the type of the medium). In this case the dissipation changes the character of

the evolution of the 3D nonlinear pulse, and in evolution of the Alfvén wave the exponential decrease of its amplitude with time is observed:

$$|h|^2 = (1+e^2)\hbar^2(t) = (1+e^2)\hbar^2(0)\exp(\Gamma t),$$

where $h = (1+ie)\hbar$. In this case, the damping rate is of the same order of magnitude as in the BK model [27] (we have obtained in our numerical simulations the averaged value $\Gamma \sim -3.1$). Moreover, similar to the BK model, some steepening of the pulse's front takes place, and the back slope of the pulse decreases. The proof of that behavior is, in particular, in the different character of the change of the integrals of motion,

$$P = (1+e^2)\int \hbar^2 d\mathbf{r} \qquad \text{and}$$

$$\text{H} = \int_{-\infty}^{\infty}\left[\tfrac{1}{2}(1+e^2)^2\hbar^4 + \lambda s(1-e^2)\hbar^2\partial_x\varphi + \tfrac{1}{2}\sigma(\nabla_\perp\partial_x w)^2\right]d\mathbf{r},$$

$$\partial_x^2 w = (1+ie)\hbar, \qquad \varphi = \arg\left[(1+ie)\hbar\right],$$

in the regions behind and in front of the main maximum. Indeed, in all cases P and $|\text{H}|$ decrease faster in front of the pulse. For various values of the coefficients in the 3-DNLS equation, the character of the evolution is the following:

1. For $\lambda = 1$, $s = -1$, and relatively large $\kappa > 0$, the initial pulse is weakly limited in the direction perpendicular to its propagation, and loses its energy with evolution ($\text{H} \to 0$ with $t \to \infty$). In this case, the amplitude of the pulse decreases with time (as we noted above, exponentially, with the rate proportional to ν) and, as a result, the solitary wave disperses. Recall here, that in the case of $\nu = 0$, the evolution after initial "sub-focusing" of the pulse leads to the formation of the stable 3D Alfvén soliton (see above).

2. For $\lambda = -1$, $s = 1$, when the Hamiltonian becomes negative and the Alfvén wave pulse for $\nu = 0$ spreads with its evolution, the presence of the dissipation accelerates this process significantly (for $\nu \sim 1$ we have obtained in the simulations averaged $\Gamma \sim -3.4$). The effect of the steepening of the front of the pulse takes place as well in this case.

3. For $\lambda = 1$, $s = -1$, relatively small $\kappa > 0$, and the initial pulse strongly limited in the transverse ρ-direction, when development of the wave collapse is observed in the simulations for $\nu = 0$, the presence of the dissipation can rapidly delay or (for large $\nu > 0$) even stop this process. In this case, the role of the dissipation in the 3-DNLS model is different from that in the model of the 3D BK equation: it is now the decisive factor in the stopping of the wave collapse.

Figure 1.4.13 shows the change with time of the amplitude and the integrals P and H (averaged throughout the region of numerical integration) for the three cases described above and $\nu = 1$.

In conclusion, we have considered analytically and numerically the nonlinear dynamics of the 3D solitary nonlinear Alfven waves propagating nearly parallel to the external homogeneous magnetic field in a plasma on the basis of model of the 3-DNLS equation. For non-dissipative case we have obtained the analytical estimates and the sufficient conditions for the stability of 3D solutions of the 3-DNLS equation and proved that the equation can have the stable 3D solutions in the form of the 3D Alfvén solitons, and also on a level with them the 3D solutions collapsing or dispersing with time. The asymptotics of the solitary solutions were studied. Our numerical experiments showed that in terms of the self-focusing phenomenon one can observe as a result of the evolution the formation of the stationary Alfvén wave beam propagating along the

external magnetic field as well as Alfvén wave beam spreading or the self-focusing of the Alfvén wave beam. The influence of the dissipation of viscous type in a plasma on structure and character of evolution of 3D Alfvén waves was studied. In our research we have not taken into account the possible effects of magnetic field inhomogeneity and non-stationarity which can take place in the Earth's ionosphere and magnetosphere. So, inhomogeneity can result, for example, in soliton acceleration [89] and other phenomena associated with infringement of balance between nonlinear and dispersive effects, for example, in destruction of the soliton, jast as it takes place for the FMS waves propagating in the ionosphere and magnetosphere [27],[35]. In our model the effect of the inhomogeneous magnetic field can be accounted if we assume that $\mathbf{B}_0 = f(\mathbf{r})$ and, hence, β, κ and v_A are the function of $\mathbf{r}$ in (1.4.24)-(1.4.27). To study the effects of non-stationarity of the magnetic field we can assume that $\mathbf{B}_0 = f(\mathbf{r})$ or, by analogy with the Kadomtsev-Petviashvili (KP) equation [14], introduce into the 3-DNLS equation the term which describes the wave fluctuations of the magnetic field in time. Thus, we can expect the effects of formation of short-wave structures with soliton destruction and development of turbulence of the wave field, being similar to that for the KP model [27]. However the generalizations of the 3-DNLS model mentioned above leave beyond our research here.

The results obtained are very important for the best understanding of physics of nonlinear wave processes in plasma of ionosphere and magnetosphere and can be rather useful at interpretation of the results of experimental studies in laboratory and space experiments on excitation, evolution and interaction dynamics of the Alfvén solitons as well as the self-influence effects (the wave collapse and the wave self-focusing of the wave beams).

1.4.4. IGW and TID in the ionosphere of the Earth

Structure and dynamics of internal gravity waves (IGW) and associated traveling ionospheric disturbances (TID) have been extensively studied for more than forty years [53]-[56]. Despite extensive observations involving numerous various technics such as, e.g., vertical and slanted ionospheric as well as satellite sounding [39] and recently developed imaging technique using multipoint GPS networks [96], the associated theory is less developed.

To solve the wide range of problems associated with wave perturbations at the ionospheric *F*-layer heights, it is necessary to take into account essential factors such as the middle- and large-scale traveling ionospheric disturbances (TID). TID directly affect variability of the ionospheric parameters as well as those of the Earth's ionosphere waveguide. One of the most convenient approaches to these problems is to study TID dynamics in terms of the internal gravity waves (IGW) [27]. Of special interest are the IGW solitons and soliton-like wave structures as traveling in the *F*-layer stable large-scale wave formations, caused by various reasons such as the isolated magnetic substorms [10] and shear flows [5-7], solar terminator and solar eclipse [40], seismo-volcanic processes, and high-power artificial explosions [27],[40]. Here we first investigate the dynamics of the solitary nonlinear IGW (as well as TID excited by them at the heights of the ionosphere's *F*-region) for conditions close to those of the *F*-layer, by omitting the physical nature of the sources, but assuming that it has the pulse character (more details about excitation of the pulse disturbances by various physical sources are given below as well as in the references listed above). Then we consider applications of the obtained results to the problems of the generation of IGW in the regions with sharp gradients of the ionospheric parameters such as electron density,

temperature, scale heights for the ions and neutral particles, etc. As particular cases we consider the frontal regions of the solar terminator and solar eclipse. To confirm our conclusions we give some results of natural radiophysical experiments in the end.

For the isothermal model of Earth's atmosphere, we take into account $k_\perp^2 \gg k_y^2$, and $|Hk_x| \ll 1$ in the linear approximation, and expanding in k up to the fifth order, write the dispersion law as [27]

$$\omega = Vk_x \left\{ 1 + \frac{k_y^2}{2k_x^2} \pm \frac{(\gamma-2)^2}{\gamma^2} H^2 k_x^2 \left[2 + \frac{(\gamma-2)^2}{\gamma^2} \varepsilon H^2 k_x^2 \right] \pm H^2 k_z^2 \right\} \qquad (1.4.37)$$

where the second term in the right-hand side describes the diffraction divergence in the transverse direction of the wave propagation, the third and the fourth terms describe the dispersive effects of corresponding order, and the last term is the same in vertical direction; $V = 2\omega_g H$, $\omega_g = [(\gamma-1)g/\gamma H]^{1/2}$ is the Brunt–Väisälä frequency, H is the scale height of the neutral atmosphere, and $\varepsilon = -V/V_{min}^{ph}$, where V_{min}^{ph} is the minimum phase velocity of the linear oscillations. In this case, taking into account the weak nonlinearity of the dimensionless function $u = u_z/ac$ which has a sense of vertical velocity of the neutral particles, $a = \exp(z/2H)$, $c = \sqrt{gH}$ and neglecting dissipative effects, from the hydrodynamic equations for the neutral gas we obtain the equation

$$\partial_t u + ac \frac{2\gamma-1}{\gamma^2} u \partial_\xi u \pm \frac{(\gamma-2)^2}{\gamma^2} VH^2 \partial_\xi^3 \left[2u + \frac{(\gamma-2)^2}{\gamma^2} \varepsilon H^2 \partial_\xi^2 u \right] = \frac{V}{2} \int_{-\infty}^{\xi} \partial_y^2 u \, d\xi \quad (1.4.38)$$

which is written in the reference frame moving along the x-axis with the velocity V ($\xi = x - Vt$). The upper signs in (1.4.37) and (1.4.38) correspond to the positive wave dispersion, and the lower signs correspond to the negative one (without loss of generality we further assume that $V < 0$ and, as can be easily seen from (1.4.37), $\varepsilon < -1$). The obtained equation is the generalization of the Kadomtsev-Petviashvili equation (so-called Belashov-Karpman (BK) equation), for the first time it has been obtained in [10],[61] and investigated in detail in a number of works (see [27]). It is written here for the velocity of the neutral component at the heights of the F-region with $\partial_z = 0$ without dissipation and describes the nonlinear IGW solitons and nonlinear wave packets, with the structure determined by both the coefficients and the function $u(0, \xi, y)$ corresponding to the initial condition, i.e., it depends on the sort of perturbation and accordingly the type of the source as well.

The structure of the solutions for the initial disturbance of the wave pulse type corresponding to various physical sources as, for example, the terrestrial and anthropogenic factors [as well as the "quasi-one-dimensional" sources of the global character, such as the solar terminator (ST) and solar eclipse (SE)], is described in detail in [27] and depends on ε. Indeed, the 2D solitons with the algebraic (for $\varepsilon \ll -1$) or the oscillating (in the direction of propagation, for $\varepsilon \le -1$) asymptotics correspond to the upper sign in (1.4.38), whereas the dispersing wave packets and/or the 1D solitons which are stable in the case of the negative dispersion [27] correspond to the lower sign.

Let us consider the case of the upper sign in (1.4.37) and (1.4.38) and study the excitation by the IGW solitons of the middle- and large-scale TID for the conditions close to those in the F-layer. Considering the solitary IGW traveling at the near-to-horizontal angles, the continuity equation for the electron density in the F-layer is given by [27]

$$\partial_t N = \partial_z\left[(\partial_z N + N/2H_i)D_0 e^{z/H_i} - u_z\left(1 - e^{-vt'}\right)N\sin I\cos I\right] - \beta N + Q \quad (1.4.39)$$

where $N(t,\ z)$ is the total electron density, $D_0\exp(z/H_i)=D_\alpha\sin^2 I$, D_α is the ambipolar diffusion coeffcient, H_i is the scale height for ions, I is the magnetic inclination, $\beta=\beta_0\exp(-Pz/H_i)$ and Q are, respectively, the recombination rate and the ion production rate, the exponent $0\leq P\leq 2$ characterizes the gas intermixing, $u_z = acu$ is the vertical component of the velocity of neutral particles, and $t'=t-t_0$, t_0 is the moment of the start of the neutral component's perturbation. Now we approximate the profile of the electron density at the height z for fixed time momentby $N=N_1\exp(z/H_i)$, $N_1 = N\big|_{z=0}$, and obtain that solution of (1.4.39) is given by [27]

$$N(u,t) = N(u,t_0)\exp[\mathrm{G}(u,t)], \qquad \mathrm{G}(u,t) = \int_{t_0}^t g(u,t)\mathrm{d}t \qquad (1.4.40)$$

where

$$g(u,t) = C - (1/H_i + 1/2H)f(u,t), \quad C = 3a_1/H_i^2 - \beta(1-q),$$
$$f(u,t) = acu\left[1 - \exp(-vt')\right]\sin I\cos I,$$
$$a_1 = D_\alpha\sin^2 I, \quad q = Q/\beta N.$$

Here, the function u satisfies (1.4.38). When $\varepsilon\ll -1$ and the solution of (1.4.38) is the 2D soliton with the algebraic asymptotics, the solution (1.4.40) for the quasi-pulse source of IGW is shown in Fig. 1.4.14. In Fig. 1.4.15 the results of numerical simulation for initial IGW disturbances normalized on 1, $\bar{u} = u(0,\xi,y)/\max\limits_{\xi,y}\left[u(0,\xi,y)\right]$, are presented. If $\varepsilon\leq -1$ then the perturbation of the electron density N as well as the IGW soliton has the oscillating asymptotics shown in Fig. 1.4.15a.

The solution of (1.4.38) and (1.4.40) for the conditions typical for the *F*-layer gives us the following results. The solitary IGW excite in the *F*-region the solitary TID of the electron density, their structure depends on the form of IGW and the ionospheric parameters determined by the photo-chemical and dynamic processes at the height considered. The amplitude of TID increases in the direction of the geomagnetic latitude $\varphi_m=45°$, the wave front steepens, and at the latitude $\varphi_m=45°$ the wave becomes similar to the shock wave.

The two-fold increase of the IGW amplitude results in the increase of the TID amplitude: 35% for $\varepsilon\ll -1$; close to 100-105% for $\varepsilon\leq -1$. For all the studied cases we note the phase shift of TID relative to the phase of IGW ($\Delta t\sim 0.5-5$ min) and the effect of the relaxation of the electron density perturbations which increase with the decreasing ε characterizing essentially the medium's dispersion. Figure 1.4.15 shows the simulation results for IGW solitons with a velocity on the order of 200 m/s at $z=0$ and $I = 63.4°$.

Thus such ionospheric characteristics as the height of the maximum and the critical frequency of the *F*-layer increase proportionally to the TID amplitude when the 2D nonlinear IGW propagates, as well as experience relaxation similar to the relaxation of the electron density N'.

In addition to the general study of the dynamics of solitary waves in the *F*-region of the Earth's ionosphere, the middle-scale and large-scale wave effects associated with
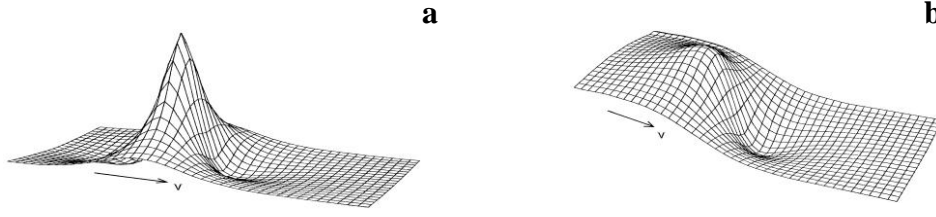
a **b**

Figure 1.4.14. IGW soliton $u(\xi,y)$ for $\varepsilon = -12$ (a) and associated perturbation of the normalized electron density $N' = \{[N(u,t) - N(0,t)]/N(0,t)\} \times 100\%$ (b).
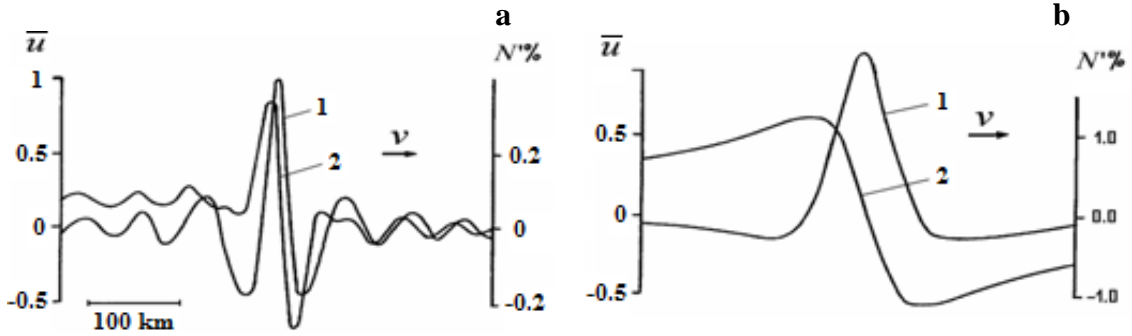
a **b**

Figure 1.4.15. Profiles of the perturbations (in the relative values of u where the amplitude of the initial condition $u(0, \xi, y)$ is normalized on 1) at $y=0$: IGW (the curve 1) and TID (N') (the curve 2): $\varepsilon = -1.2$ (a) and $\varepsilon = -12$ (b).

motions of the fronts of ST and SE were investigated numerically within the framework of the above developed weakly nonlinear approximation neglecting the dissipation effects. Following [40] let us consider, at first, the wave effects caused by ST motion. Let's define ST as the area separating space, shined by a full disk of the Sun, from area of the full shadow rejected by the Earth.

At heights of the *F*-layer of ionosphere where concentration of the charged particles is a lot of above, than in underlaying areas, at the ST movement, in connection with infringement of balance of ionization and the dynamic balance by it, caused by fast change of a degree of light exposure in the frontal zone of ST, the area of sharp gradients of the basic ionospheric parameters (electron density, electron and ion temperature, recombination rate, ion production rate, etc.) moving with a ST speed (linear speed of rotation of the Earth at height of *F*-region) is formed.

Let us consider the dynamical model of the *F*-layer [40] considering time (of corresponding periods) dependences of ionospheric characteristics, defining processes of diffusion, ionization and recombination at heights of *F*-region, i.e. effects of influence of ST on a plasma, associated with sunrise-sunset processes. This dynamical model is the following set of the equations:

$$N_0 = N_{0m} \exp\left[-\gamma_N (t - t_m)^2 / t_{ch}^2\right],$$

$$Q(z,\chi) = Q(h_0,0) \exp\left(1 - \sec\chi\, e^{-\zeta}\right) \exp(-\zeta), \quad \beta_0 = Q(h_0,0)/N_{0m},$$

$$D_0 = D_{0m} T_i, \quad H = (kT_e)/(m_e g), \quad H_i = k(T_e + T_i)/(m_i g), \quad (1.4.41)$$

$$T_e = T_{em} \exp\left[-\gamma_e (t - t_m)^2 / t_{ch}^2\right], \quad T_i = T_{im} \exp\left[-\gamma_i (t - t_m)^2 / t_{ch}^2\right],$$

$$P = 1 + \exp\left[-(t - t_m)^2 / t_{ch}^2\right],$$

where the functions describe background (in relation to time scales of investigated disturbances) changes at heights of the *F*-region and are defined by the expressions

$$N(t) = N_0(t)N_1(z), \ \beta = \beta_0 \exp\left(-P\zeta\right), \ D_0 = D_\alpha \sin^2 I \exp\left(-\zeta\right) \tag{1.4.42}$$

where $\zeta = z/H_i$, $z = h - h_0$, $h_0 = H_i \ln \alpha$ corresponds to the electron density maximum; $\alpha = 2H_i\sqrt{\beta_0/D_0}$; χ is the zenith angle of Sun; t_{ch} characterizes the time scale, the index *m* corresponds to the maximal value of function; γ_k are some functions defining effect of influence on corresponding component; other designations are standard in physics of ionosphere.

Let's note the following important circumstance. At a choice of corresponding scales and a kind of functions γ_k the generalized dynamic model (1.4.41), (1.4.42) will describe a time course of the basic ionospheric parameters for corresponding "source", that is equivalent to the complement of the problem by initial and boundary conditions.

If, for example, to assume that $t_{ch} = 24$ hours and choose the characteristic for the *F*-layer values of the amplitudes of $N_{0m}, Q(h_0,0), D_{0m}, T_{em}, T_{im}$ and time momentes t_m corresponding to the maxima of corresponding functions, we obtain that the model (1.4.41), (1.4.42) describes in some approach (the degree of approach is defined by a choice of functions γ_k, at $\gamma_k = \text{const}_k$ we have zero approach) a daily course of the basic ionospheric parameters [40]. In this case, besides other, the model can be used for investigation of dynamics of middle- and large-scale wave structure of the *F*-layer in areas with sharply expressed gradients of the ionospheric characteristics (morning and evening sectors) on a background of slow (daily) changes.

From the continuity equation for the electron density in the *F*-layer (1.4.39), considering the wave disturbances propagating under corners, close to a horizontal, at $N_1(z) = \exp\zeta$ with due account of the change $t \to \xi - Vt$ it is easy to obtain (where *V* is the ST velocity at the corresponding height *h*, and ξ is the spatial coordinate along **V**) in the reference frame related to the source the expression for vertical component of the neutral particles' velocity [27]:

$$u_z = \left[ac\left(1 - e^{-vt'}\right)\sin I \cos I\right]^{-1}$$
$$\times \left\{ V\frac{H_i}{N_0}\partial_\xi N_0\left(1 - e^{-\zeta}\right) + \left[\beta\frac{H_i}{1-P}\left(1 - e^{(1-P)\zeta}\right) + \frac{Qz}{N_0}\right]e^{-\zeta} + \frac{3}{2}\frac{D_0}{H_i}e^\zeta \right\} \tag{1.4.43}$$

where $t' = \xi/V$, and the values of parameters are defined by the dynamical model of the *F*-layer (1.4.41), (1.4.42) with due account of dependences of basic parameters on time.

In approach of an isothermal ionosphere, taking into account the weak nonlinearity of the function $u = u_z/ac$, $a = \exp(z/2H)$, $c = \sqrt{gH}$ and weak dispersion ($|Hk_x| \ll 1$), the BK equation (1.4.38) and corresponding dispersive equation (1.4.37) are valid. For such global phenomenon as ST it is possible with sufficient accuracy to suppose that $\partial/\partial y = 0$. Making the changes $u \to Vu/\alpha$, $\xi \to (-\delta/V)^{1/4}\xi$, $t \to (-\delta/V^5)^{1/4}t$, where $\alpha = ac(2\gamma - 1)/\gamma^2$, $\delta = [(\gamma - 2)/\gamma]^4 \varepsilon VH^4$, $\varepsilon = -V/V_{min}^{ph}$, $\gamma = c_p/c_v$ and omitting strokes, write eq. (1.4.38) for $\partial/\partial y = 0$ in a more convenient form:

$$\partial_t u + u\partial_\xi u + 2(-\varepsilon)^{-1/2}\partial_\xi^3 u - \partial_\xi^5 u = 0. \tag{1.4.44}$$

Equation (1.4.44) is the 1D analogue of the BK equation and it is written in the

reference frame connected with ST. For eq. (1.4.44) with the initial condition (1.4.43) and zero boundary conditions (the last are valid for the characteristic periods of a problem, sufficiently small in comparison with the length of a day), using the model (1.4.41) and algorithms developed in [21], we solved the Cauchy (initial) problem at $z = 0$, H, $2H$. The values of the ionospheric parameters of model were chosen close to characteristic ones for F-layer in conditions of a daily cycle of winter and summer seasons.

Figure 1.4.16 shows the examples of simulation results obtained in [40] for geomagnetic latitude $\varphi_m=45°$. As one can see from figures the obtained solutions testify to generation by the ST front both in morning, and in evening sectors some kind of solitons-like wave "forerunners" in the neutral particles velocity u with the periods ~40-60 mins which scales are essentially various for summer and winter seasons and are defined by a lot of factors: height z, geomagnetic latitude, value of dispersion ε depending, in its turn, from values of some ionospheric characteristics, and also features of change of ionospheric parameters in a concrete daily cycle. Simulation for $\partial/\partial y \neq 0$ [eq. (1.4.38)] shows that, generally, the picture for $z=0$ is the train of 2D solitons-like waves (with $k_x \gg k_y$) similar to the multisoliton solutions of the KdV equation (the case $y=0$). For $z = H$, $2H$ the qualitative form of the solution is maintained, although they are less regular and (on the average) the largeramplitude waves. The characteristics of such soliton-like formations strongly depend on the season and the ionospheric parameters.
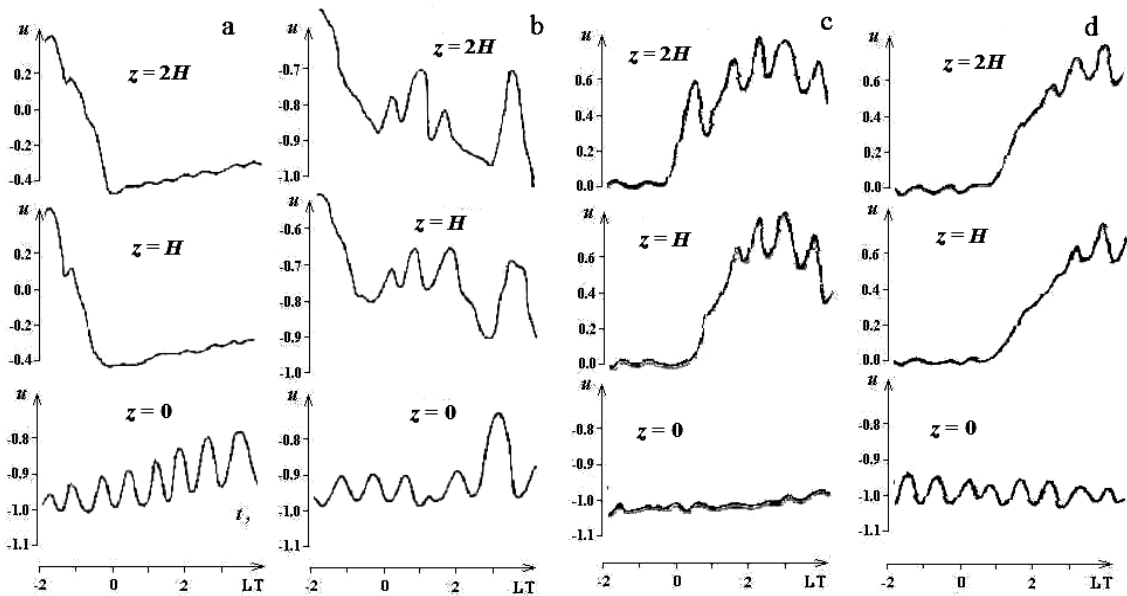

Figure 1.4.16. Perturbations of the neutral particles velocity u in the F-layer of ionosphere caused by ST (a, b – morning sector; c, d – evening sector): a, c) winter, b, d) summer; $t=0$ corresponds to the moment of sunrise (a, b) and sunset (c, d) at height $z=0$.

Figures 1.4.17 and 1.4.18 show the results, obtained in the experiments of 1-min vertical sounding of the ionosphere fulfilled in the radioobservatory of Kazan Federal University (Nasyrov, Personal communication, 2014). In both figures one can see also the solitons-like wave "forerunners" in the electron density in the maximum of the F-layer N_mF2 with T ~50-60 mins. Figure 1.4.18 shows also daily course of N_mF2

calculated with the use of model IRI-2012 (curve 2) for the same time. One can note that this ST effect is not account in any way by IRI-2012 model.

If in eqs. (1.4.41), (1.4.42) to choose t_{ch} corresponding such source as a SE spot, that the model will describe quite adequately the wave effects in the *F*-layer of the ionospheres associated with passage of such disturbing factor as SE [40]. Such investigations showed (see example in Fig. 1.4.19) that the characteristic periods of "forerunners" of the SE front are ~3-10 min, and its spatial scales are defined by the parameters of the *F*-layer.
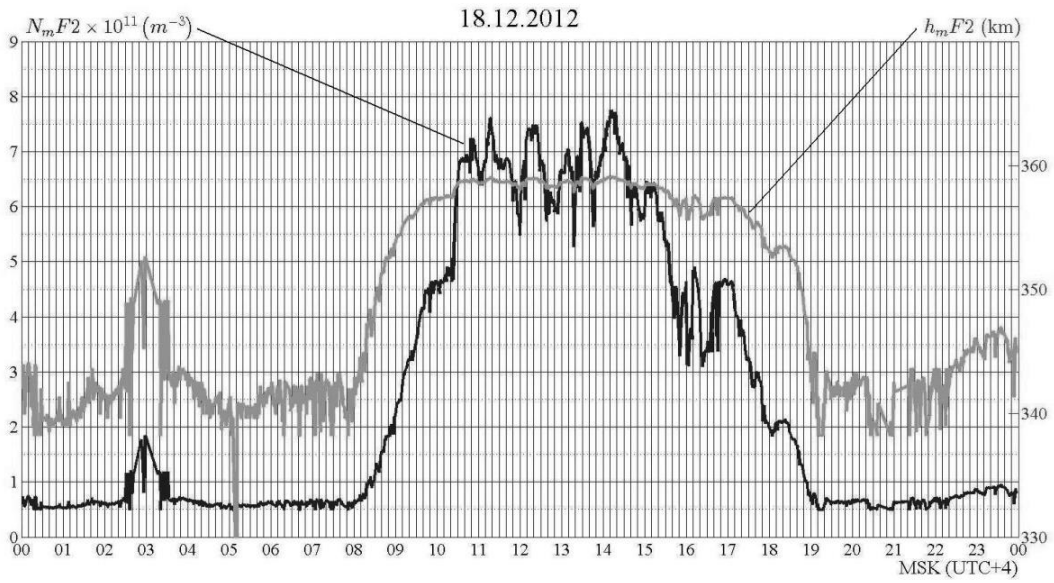

Figure 1.4.17. Daily course of parameters h_mF2 and N_mF2 (winter, 1-min vertical sounding) (Nasyrov, Kazan Federal University, Personal communication, 2014).
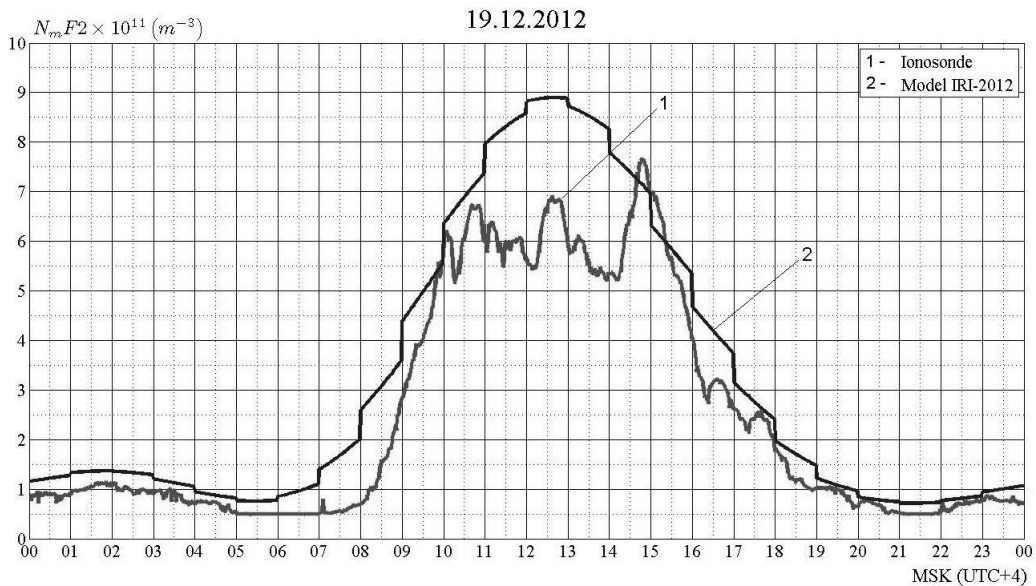

Figure 1.4.18. Daily course of N_mF2 (winter, 1-min vertical sounding) and model IRI-2012 (Nasyrov, Kazan Federal University, Personal communication, 2014).

Simulations for the conditions corresponding to the partial solar eclipse observed on March 18, 1988, and the sunrise and sunset periods on March 1–10, 1990, (an

interval of the International Geophysical Calendar) agree well with the results of special targeted experiments on the passive slanted sounding of the ionosphere done in these periods in the Far-Eastern region of Russia (see refs. in [27]). Thus we conclude that despite some idealization of the problem, the approach based on the generalized KP equation allows us to predict the effects of the TID dynamics in the *F*-region of the Earth's ionosphere reasonably well.

In conclusion, we note that in real conditions in the ionosphere it is necessary to take into account dissipative processes which really lead to decreasing of the perturbations. In this case eq. (1.4.38) should be complemented by the dissipative term of form in the left-hand side [27] with the factor

$$\nu = (\rho_0/2\rho)\left(c_\infty^2 - c_0^2\right)\tau\int_0^\infty \mu\phi(\mu)\,d\mu = (2\rho_0)^{-1}\left[4\eta/3 + \varsigma + \gamma(1/c_v - 1/c_p)\right]$$

where c_∞ and c_0 have a sense of the "highfrequency" and "lowfrequency" sound. The case $\nu \neq 0$ was investigated in detail in [27], where it was shown that the presence of
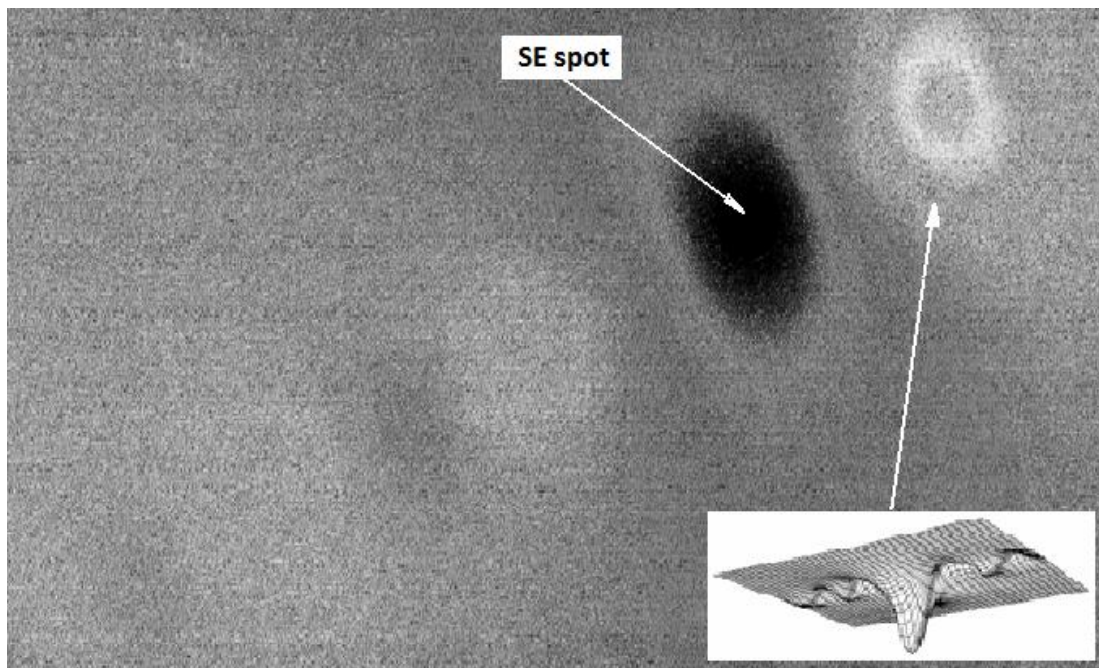

Figure 1.4.19. General view of numerical solution of the GKP equation [function $u(\xi, y)$] for the pulse source of type of the SE spot [(x, y)-plane] $V \approx 1667$ km/h = 463 m/c (linear velocity of the Earth rotation at height of the *F*-layer maximum).

dissipative term leads to both the exponential decrease of the amplitude with the rate $\Gamma(t) \sim \nu$ and effects of destruction of the structure and the symmetry of the IGW soliton (see example in Fig. 1.4.20) accompanied by the relaxation in the recovery of the electron density after the wave passes [40].

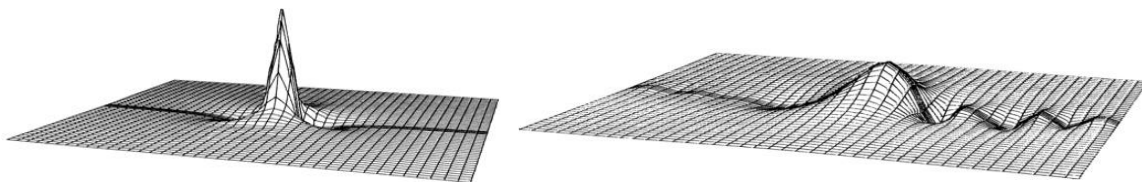The effects of stochastic fluctuations of the wave field $u(t,x,y)$ on the evolution of

Figure 1.4.20. Evolution of 2D IGW soliton for $\nu = 1$, $\varepsilon = -1.2$: $t = 0$, 0.2.

the ionospheric perturbation can also be accounted for in the basic equations. Thus, accordingly, (1.4.38) should be complemented by the term like $\chi(t, x, y)$. In the case of the lowfrequency fluctuations when $\chi=\chi(t)$, eq. (1.4.38) for $\varepsilon=0$ was investigated analytically in [14].

   The obtained results can be easily applied to (1.4.38) with $\chi=\chi(t)$ on the left-hand side. Thus the interpretation of the results [14] in terms of problem (1.4.38) and (1.4.39) enables us to conclude that even small stochastic fluctuations of the wave field lead to the damping of the solitary IGW (with its propagation) accompanied by the transform of the wave to an oscillatory structure. Figure 1.4.21 shows an example of the results of numerical simulation of the IGW soliton evolution in medium with presence of stochastic fluctuations of the wave field in the form of a Gaussian noise. One can see that soliton with evolution acquires a short wave structure and it is destroyed. In the case $\chi(t, x, y)$, however, the analytical study of the process becomes too complicated,
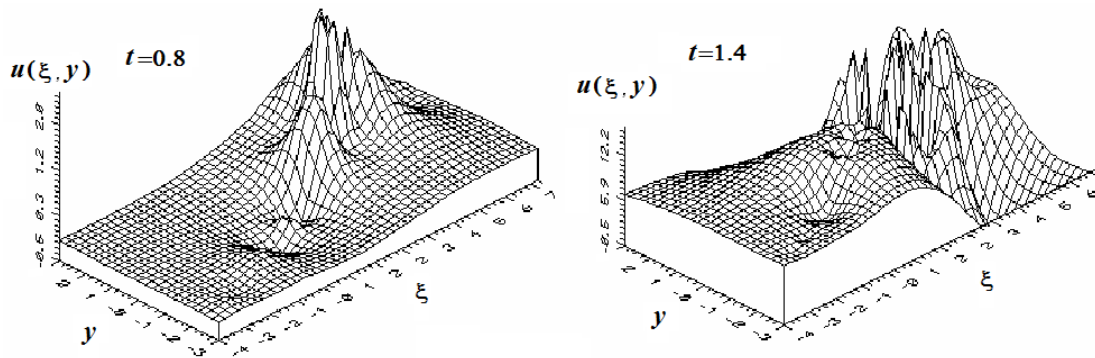
Figure 1.4.21. Evolution of 2D IGW soliton with presence of stochastic fluctuations of the wave field: the Gaussian noise $\chi=\chi(t)$ for the standard deviation $\sigma = 0.02$ ($\varepsilon<<-1$).

and in [27] numerical integration of (1.4.38) and (1.4.39) with the stochastic term was done. The obtained results appear to be qualitatively similar to the case $\chi=\chi(t)$, namely, the decrease of the amplitude of the solitary oscillating IGW is observed, with the subsequent destruction of the wave.

   Let us note that the problem of destroying the large-scale wave disturbances and transit of them into chaotic regime was solved also in [66],[67], and physical reasons which lead to developing of chaos and order-disorder transition can be the same as we noted above, on a level with other reasons noted in [66],[67].

2. VORTICAL STRUCTURES IN COMPLEX CONTINUOUS MEDIA

2.1. Introduction

In this part the results of analysis and numerical simulation of evolution and interaction of the *N*-vortex structures of various configuration and different vorticities in the continuum including atmosphere, hydrosphere and plasma are presented. It is found that in dependence on initial conditions the regimes of weak interaction with quasi-stationary evolution and active interaction with the "phase intermixing", when the evolution can lead to formation of complex forms of vorticity regions, are realized in the *N*-vortex systems. For the 2-vortex interaction the generalized critical parameter determining qualitative character of interaction of vortices is introduced. It is shown that for given initial conditions its value divides modes of active interaction and quasi-stationary evolution. The results of simulation of evolution and interaction of the two-dimensional and three-dimensional vortex structures, including such phenomena as dynamics of the atmospheric synoptic vortices of cyclonic types and tornado, hydrodynamic 4-vortex interaction and also interaction in the systems of a type of "hydrodynamic vortex – dust particles" are presented. The applications of undertaken approach to the problems of such plasma systems as streams of charged particles in a uniform magnetic field **B** and plasma clouds in the ionosphere are considered. It is shown that the results obtained have obvious applications in studies of the dynamics of the vortex structures dynamics in atmosphere, hydrosphere and plasma.

2.2. Basic equations

Here we study numerically the interaction of the vortex structures (so-called FAVRs, see [101]) in the continuum, and, specifically, in fluids (such as atmosphere and hydrosphere) and plasmas in two-dimensional (2D) approximation, when the Euler-type equations are applicable. The Euler equation for the inviscid incompressible fluid $\frac{d\boldsymbol{u}}{dt} = \boldsymbol{F} - \frac{1}{\rho}\operatorname{grad} p$ in the 2D case takes form of the following set:

$$\frac{\partial u}{\partial t} + u\frac{\partial u}{\partial x} + v\frac{\partial u}{\partial y} = F_x - \frac{1}{\rho}\frac{\partial p}{\partial x},$$

$$\frac{\partial v}{\partial t} + u\frac{\partial v}{\partial x} + v\frac{\partial v}{\partial y} = F_y - \frac{1}{\rho}\frac{\partial p}{\partial y}. \tag{2.1}$$

Add here the equation of continuity:

$$\frac{d\rho}{dt} + \rho\left(\frac{\partial u}{\partial x} + \frac{\partial v}{\partial x} + \frac{\partial w}{\partial x}\right) = 0$$

where for ideal incompressible fluid $d\rho/dt = 0$ and, hence,

$$\frac{\partial u}{\partial x} + \frac{\partial v}{\partial x} + \frac{\partial w}{\partial x} = 0. \tag{2.2}$$

Introduce further the flow function

$$\psi = \int |\boldsymbol{u}|\sin\alpha\, ds$$

where $\boldsymbol{u}$ is a fluid velocity, s is a displacement, α is an angle between $\boldsymbol{u}$ and s (function ψ is positive when the streamlines are directed clockwise). It is easy to show, that

$$u = \frac{\partial\psi}{\partial y}, \qquad v = -\frac{\partial\psi}{\partial x}. \tag{2.3}$$

Function

$$\text{rot } \mathbf{u} = \begin{vmatrix} \mathbf{i} & \mathbf{j} & \mathbf{k} \\ \dfrac{\partial}{\partial x} & \dfrac{\partial}{\partial y} & 0 \\ u & v & 0 \end{vmatrix} = \left(\dfrac{\partial v}{\partial x} - \dfrac{\partial u}{\partial y} \right) \mathbf{k}$$

is the vector of vortex, and for flat motion

$$\zeta = \frac{\partial v}{\partial x} - \frac{\partial u}{\partial y} \tag{2.4}$$

is a vorticity.

Now present the Euler equations in new variables – vorticity and flow function, making differentiation of the equations in (2.1) on y and x accordingly. Then, in the absence of external forces, after elementary transformations we obtain:

$$\frac{\partial \zeta}{\partial t} + u \frac{\partial \zeta}{\partial x} + v \frac{\partial \zeta}{\partial y} + \zeta \left(\frac{\partial v}{\partial y} + \frac{\partial u}{\partial x} \right) = 0. \tag{2.5}$$

As, according to eq. (2.2) for a flat motion $\dfrac{\partial v}{\partial y} + \dfrac{\partial u}{\partial x} = 0$, that from eq. (2.5) we have

$$\frac{\partial \zeta}{\partial t} + u \frac{\partial \zeta}{\partial x} + v \frac{\partial \zeta}{\partial y} = 0. \tag{2.6}$$

Equation (2.6) in variables "vorticity – the flow function" is the equation of carry of a vortex and is nonlinear, as u and v are the functions of ζ. The last two terms in (2.6) are convective ones, and the convection in this case means that the vortex is carried on a current.

With due account of (2.3) we can rewrite (2.4) in the form $\zeta = \dfrac{\partial}{\partial x} \left(-\dfrac{\partial \psi}{\partial x} \right) - \dfrac{\partial}{\partial y} \left(\dfrac{\partial \psi}{\partial y} \right)$, that is the Poisson equation for the flow function

$$\Delta \psi = \frac{\partial^2 \psi}{\partial x^2} + \frac{\partial^2 \psi}{\partial y^2} = -\zeta. \tag{2.7}$$

Thus, the dynamics of vortical structures in their flat movement for the case of an inviscid incompressible fluid is described by the set of equations of carry of a vortex (2.6) and the Poisson equation (2.7) for the flow function.

Simple model of 2D magnetized plasma [94] is the quasi-particles (or the charged filaments aligned in a uniform magnetic field $\mathbf{B}$) which move with the central-directed velocity $\mathbf{E} \times \mathbf{B} / B^2$. The equations of motion of these quasi-particles (filaments) have the form

$$e_i \frac{\mathrm{d}\, x_i}{\mathrm{d}\, t} = \frac{1}{B} \frac{\partial \mathrm{H}}{\partial y_i}, \qquad e_i \frac{\mathrm{d}\, y_i}{\mathrm{d}\, t} = -\frac{\partial \mathrm{H}}{\partial x_i} \tag{2.8}$$

where e_i is the charge per unit length of the filament and

$$\mathrm{H} = \sum - e_i e_j \ln \left(\left| \mathbf{r}_i - \mathbf{r}_j \right| \right) \tag{2.9}$$

is the Hamiltonian which has the sense of energy of Coulomb interaction.

In a continuous limit this 2D plasma satisfies the equations:

$$\frac{\partial \rho}{\partial t} + \boldsymbol{v} \cdot \nabla \rho = 0, \quad \boldsymbol{v} = -\frac{\widehat{z} \times \nabla \psi}{B}, \tag{2.10}$$

$$\nabla^2 \psi = -\rho, \tag{2.11}$$

where ρ is the charge density, $\boldsymbol{v} = (v_x, v_y)$, ψ is the potential of an electric field and $\nabla = (\partial/\partial x,\ \partial/\partial y)$. Independently on the scale of coefficient B these continuous equations are formally identical to the equations for the 2D movement of an inviscid incompressible fluid (2.6), (2.7) where ρ is the *z*-component of vorticity ζ, and ψ is the flow function. If the vorticity is presented by discrete vortexes (with circulations e_i) then the motion of a fluid is described by the Hamilton equations with *B*=1. Note, that the equations of motion of clouds of ideal ionospheric plasma have a similar form.

Another 2D continuous models can be represented by vortexes or the filaments (quasi-particles) with the Coulomb interaction [95] and include the Debye radius of shielding in the Poisson equation (2.11). At this, it is necessary to proposed that the ions move with the guiding-centre velocity, and electrons (for example, moving along a field **B**) have the Boltzmann distribution. Then ionic current is still described by (2.10), and eq. (2.11) is rewritten in the form of

$$\nabla^2 \psi - k^2 \psi = -\rho, \tag{2.12}$$

where $k^2 \psi$ is the Debye shielding. This model is also presented by charged filaments (quasi-particles) satisfying (2.8), but, unlike (2.9), with the Hamiltonian

$$\mathrm{H} = \sum -e_i e_j k_0(k\,|\mathbf{r}_i - \mathbf{r}_j|), \tag{2.13}$$

which describes the shielded Coulomb interaction between filaments.

One more model of plasma which can be expressed in the similar form, has been introduced in [52]. Its distinctive feature is inclusion of the ionic-polarized current through the equation of motion of ions

$$\frac{\mathrm{d}\mathbf{v}}{\mathrm{d}t} = \frac{e}{M}(-\nabla\varphi + \mathbf{v} \times \mathbf{B}). \tag{2.14}$$

The electrons have also the Boltzmann distribution here but the Debye length is supposed tending zero so, that full charging neutrality is conserved. In this case k^{-1} is not Debye length, but it is the ion Larmour radius (electron temperature), and shielding is an indirect effect of the ion-polarized current. Let us note here that in space plasmas, in addition to vortices with dimensions of the order of the ion Larmor radius calculated at the electron temperature the vortical structures with spatial scales of the order of the Larmor radius calculated at the ion temperature can exist [1], however "classic" model of Hasegawa-Mima [52] does not take into account them. In this case the general structure of the equations is the same, but it is necessary to consider k^{-1} as some generalized ion Larmour radius.

The hydrodynamical model of a rotating fluid [43] describing a motion of the Earth atmosphere also corresponds to shielded interaction. Atmospheric currents in a horizontal plane are described by the equation:

$$\frac{\mathrm{d}\mathbf{v}}{\mathrm{d}t} = -g\nabla h + \mathbf{R}v \times \widehat{\mathbf{z}}, \tag{2.15}$$

where *h* is atmospheric depth, and **R** is the Coriolis force. Small change of *h* satisfies the equations identical to model of shielded guiding-centre plasma and a role of length of shielding plays the Rossby radius, $\sqrt{gH_0}/R$.

There are also some other examples of vortex motion in plasmas and rotating fluids which were discussed in detail, for example, in [77],[85]. They also use hydrodynamic description and can be reduced to the equations similar to the presented above.

Thus, write a set of equations describing a motion of a fluid, gas or plasma in the

generalized variables:

$$\frac{\partial \rho}{\partial t} + \mathbf{v} \cdot \nabla \rho = 0, \qquad \mathbf{v} = -\frac{\hat{\mathbf{z}} \times \nabla \psi}{B},$$ (2.16)

$$\nabla^2 \psi - f = -\rho.$$

In dependence on the considering medium the functions and variables in eqs. (2.16) will have various physical sense (Table 2.1), and the set (2.16) will get the form of one of described by the eqs. (2.6)-(2.15) ones.

Table 2.1. Sense of the variables in dependence on type of medium

Function	Fluid, gas	Plasma
B	$B = 1$	module of a vector of a magnetic induction
ψ	flow function	potential of an electric field
ρ	z-component of vorticity	line density of a charge
F	$f = 0$	$f = 0$ – plasma with Coulomb interaction; $f = k^2 \psi$ – plasma with shielded Coulomb interaction

Note that function f has various sense in dependence on considering model of medium. So, for an inviscid incompressible fluid and also for charged filaments (quasi-particles) with the Coulomb interaction $f = 0$, for filaments (particles) with the shielded Coulomb interaction $f = k^2 \psi$. Further we consider only a case when $f = 0$, which corresponds to rotation of local vortical structures in a fluid or to evolution of the charged filaments (quasi-particles) in a homogeneous magnetic field. Generalization for $f = k^2 \psi$ is rather trivial.

2.3. Modeling technique

For numerical simulation we used the contour dynamics (CD) method [101], to some extent modified (see [26] for detail). This has yielded us a possibility not only to observe evolution of a single vortex, but also to study the interaction between vortices having different sizes, vorticities and symmetry orders (different modes), and also to simulate the 3D vortex structures. A general idea of CD method is that the interaction between the boundaries of the regions with constant ζ is considered, and due to this the dimension of the problem decreases on unit. Analytical solution of the Poisson equation (2.16) with $f = 0$ for flow function ψ has the form [23]

$$\psi = -\frac{1}{2\pi} \iint d\xi\, d\eta\, [\ln r] \rho(\xi, \eta),$$ (2.17)

where $\ln r$ is Green's function of eq. (2.2), and $r = [(x-\xi)^2 + (y-\eta)^2]^{1/2}$. Then a value of velocity can be obtained by differentiation of integral (2.17), namely:

$$\mathbf{u}(x, y) = \rho_0 \oint_{\Gamma} [\ln r][\mathbf{e}_x\, d\xi + \mathbf{e}_y\, d\eta].$$ (2.18)

Further, obtain the change of the contour coordinates with time by solving differential equation $\mathbf{u}(x, y) = \dot{x}\mathbf{e}_x + \dot{y}\mathbf{e}_y$. For the computer simulation of the vortex structures the

contour's boundary is divided into *N* lattice points (moreover, the point quantity should be rather great), and the temporal evolution is computed for each point. Thus eq. (2.18) is written in the discrete form using the 3-layer difference scheme with approximation order $O(\tau^2)$:

$$\boldsymbol{x}_m^{p+1} - \boldsymbol{x}_m^{p-1} = 2\tau \sum_{n=1}^{N} (\Delta u)_n^p \left(\cos \theta_n^p \, \boldsymbol{e}_x + \sin \theta_n^p \, \boldsymbol{e}_y \right), \qquad (2.19)$$

where $\operatorname{tg} \theta_n = \dfrac{y_m - y_n}{x_m - x_n}$, which stability is guaranteed by the condition $\tau \le h_n / \max\limits_{x,y} \{u,v\}$ where *u* and *v* are the *x* and *y* components of the velocity of the contour point, respectively. We omit here the details of the CD method and nuances of its modification for modeling of the FAVR evolution. You can find them in [26]. Equation (2.19) allows us to found a value of velocity of each point of contour in dependence on influence to it of the points of both the same contour and the contour interacted with it. So, one can observe the time evolution of the vortex structure setting its initial form.

2.4. Numerical simulation and discussion

Let us consider the results of numerical simulation in terms of the vortex motion of the inviscid incompressible fluid, as more visual and directly applicable to physics of the atmosphere and hydrosphere.

For the first time the CD method has been used for simulation of evolution of 2D 2-vortex systems of FAVRs in [101], after that there was a whole series of similar studies of different authors in which, however, the problems of evolution of more general *N*-vortex systems and possible modes of vortical interaction depending on their initial configuration were not considered. For the first time such studies have been undertaken in [20].

In general, to study the evolution of vortex structures with different symmetry orders it is necessary to insert a small amplitude perturbation $r = R_0 [1 + \varepsilon \cos (m\alpha - \omega_m t)]$ (where R_0 is a conditional radius, ε is an eccentricity, *m* is symmetry order (mode), α is an angle and $\omega_m = \rho_0 (m-1)/2$) to the circle region with constant vorticity. But, taking into account that the results of evolution for one and two vortices with different *m* were described in detail in [33],[36], let us stay on results on interaction of FAVRs and consider the most simple cases of circle vortices when *m*=1 and, therefore, $\omega_m = 0$. As it was found in [25] for such FAVRs the result of the evolution depends on sign of vorticity ("polarity" of vortex) ζ [$\zeta = \rho$ in eqs. (2.16)] and the distance δ between boundaries of vortices. We fulfilled a number of the series of numerical simulations for study of 2-vortex interaction, the interaction in the *N*-vortex systems, including interaction between the hydrodynamical vortex structures and the dust particles in a plasma, and also interaction of two 3D plane-rotating vortex structures within the framework of many-layer model of medium, in dependence on some parameters: initial distance between vortices, value and sign of their vorticities, and spatial configuration of the vortex system. Consider the examples of the basic results.

2.4.1. Two-vortex interaction

For two circle vortices having opposite polarities we observed that at an initial stage they approach and further move in the same direction, rotating in opposite directions (Fig. 2.1). Thus, the vortices practically don't interact independently on value of δ.
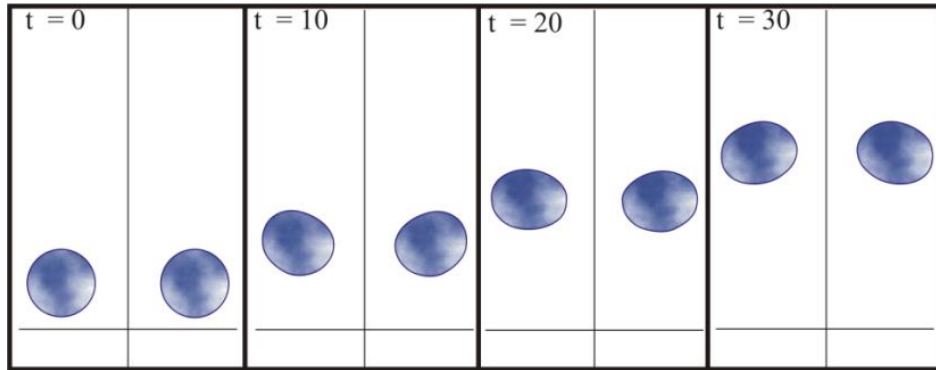

Figure 2.1. Evolution of two circle vortices with opposite polarities
($\zeta_1 = -1$ and $\zeta_2 = 1$).

For the circle vortices having the same polarities the result of evolution depends essentially on δ. So, our results show that at interaction of a pair of circle vortices some cases can take place:

1.   For rather big δ they, on a level with rotation about their own axes, rotate around the common center and one can observe a deformation of the vortices − they are drawn out, taking the form close to elliptical, but in due course return to an original state [Fig. 2.2(a)], thus their interaction is weak and it is reduced to a cyclic change of their shape (so-called "quasi-recurrence" phenomenon [101] is observed).
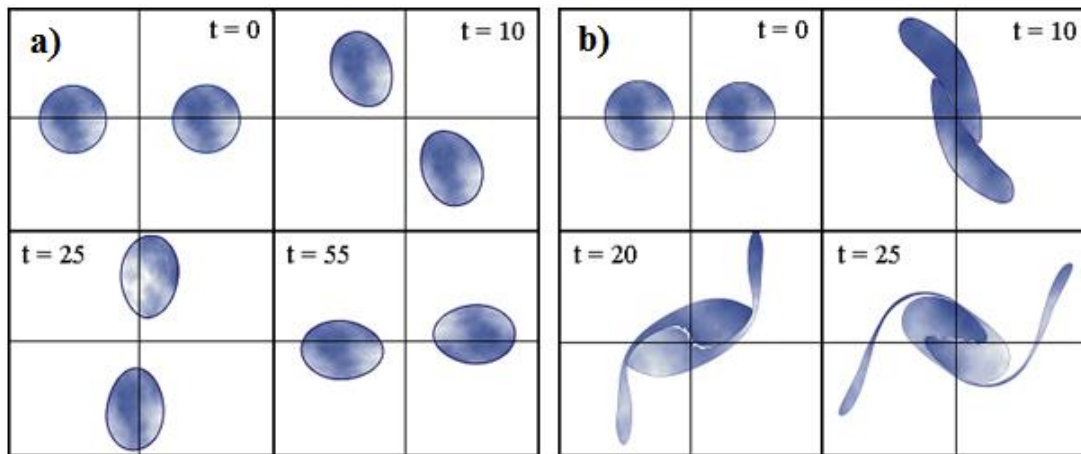

Figure 2.2. Interaction of two vortices with $\zeta_1 = \zeta_2 = -1$ at initial distance
between each other: a) δ = 2*d*; b) δ = *d*/2.

2.   With decreasing of a distance the vortices start ever more to be deformed during interaction, that results in formation of the cusps [20]. At further evolution it causes appearance of the filaments of vorticity [20] (see. Fig. 2.3) and, as a result, the vortices disintegrate.

3.　For rather small δ the vortices, on a level with rotation about their own axes and around their common center, interact forming a common vortex region which consists of the vorticities of more small scales [Fig. 2.2(b)]. Thus, in this case the regime of active interaction with the "phase intermixing" takes place, and different configurations are possible too from small coupling of the vortices down to full junction of two vortices [68].
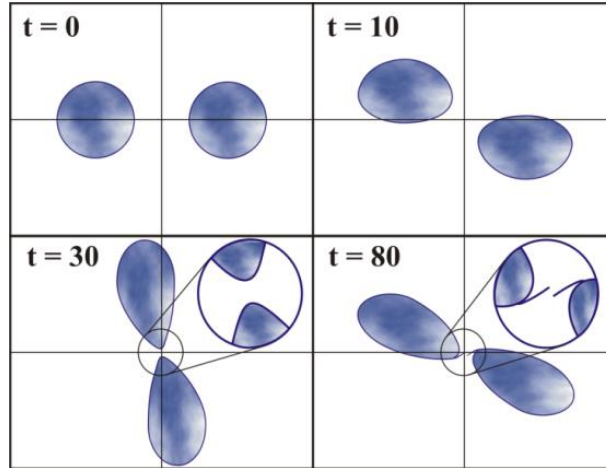

Figure 2.3. Formation of filaments of vorticity.

In our numerical experiments we have found that critical initial distance for two interacting vortices dividing these two types of interaction $\delta_{cr} = 3d/4$, where d is the vortex diameter.

Note, that qualitative character of interaction of the vortices with different symmetry orders is, in general, the same, but in this case the vortex structures with more high symmetry order m liable to more high deformation (the vortex filaments appear) and have the greater tendency to destruction [24].

To make more strong analysis we shall suppose, that the qualitative change (some kind of a "jump") in a character of interaction of two vortex regions happens with transition to a "phase intermixing" state. The problem is to find some generalized critical parameter describing the interaction of the vortices in terms of such jump, which value would allow us to predict the qualitative character of the result of vortex interaction.

As such parameter we offer to use the following function of the basic characteristics of interacting vortex structures corresponding to their state at $t = 0$:

$$\xi = \frac{S}{l^2} \frac{\zeta_1}{\zeta_2} \left(1 - e_0\right)^{-1} \left(1 + \sin^2 \theta\right),$$ (2.20)

where S is the area of each interacting FAVR[3], l is the distance between their centers, ζ_1 and ζ_2 are the values of the vorticities (and $\zeta_1 \geq \zeta_2$), $e_0 = (e_1 + e_2)/2$ is the eccentricity averaged on two vortices, and $\theta = \theta_1 + \theta_2$ is the sum of angles of inclination of large axes of the vortex ellipses concerning a line, connecting their centers (see Fig. 2.4).

---

[3] Suppose, for a determinacy, that the areas of interacting vortices $S_1 = S_2 = S$.
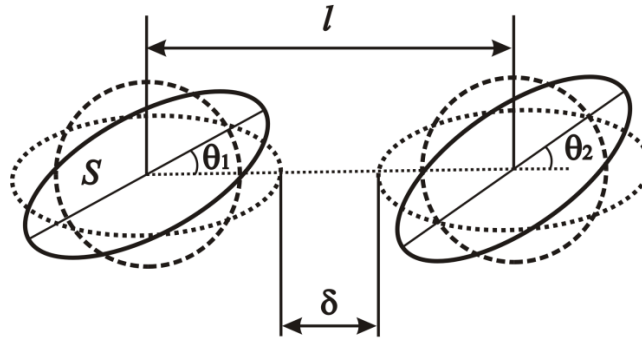
Figure 2.4. Illustration to definition of the initial state parameters of vortex system.

Let us introduce the following denotations for critical parameters corresponding to an initial state of a vortex system and determining the transition to the "phase intermixing" state with change of the sizes and positional relationship of vortices, ratio of their vorticities, eccentricity and angle θ, respectively:

$$\alpha = S/l^2, \quad \beta = \zeta_1/\zeta_2, \quad \gamma = (1-e_0)^{-1}, \quad \theta_0 = 1 + \sin^2\theta$$

and write function ξ (2.20) in the following form

$$\xi = \alpha\beta\gamma\theta_0. \tag{2.21}$$

To justify the expediency of offered criterion (2.21) we fulfilled some series of numerical experiments in which the critical values of parameters α, β, γ and θ_0 for vortex regions of the circle and elliptical form, as the models most often meeting in numerous applications, were calculated.

With the purpose finding of the critical value of the parameter α, the system consisting of two circle vortices with equal values of vorticities and radiuses was considered: at fixed distance between the centers of two vortices we increased their radiuses (and, accordingly, areas) until there was an interaction. Thus the parameters corresponding to the critical state of vortex pair were fixed. The quantities which uniquely determinate initial configuration of the system of two circle vortices are shown in Fig. 2.4.

In our numerical simulations for the cases corresponding the initial states between the centers of vortices $l = 1, 2, \ldots, 5$ we have found that the beginning of interaction in all cases responds the approximately same value of parameter α. The values of parameters, at which there is a qualitative change in the character of interaction – the transition from steadily rotated pair to the "phase intermixing" state, are shown in Table 2.2. So, the results of numerical simulations enable us to conclude that the critical value of parameter α, at which there is qualitative change in the interaction of the vortices, equals $\alpha_{cr} = 0.267$. For $\alpha < \alpha_{cr}$ the merging of the vortex regions does not happen during interaction, but as soon as parameter αreaches its critical value, there is a qualitative jump in behavior of the vortex system, and the vortices start to be intermixed.

The next series of the numerical simulations purposed a calculation of the critical value of the parameter β. Our results showed that the vortices with the greater value of β are exposed to the greater deformation, their filamentation (i.e. formation of the filaments of a vorticity) happens faster, thus the change in character of the interaction happens at the ratio of vorticities $\zeta_1/\zeta_2 > 1.11$ (remind, that $\zeta_1 \geq \zeta_2$), therefore, $\beta_{cr} = 1.11$.

Table 2.2

S	l	δ/l	α
0.267864	1	0.416	0.267864
1.067791	2	0.417	0.266947
2.399785	3	0.417	0.266642
4.271168	4	0.417	0.266947
6.669121	5	0.417	0.266764

To answer a problem on the critical value of the parameter γ a series of simulations for vortices of elliptical form was conducted (Fig. 2.4). We fixed the area S, at which the circle vortices still save a stable state, and at $S = \mathrm{const}$ changed the eccentricities e_1 and e_2. Further, we found the critical value e_0, at which the vortex system loses its stability transferring to the "phase intermixing" state. Thus, we considered the cases corresponding to the initial states between the centers of vortices $l = 1, 2, \ldots, 5$. The values of critical parameters, at which there is a qualitative change in the behavior of the system of two elliptical vortices, are presented in Table 2.3.

Table 2.3

L	δ/l	α	e_0
1	0.180	0.266033	0.863847
2	0.180	0.266033	0.866426
3	0.183	0.266033	0.863834
4	0.180	0.266490	0.863341
5	0.180	0.266764	0.863037

Numerical simulations have shown that there is the same for all cases a critical value of the averaged eccentricity, at which the "phase change" happens $- e_0 \approx 0.864$, that corresponds to $\gamma = 7.143$. Thus, as one can see from Table 2.3 the ratio δ/l is also a constant in a critical region, however it cannot be used as the critical parameter for the description of interaction, because, at first, it takes different values for elliptical and circle vortices (see Table 2.2), secondly, it is less information as determines only a distance between boundaries of the vortices, to say nothing about their form. Therefore, for definition of the function ξ we use parameter γ, expressed through the averaged eccentricity.

Further investigations have been connected with finding of the critical angle of inclination (see Fig. 2.4) of the elliptical FAVRs for the initial state of a system, at which the evolution results in qualitative change in character of their interaction. The simulations fulfilled show that increase of the angle of declination of the vortex regions θ at $t = 0$ more than on $4°$ leads to the transition to the unstable state. Thus, we mean as angle of inclination the summing angle $\theta = \theta_1 + \theta_2$, and, for example, the case when $\theta_1 = \theta_2 = 2°$ is analogous to the case $\theta_1 = 4°$, $\theta_2 = 0$. As it follows from processing of the results of this series of the simulations, the critical value of the corresponding parameter is $\theta_0 = 1.005$.

Summing all presented above results we can define a critical value of the generalized parameter ξ (2.21) as a multiplication of four parameters α_{cr}, β_{cr}, γ_{cr} and θ_{0cr}:

$$\xi_{cr} = \alpha_{cr}\beta_{cr}\gamma_{cr}\theta_{0cr} = 2.129.$$

Numerical simulations for $|\xi| \geq \xi_{cr}$ with simultaneous variation of critical parameters α, β, γ and θ_0 corresponding to the change of sizes and positional relationship of vortices, the ratio of their vorticities, eccentricity and the summing angle of inclination of their major axes θ, respectively, have confirmed capability and expediency of usage of the parameter ξ for prediction of character of interaction of the 2D vortex structures.

Note that the obtained results, despite their general significance in theory of vortex dynamics, can help to predict the temporal behavior of 2-vortex system in real physical media such as atmosphere, hydrosphere and plasma.

2.4.2. Interaction in N-vortex systems

To study the interaction in more complex *N*-vortex systems we considered the problems with $N=3$ and $N=4$ in two variants: 1) for vortices linearly disposed at initial time, and 2) for vortices disposed at initial time in the corners of appropriate equilateral figures, and we used the critical parameter δ in the analysis of obtained results. Fig. 2.5(a) shows an example of simulation of the interaction for initially linear disposition of four vortices. One can see that for rather big and equal initial distance between vortices the evolution leads to formation of two vorticity regions as a result of more strong interaction of each of the "outer" vortices with closest "inner" vortex. Thus, the interaction of forming pairs is similar to that of two vortex cases. In case $\delta_i = d/2$ we observed the formation of a complex vortex structure which consists of many vorticities of more small scales [Fig. 2.5(b)]. Further evolution of such structure leads to formation of complex turbulent field. Note that in the last case we can also see that the interaction between outer vortices is stronger.
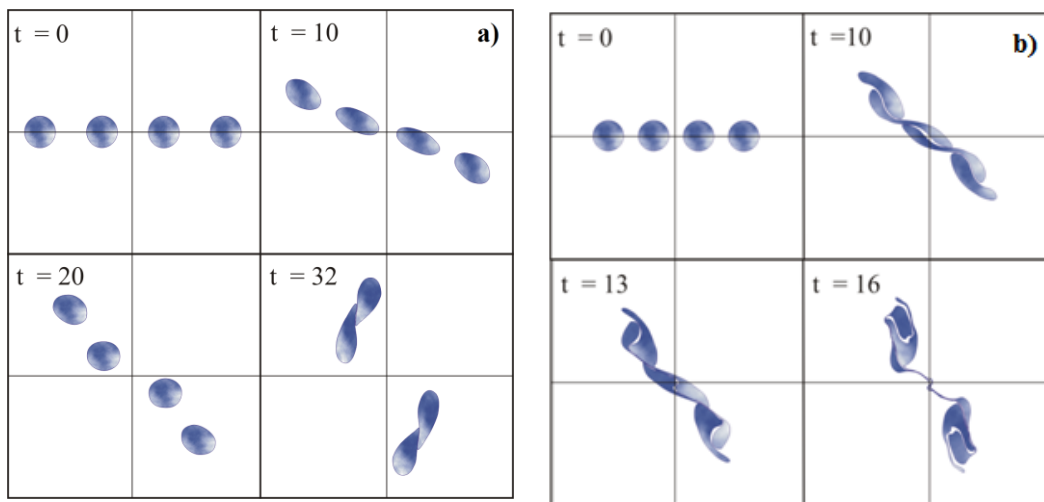

Figure 2.5. Interaction of four linearly disposed vortices with $\zeta_1 = \zeta_2 = -1$: a) $\delta_i = d$; b) $\delta_i = d/2$.

This can be explained by the fact of more strong "attraction" of outer vortices to the "center of mass" of the vortex system because the outer vortex is attracted to the center by three other vortices, and the inner vortex is attracted to the center by two vortices and, to opposite side − by one outer vortex. To test this statement, in the next series of numerical experiments we have arranged outer and inner vortices on different initial

distances. As a result, we observed the formation of common vortex structure from two inner vortices (see Fig. 2.6). The results obtained for the 4-vortex system and the simulations for the 3-vortex system showed that in both cases, owing to effect noted above, the critical initial value δ_{cr} dividing quasi-stationary and active types of interaction is less than that for 2-vortex case.
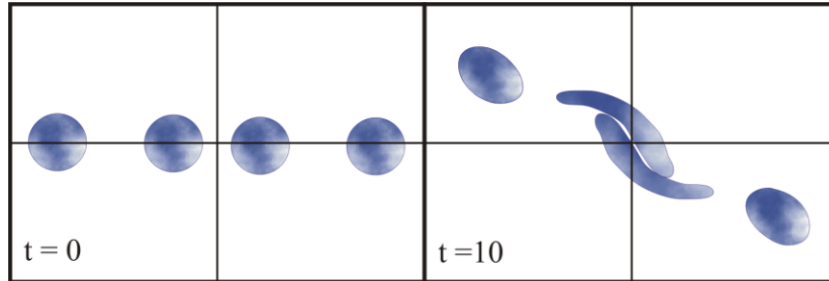

Figure 2.6. Interaction of four linearly disposed vortices with
$\zeta_1 = \zeta_2 = -1$ for $\delta_{out} = d$ and $\delta_{inn} = d/2$.

In the next series of numerical experiments we studied the interaction between the vortices disposed at initial time in the corners of appropriate equilateral figures. The following results were obtained. In case of evolution of three vortices with different signs of ζ being at initial time in the corners of a triangle, we observed that a pair of them, having opposite polarities, behaves as well as a pair of vortices with opposite polarities in 2-vortex case, and third vortex does not participate in interaction almost, practically independently on the value of δ_i $(i = 1, 2, 3)$. The similar character of interaction is observed for four vortices with different signs of ζ being at $t = 0$ in the corners of square (see Fig. 2.7, numbering of the vortices – clockwise, since the upper left corner).
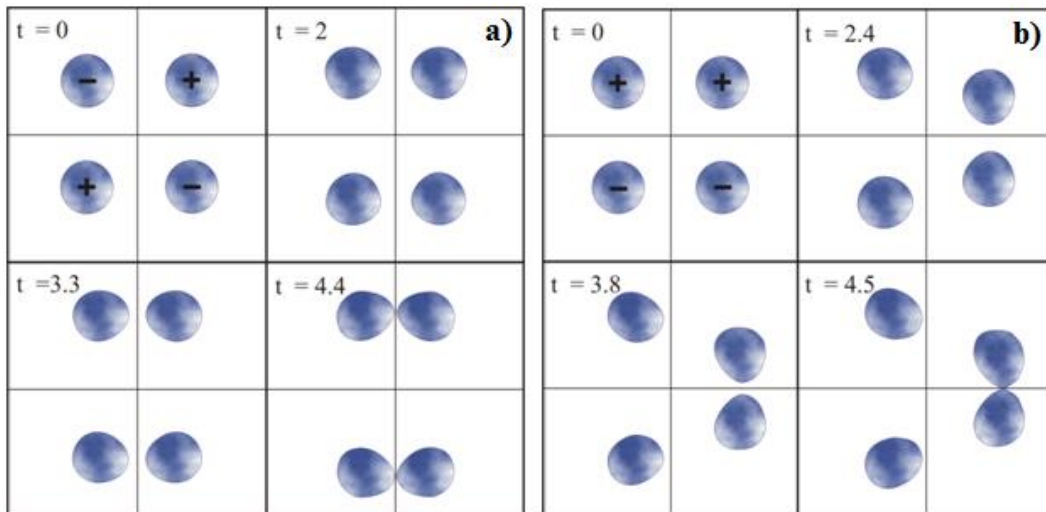

Figure 2.7. Interaction of four vortices for $\delta_i = d$ with: a) $\zeta_1 = \zeta_3 > 0, \zeta_2 = \zeta_4 < 0$;
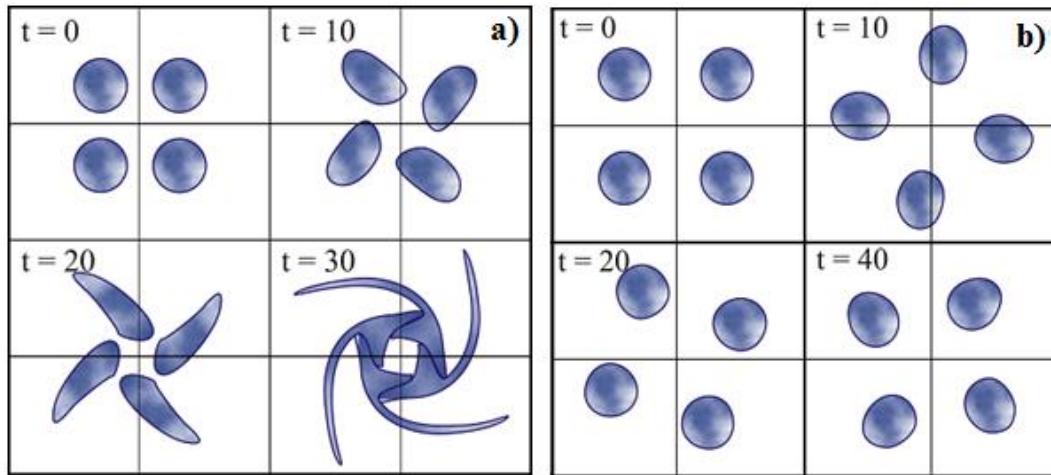b) $\zeta_1 = \zeta_2 > 0, \zeta_3 = \zeta_4 < 0$.

Figure 2.8. Interaction of four vortices with the same polarities for:
a) $\delta_i = d/2$; b) $\delta_i = d$.

The character of interaction in the 3- and 4-vortex systems consisting of vortices having the same polarities depends essentially on the distances between them like that in the 2-vortex case. The examples of such interaction for $\delta = d/2 < \delta_{cr}$ and $\delta = d > \delta_{cr}$ are shown in Fig. 2.8. One can see that in the first case the four vortices are rotated forming one big vortex structure which consists of many vorticities of more small scales. In the second case we observed a "quasi-recurrence" phenomenon. Similar pictures take place in the 3-vortex systems when at $t = 0$ the vortices are in the corners of triangle on the distances $\delta < \delta_{cr}$ or $\delta > \delta_{cr}$ one from another.

2.4.3. Three-dimensional vortices interaction

Our modification of the CD method enables also to simulate the interaction dynamics of the three-dimensional plane-rotating vortex structures in the "two-dimensional approximation" within the framework of multilayered model of medium. Fig. 2.9 shows an example of results of numerical simulation of interaction of two three-dimensional vortices with the exponential decreasing of their vorticity in (x, y)-planes of rotation with z-coordinate. One can see that, in the beginning, the vortices' central regions start to interact and only then other their areas are involved in the interaction. Such behavior is explained by stronger interaction of central regions, which are located at the relatively short distance from each other and their vorticities have relatively big values, so that the ratio ζ/δ is big in comparison with that for top and bottom of vortices.More strong analysis, however, requires a more detailed study of the regimes of this interaction, that has been discussed in detail above.

2.5. Some examples of applications

Consider now some examples of applications of our results to the problems of study of vortex motions in the atmosphere, hydrosphere and in a plasma of ionosphere.

2.5.1. Vortical motions in the atmosphere and hydrosphere

Using our technique we studied numerically the evolution and interaction of synoptic vortices and vortical structures in a fluid such as atmosphere and hydrosphere. Figures 2.10 and 2.11 show the examples of our results on modeling the evolution of the

cyclonic type synoptic vortex in the atmosphere and of the 4-vortical interaction in the channel Naruto (Japan), respectively, in comparison with photos of real systems. Here we used our modified CD method for vortex structures with due account of scale parities of parameters of the model and real vortices which were simulated (see Table 2.4 below for detail).
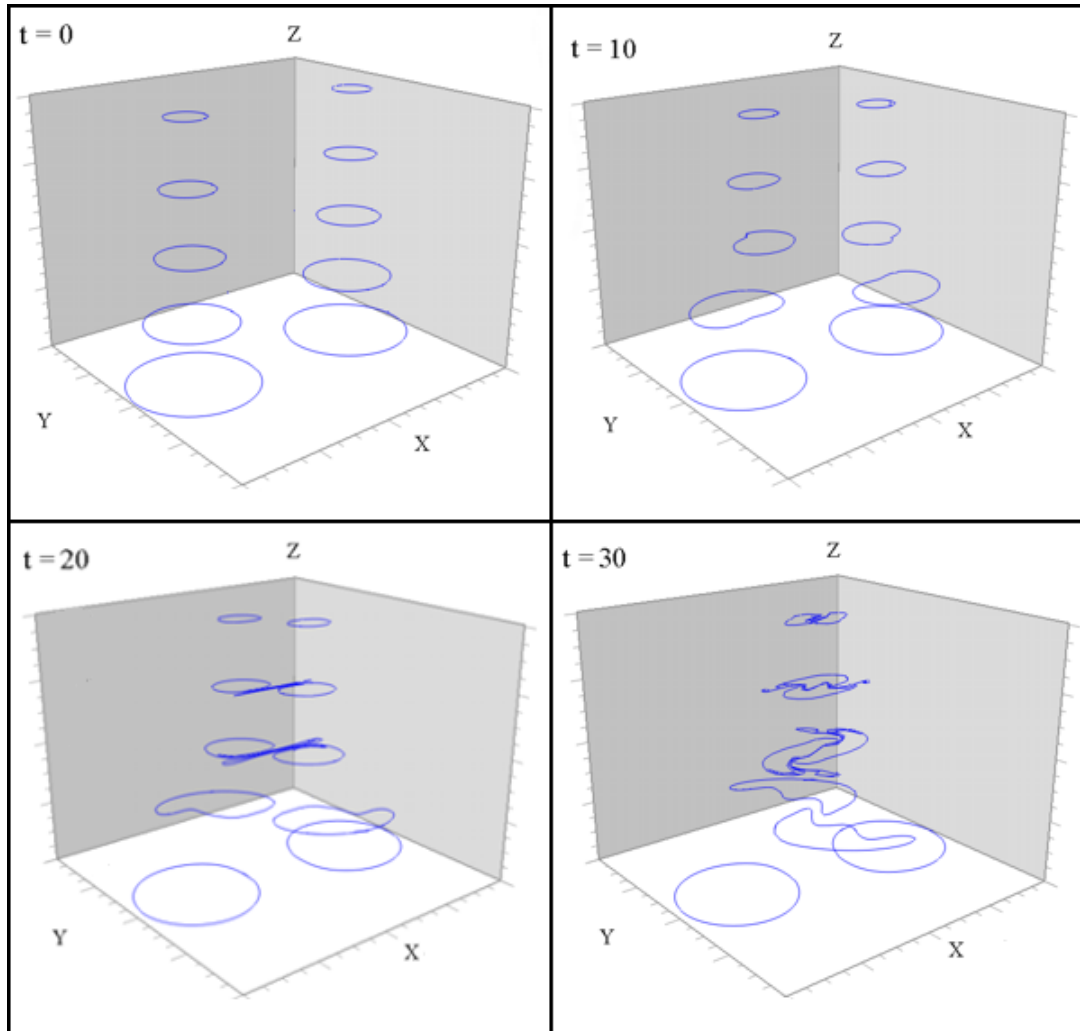

Figure 2.9. Interaction of three-dimensional plane-rotating vortex structures in the many-layer model.

In these figures one can see that our numerical results qualitatively coincide with the real systems which are simulated.

Using the quasi-2D approach with many-layer approximation of the 3D vortical structure by the FAVR system we studied also the time evolution of a tornado, and our model vortex (FAVR system) has been associated with real tornado from video-record (see Fig. 2.12). One can see that our simulation reflects the basic features of evolution of a tornado such as its form, spatial structure and dynamics of evolution. In particular, we investigated an influence of the perturbation imposed on the tornado axis on its dynamics. We established as a result, that small cross-section indignation leads to inappreciable fluctuations of an axis and, as a whole, does not influence on structure and stability of a vortex. Let us note also that vertical motions in tornado, which are sufficient in such 3D natural vortices, are taken into account implicitly by the modified
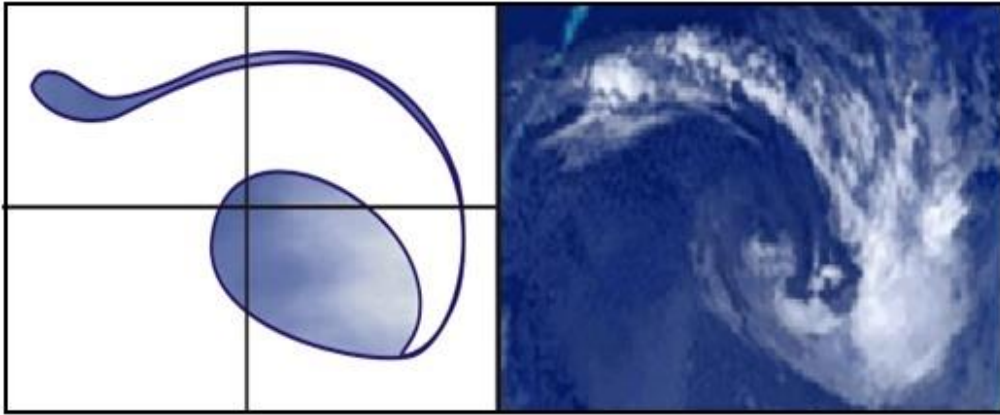
Figure 2.10. Modeling of evolution of the cyclonic type synoptic vortex
(numerical result and satellite photo).

CD method as each point of the contour of each layer interacts with each point of the contours of other layers. So, using our approach we can forecast tornado evolution and simulate interaction of such type of vortices.
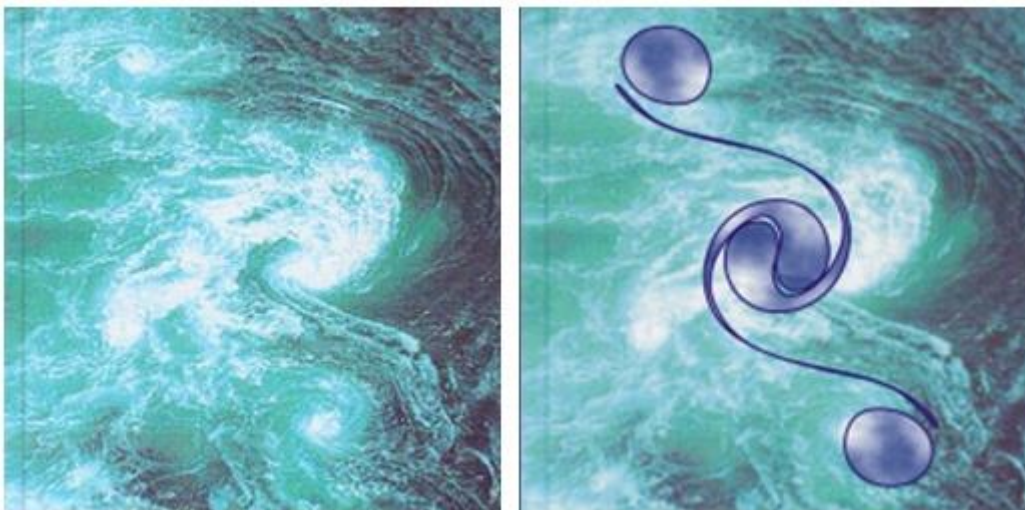

Figure 2.11. Modeling of the 4-vortical interaction in channel Naruto,
Japan (numerical result and air photography).

As we mentioned above, to make modeling it is necessary to know the scale parities of parameters of the model and the real system which is simulated. One can see some of them in Table 2.4.

2.5.2. Vortical structures in a plasma

Using 2D model of plasma of Taylor-McNamara [94] we studied the dynamics of charged filaments which represent streams of charged particles in a uniform magnetic field **B**. Figure 2.13 shows the examples of our results for a few cases of the particles' streams with their cross-section perturbations. As is known such perturbations lead to deformations of a magnetic field in a zone polar cusp, which influence on dynamics of streams of the charged particles.
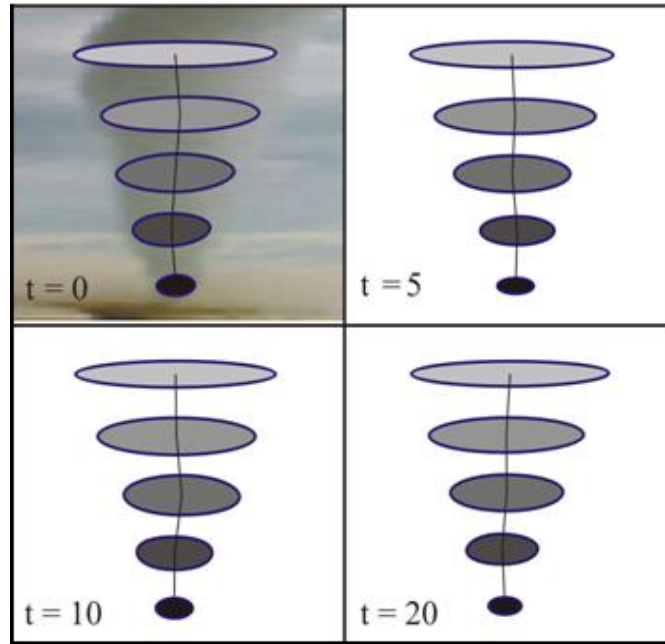
Figure 2.12. Evolution of the 3D tornado vortex.

Table 2.4. Scale parities of parameters of modeling and some real vortex systems

Parameter	Model values	Tornado	Tropical cyclones	Ocean vortices
R	1	$10^2 m$	$10^5\,m$	$2.5\times10^4 m$
V	1	100 m/s	10 m/s	2.5 m/s
ζ	1	1 s^{-1}	$10^{-4}\,s^{-1}$	$10^{-4} s^{-1}$
T	2π	$2\pi\,s$	$2\pi\times10^4\,s$	$2\pi\times10^4 s$

We have found that the structures of vortical type are formed especially quickly and more intensively, than more amplitude of perturbations and quantity of the filaments participating in interaction, and also than more close to each other filaments are located. One can see also that the cross-section perturbations of velocity of a stream lead to its transition in a unstable state with formation of folds and complex vortical structures.

Next example is the interaction in the vortex-dust particles system. The theoretical analysis and the experimental results [98] show that in a plasma with gradient of dust charge the vorticity of dust particles can exist. (In particular, it was found that vertical vortices rotate with frequency 0.2-1.5 s^{-1}. Experiments were made in argon with the particles of melanin (the size of particles is about 3 microns). During electrical discharge the formation of two vortices with opposite signs of vorticity was observed.) This gives a possibility to study the interaction between the "hydrodynamic" vortex structures and dust particles by use of the CD-method considering the dust particles as vortices of very small scales [23]. We studied numerically the interaction of the particles having nonzero value of a vorticity with the vortical area of greater size. The results of our numerical simulations showed that the character of interaction in this case depends on the value of particles' vorticity. If this value is very small then the interaction is not observed. When the vorticity of dust particles becomes like vorticity of the "hydrodynamic" vortex, the interaction becomes significant. The examples of simulation for both linear dust layers and dust cloud are presented in Fig. 2.14, where one can see that the dust particles are involved by a vortex in large-scale rotation.
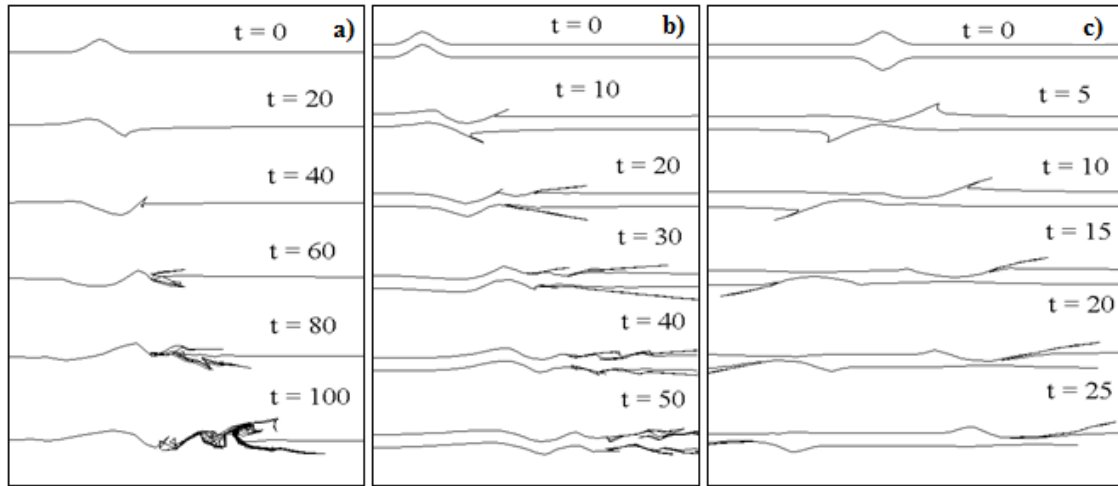
Figure 2.13. Vortex structures formation at cross-section perturbations of the charged filaments: (a) one perturbed line; (b) and (c) two lines with perturbations of the same and opposite polarities.

This result is especially important for numerous possible applications in physics of an atmosphere and plasma where presence of dust particles practically always takes place.

Next example of the application of our approach is investigation of the evolution of plasma clouds in the ionosphere. Such clouds are formed in the ionosphere under the influence of solar ionization of artificial injected Ba in rocket experiments at heights of the *F*-region of ionosphere [78]. An example of our modeling results is presented in Fig. 2.15. One can see, that such plasma structures, that lead to formation of the aligned along magnetic field **B** electron-ionic irregularities (mainly in collision plasma with small $\beta = 4\pi nT / B^2$), diffusing across field **B** at evolution, get irregular "striped" structure. This effect is rather new because it was not found earlier (see, for example, [82]). Our result coincides with the experimental data obtained in rocket experiments [78]. Such irregularities lead to development of nonlinearity in a *F*-layer and can lead to dispersion and fading of HF and VHF radio waves.

2.5.3. Other possible applications

Our approach can be useful in studies of other applications which are connected with dynamics of vortex and spiral structures in space and laboratory plasmas. One can note, for example, such of them as modeling of formation and evolution of vortical structures in astrophysics (such as spiral structure of Galaxies and solar flare activity associated with the dynamics of magnetic loops and magnetic tubes in the solar corona). Next examples are related to hydro- and aerodynamics (formation of vorticities and vortical chains at flowing of solid bodies by streams of gas and a fluid), and to the problem of magnetic confinement of plasma and controlled fusion, and also to some plasma technologies.

2.6. Conclusion

So, we have presented here the results of analysis and numerical simulation of evolution and interaction of the *N*-vortex structures of various configurations and different vorticities in the continuum including atmosphere, hydrosphere and plasma on
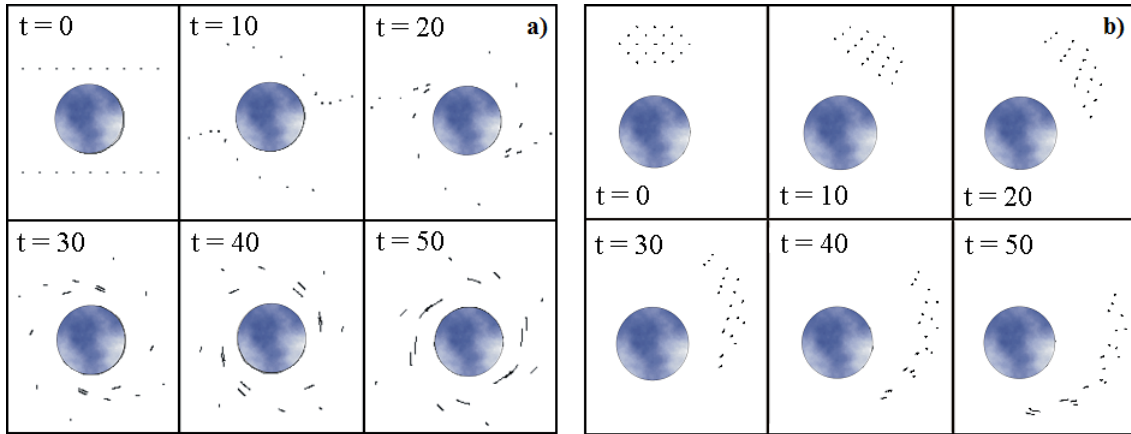
Figure 2.14. Interaction of dust particles with rather big values of vorticity with "hydrodynamic" vortex: a) linear dust layers; b) dust cloud.
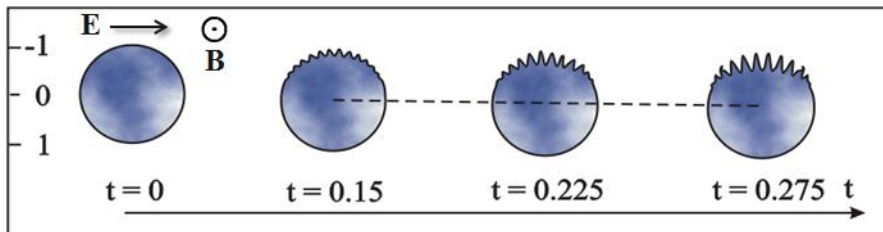

Figure 2.15. Evolution of artificial electron-ionic ionospheric inhomogeneity, cross-section section.

the basis of the model described by eqs. (2.16) in terms of the vortex motion of the inviscid incompressible fluid. We have found that in dependence on initial conditions the regimes of weak interaction with quasi-stationary evolution and active interaction with the "phase intermixing", when the evolution can lead to formation of complex forms of vorticity regions, are realized in the *N*-vortex systems. For the pair of the vortices at 2-vortex interaction we managed to find the function ξ having the sense of critical parameter which uniquely determines a qualitative character of their interaction. It was shown that for given initial conditions its value divides modes of active interaction and quasi-stationary evolution. Thus, comparing the value of ξ with its critical value ξ_{cr} we can predict the result of interaction of the vortices, namely: if $\xi < \xi_{cr}$ then "phase intermixing" of vortices is not observed with evolution, in the opposite case, when $\xi \geq \xi_{cr}$, the merging of vortices with further formation of the vorticities of more small scales is happen. For the vortices of the circle and elliptical (or close to elliptical) form, the value of generalized critical parameter $\xi_{cr} = 2.129$ corresponds to the "phase change" point. This result concerns only the systems which consist of two vortices. The generalization for a case of arbitrary number of vortex regions (in particular, for the 2D and quasi-3D *N*-vortex cases considered here and in [36]) requires padding investigations.

The results of simulation of evolution and interaction of the 2D and 3D vortex structures, including such phenomena as dynamics of the atmospheric synoptic vortices of cyclonic type and tornado (on the basis of the multilayered model of medium [37]), hydrodynamic 4-vortex interaction and also interaction in the systems of a type of

"hydrodynamical vortex–dust particles" (when the dust particles are involved in rotation by hydrodynamic vortices), and dynamics of plasma clouds in the ionosphere of the Earth were presented. Other possible applications of the results obtained can be associated with the study of dynamics of the Alfven vortices in plasma of the ionosphere and magnetosphere of the Earth [88], stability of vortex structures of different types and origins, including the quasi-geostrophic vortices in an ocean [68], dynamics of the acoustic-gravity waves in the Earth atmosphere [57], self-organization of the large-scale nonlinear vortex structures in an inhomogeneous ionosphere [2]-[4],[7],[65], and motions in dust devils on surfaces of Earth and Mars [58]. The approach proposed in the paper enables also to study the motions in the hydrodynamic model of rotating fluid that corresponds to the screening interaction [43], and it can be useful for description of zonal flows in vortices in the ionospheric plasma [41].

We have shown that the generalized set (2.16) with $f = 0$ can describe also the dynamics of quasi-particles with Coulomb interaction model [see eqs. (2.10) and (2.11)], and the results obtained and presented in the paper can be easily extended to the 2D simple systems where the plasma is represented by charged filaments, aligned with a uniform magnetic field $\mathbf{B}$, that move with the guiding-centre velocity $\mathbf{E} \times \mathbf{B} / B^2$. We have demonstrated the application of undertaken approach developed in [33],[36] to the problems of such plasma systems as streams of charged particles in a uniform magnetic field $\mathbf{B}$. Note, that this approach can be useful and also for other 2D continuum models when $f \neq 0$ in the Poisson equation (2.16). They can describe the vortices or filaments with the non-Coulomb interaction. In the last case it is assumed that ions move with the guiding-centre velocity but electrons have a Boltzmann distribution, thus the additional term $f = k^2 \psi$ describes the Debye screening – see models (2.10), (2.12), (2.13) and the Hasegawa-Mima model [52] which includes additionally the ion equation of motion (2.14).

In conclusion, in this Part of the book we have proposed the approach for investigations of the evolution and dynamics of the vortices of different types and origin in a continuum, have considered some problems on the basis of the modified CD method developed, and have shown that the results obtained have obvious applications in studies of the problems associated with the vortex movements in the atmosphere and hydrosphere, and in a plasma of the ionosphere and magnetosphere of the Earth.

References

1. Aburdzhaniya, G.D., Kamenets, F.F., Lakhin, V.P., Mikhailovskii, A.B., Onishchenko, O.G. Electron-drift solitons in an inhomogeneous magnetized plasma. *Phys. Lett. A*, 105, 48-50, 1984.

2. Aburjania, G.D., Khantadze, A.G., Kharshiladze, O.A. Nonlinear electromagnetic planetary vortex structures in *F*-region of the ionosphere. *Plasma Phys. Rep*, 28 (7), 633-638, 2002.

3. Aburjania G.D., Alperovich L. S., Khantadze A. G., Kharshiladze O.A. A new model for the generation of large-scale ionospheric vortex electric field. *Physics and Chemistry of the Earth.*, (Elsevier, Netherlands), V. 31. Issue 4-9. P. 482-485. 2006.

4. Aburjania G.D., Alperovich L. S., Khantadze A. G., Kharshiladze O.A. On the planetary ionospheric vortex electric field. *Advances in Space Research*. V. 34 .№ 6. P. 925-928. 2007.

5. Aburjania, G.D., Chargazia, K.Z., Kharshiladze, O.A. Shear flow driven magnetized planetary wave structures in the ionosphere, *Journal of Atmospheric and Solar-Terrestrial Physics*, 72 (13), 971-981. 2010.

6. Aburjania, G.D., Zimbardo, G., Kharshiladze O.A. Effect of the shear flow in the generation and self-organization of internal gravity wave structures in the dissipative ionosphere. *Plasma physics reports*, 38 (12), 972-990. 2012.

7. Aburjania, G.D., Kharshiladze, O.A., Chargazia,K.Z. Self-organization of internal gravity wave structures in an inhomogeneous ionosphere: 1. Nonlinear model dynamic equations. *Geomagnetism and Aeronomy*. 53 (5), 650-654 . 2013

8. Aburjania, G.D., Kharshiladze, O.A., Chargazia,K.Z. Self-organization of IGW Structures in an Inhomogeneous Ionosphere: 2. Nonlinear Vortex Structures, *Geomagnetism and Aeronomy,* 53 (6), 750. 2013

9. Arons, J. Some problems of pulsar physics, *Space Sci. Rev.*, vol. 24, pp. 417510, 1979.

10. Belashov, V.Yu. Dynamics of the internal gravity waves at heights of the *F*-region of ionosphere. *Geomagn. i Aeron*. 30, 637-641, 1990.

11. Belashov, V.Yu. Stability of two- and three-dimensional solitons in weakly dispersive media. *Sov. Phys. Doklady* 36, 626-630, 1991.

12. Belashov, V.Yu. The methods for numerical integration of nonlinear evolutional KP-class equations, *XX International Conference on Phenomena in Ionized Gases, Pisa, Italy, 1991,* Contributed Papers, vol. 6, pp. 1241-1242, 1991.

13. Belashov, V.Yu. Nonlinear effects for FMS waves propagating in magnetized plasma. *Plasma Phys. Control. Fusion* 36, 1661-1669, 1994.

14. Belashov, V.Yu. Dynamics of KP equation solitons in media with low-frequency wave field stochastic fluctuations. *Phys. Lett., A197, 282-286, 1995.

15. Belashov, V.Yu. *The KP equation and its generalizations. Theory and applications.* NEISRI FEB RAS, 162 p., 1997, (in Russian).

16. Belashov V.Yu, Tunina S.G. Astronomy, observations and techniques. *Radiophysics and quantum electronics. Soviet Radiophys.* XL. 1, p.328-344, 1997.

17. Belashov, V.Yu. Numerical study of dynamics of 3D ion-acoustic and FMS nonlinear waves in plasma using spectral approach, *Proceedings of the 5th International*

School/Symposium for Space Simulation (ISSS-5), Kyoto, Japan, 1997, Kyoto: Kyoto University, pp. 118-122, 1997.

18. Belashov, V.Yu. Dynamics of the 3D Alfvén waves propagating in magnetized plasma and stability problem. *Proc. 1996 Int. Conf. on Plasma Physics. Nagoya, Japan, Sept. 9-13, 1996.* Contributed Papers. 1, 954-957, 1997.

19. Belashov, V.Yu. The problem of stability for three-dimensional Alfvén waves propagating in magnetized plasma. *Doklady Phys*. 44, 327–329, 1999.

20. Belashov, V.Yu., Singatulin R.M. Computer simulation of evolution of vortex structures in continuum. *Izv. Vuzov. Problemy Energetiki* 9, 103-109, 2001. (in Russian).

21. Belashov, V.Yu. *Multidimensional nonlinear waves in real dispersive media.* KSPEU, Kazan, 143 p., 2002, (in Russian).

22. Belashov, V.Yu., Belashova, E.S. and Anoshen, A.V. Ideology and realization of numerical approaches to integration of the KP and 3-DNLS classes of equations. *Dep. VINITI, N 273-B2003.* KSPEU, Kazan, 2003.

23. Belashov, V.Yu., Singatulin, R.M. Application of CD-algorithm to study of vortices in plasmas and fluids. *Proc. 4th Int. Conf. on Plasma Physics and Plasma Technologies − PPPT-4*, 892-895, Minsk, Belarus, 2003.

24. Belashov, V.Yu., Singatulin R.M. Dynamics of vortex type wave structures in plasmas and fluids. *Plasma Physics: 11th Intern. Congress on Plasma Physics: ICPP 2002, AIP Conf. Proc.,* edited by I.S. Falconer, R.L. Dewar and J. Khachan, V. 669, 609-612 (American Inst. of Physics, Melville, New York), 2003.

25. Belashov, V.Yu., Singatulin R.M. Dynamics of vortex type wave structures in plasmas and fluids. *Proc.30th EPS Conf. on Controlled Fusion and Plasma Physics*, V. 27A, P-2.200 (St. Petersburg, Russia), 2003.

26. Belashov, V.Yu., Singatulin, R.M. Algorithm of the contour dynamics method and simulation of vortex structures. *Dep. VINITI N 272-B*, KSPEU, Kazan, 2003.

27. Belashov, V.Yu., Vladimirov, S.V. *Solitary Waves in Dispersive Complex Media. Theory, Simulation, Applications.* Springer-Verlag, Berlin-Heidelberg-New York-Tokyo, 304 p., 2005.

28. Belashov, V.Yu. Dynamics of multidimensional nonlinear wave structures of soliton and vortex types in dispersive complex media. Theory, simulation, applications. *Int. Baikal School on Fundamental Physics. Plenary Lecture. Ed. Inst. Solar-Terr. Physics Siberia Div. of RAS*, pp. 3-9, 2011, (in Russian).

29. Belashov, V.Yu. Dynamics of multidimensional nonlinear wave structures of the solitons and vortex types in dispersive complex media. Theory, simulation, applications. *17th Int. Congress on Plasma Physics – ICPP 2014, Lisbon, Portugal, Sept. 15-19, 2014, Book of Abstracts*. BAP.P.35, 2014.

30. Belashov, V.Yu. Nonlinear effects of the dynamics of fast magnetosonic waves in a plasma: Self-focusing and stabilization of beams, *Trudy XXIV Vserossiiskoi nauchnoi konferentsii " Rasprostranenie radiovoln" RRV-24 (Proceedings of the XXIV All- Russian Scientific Conference "Radiowave Propagation" RWP-24)*, Irkutsk: ISZF SO RAN, vol. 3, pp. 5-12, 2014.

31. Belashov, V.Yu., Belashova E.S. Nonlinear dynamics of the 3D Alfvén waves in plasma of ionosphere and magnetosphere. *J. Atm. Solar-Terr. Phys*.136 150–154, 2015.

32. Belashov, V.Yu., Belashova E.S. Dynamics of IGW and traveling ionospheric disturbances in regions with sharp gradients of the ionospheric parameters. *Advances in Space Research* 56, 333–340, 2015.

33. Belashov, V.Yu. Modeling of vortex structures in continuous media (atmosphere, hydrosphere and plasma). Solicited paper. *Presented at IUGG General Assembly. Symposium A12 Coupling Processes in the Atmosphere-Ionosphere System* (Div. II-C/ICMA/SCOSTEP, Prague, Czech Republic, 2015. Available online at: https://www.czech-in.org/cm/IUGG/CM.NET.WebUI/CM.NET.WEBUI.scpr/SCPRsessions.aspx?conferenceid=05000000-0000-0000-0000-000000000053&sessionID=05000000-0000-0000-0000-000000003004.

34. Belashov, V.Yu., Belashova, E.S. *Solitons: theory, simulation, applications. Ed. Center "School"*, Kazan, 270 p., 2016, (in Russian).

35. Belashov, V.Yu., Belashova, E.S. Nonlinear Dynamics of 3D Beams of Fast Magnetosonic Waves Propagating in the Ionospheric and Magnetospheric Plasma. *Geomagnetism and Aeronomy* 56, 716–723, 2016.

36. Belashov, V.Yu. Dynamics of multidimensional nonlinear wave structures of the soliton and vortex types in dispersive complex media: Theory, simulation and applications. *Astrophys. Aerospace Technol.* 4(3) (Suppl), 18, 2016.

37. Belashov, V.Yu. Modeling of dynamics of vortex structures in continuous media. *Astrophys. Aerospace Technol.* 4(3) (Suppl), 28, 2016.

38. Belashov, V.Yu. Dynamics of multidimensional nonlinear wave structures of the soliton and vortex types in dispersive complex media: Theory, simulation and applications. *Astrophys. Aerospace Technol.* 4(3) (Suppl), 18, 2016.

39. Belashova, A.A., Belashov, V.Yu., Poddelskiy, I.N. Composite studies of the dynamics of wave disturbances of the ionosphere in the far-eastern USSR. *Geomagn. and Aeron.* 30, 543-549 (*Geomagn. i Aeron.* **30**, 647-654), 1990.

40. Belashova, E.S., Belashov V.Yu. *Solitons as mathematical and physical objects.* KSPEU, Kazan, 205 p., 2006, (in Russian).

41. Benkadda, S., Klochkov, D.N., Popel, S.I., Izvekova, Y.N. Nonlinear excitation of zonal flows and streamers in plasmas. *Physics of Plasmas*, 18(5), 052306, 2011.

42. Canuto, V. and Ventura, J. Quantizing magnetic fields in astrophysics, *Fundamentals of Cosmic Physics*, Gordon and Breach, vol. 2, pp. 203-353, 1977.

43. Charney, J.G. On the scale of atmospheric motions. *Geophs. Public. Kosjones Nors. Videnshap-Acad.* Oslo 17, 1-17, 1948.

44. Danilov, Yu.A. and Petviashvili, V.I. Solitons in plasma, *Itogi nauki i tekhniki. Fizika plazmy (Science and Technology Results: Plasma Physics),* Moscow: VINITI, vol. 4, pp. 5-47, 1983.

45. Das, G.C. and Paul, S.N. Ion-acoustic solitary waves in relativistic plasmas, *Phys.Fluids,* vol. 28, pp. 823-837, 1985.

46. Dawson, S.P., Fontan, C.F. Soliton decay of nonlinear Alfven waves: numerical studies. *Phys. Fluids* 31, 83-89, 1988.

47. Dawson, S.P., Fontán, C.F. Extension of the Ablowitz–Ladik method to the derivative nonlinear Schrödinger equation. *J. Comput. Phys.* 76, 192-200, 1988.

48. Elsasser, K. and Popel, S. Plasma equations in general relativity, *Phys. Plasmas*, vol. 4, pp. 2348-2356, 1997.

49. Esfahani, A. Instability of solitary waves of the generalized high-order KP equation, *Nonlinearity*, vol. 24, pp. 833-846, 2011.

50. Giamarchi, T. *Quantum Physics in One Dimension*, New York: Oxford University Press, 2003.

51. Haas, F. Relativistic hydrodynamic equations for fully degenerate plasma, *17th International Congress on Plasma Physics (ICPP-2014), Book of Abstracts,* Lisbon, Portugal, BAP.15, 2014.

52. Hasegawa, A., Mima, K. Pseudo-three-dimensional turbulence in magnetized nonuniform plasma. *Phys. Fluids* 21, 87-103, 1978.

53. Heisler, L.H. Occurrence of giant travelling ionospheric disturbances at night. *Nature.* 183, 383-384. 1959.

54. Hocke, K., Schlegel, K. A review of atmospheric gravity waves and traveling ionospheric disturbances: 1982–1995. *Ann. Geophys.* 14, 917-940, 1996.

55. Hunsucker, R.D. Atmospheric gravity waves generated in the high-latitude ionosphere: A review. *Rev. Geophys.* 20, 293-315, 1982.

56. Hunsucker, R.D. The sources of gravity waves. *Nature.* 328, 204-205, 1987.

57. Izvekova, Yu.N., Popel, S.I., Chen, B.B. Nonlinear acoustic-gravity waves and dust particle redistribution in Earth's atmosphere. *J. Atm. Solar-Terr. Phys.* 134, 41-46, 2015.

58. Izvekova, Yu.N., Popel, S.I. Charged Dust Motion in Dust Devils on Earth and Mars. Contributions to *Plasma Phys.* 56(3-4), 263-269, 2016.

59. Kadomtsev B.B., Petviashvili V.I. Instabilities and oscillations of one- and two-dimensional Kadomtsev-Petviashvili waves and solitons II. Linear to nonlinear analysis. *Soviet Phys Dokl.* 192, p.753-756, 1970.

60. Karpman, V.I. *Nelineinye volny v dispergiruyushchikh sredakh* (Nonlinear Waves in Dispersive Media), Moscow: Nauka, 1973.

61. Karpman, V.I., Belashov, V.Yu. Dynamics of two-dimensional solitons in weakly dispersive media. *Phys. Lett.* 154A, 131-139, 1991.

62. Karpman, V.I., Belashov, V.Yu. Evolution of three-dimensional nonlinear pulses in weakly dispersive media. *Phys. Lett.* 154A, 140-144, 1991.

63. Kawahara T.J. A general theory of magnetic resonance absorption. *J Phys Soc. Jap.* 33, p. 260-264, 1972.

64. Kawahara T. Fractional quantization of the hall effect, *Phys. Rev. Lett.*, 51, No 5, 381-383. 1983.

65. Kharshiladze, O.A. Physical and mathematical models for generation of large-scale internal vortical electric fields in the ionosphere. *Bulletin of the Georgian Academy of Sciences.* V 172, N 1, P 61-64. 2005.

66. Kharshiladze, O.A. Dynamical Chaos and Order-Disorder Transition in the Large-Scale Ionospheric Motions. *Abstracts of 3rd IAGA/ICMA (International Association of Geomagnetism and Aeronomy / International Commission on middle Atmosphere) Workshop on "Vertical Coupling in the Atmosphere-Ionosphere System"*, Varna, Bulgaria, 2006.

67. Kharshiladze, O.A. Ionospheric Large-Scale Motions Transition into Chaotic Flow. *ISAP2007*, *International Symposium on Antennas and Propagation*, Toki Messe, Niigata, Japan. 2007.

68. Kozlov, V.F., Makarov V.G. Simulation of the instability of axisymmetric vortices using the contour dynamics method. *Fluid Dynamics* 20(1), 28-34, 1985.

69. Krimigis, S.M. and Van Allen, J.A. Geomagnetically trapped alpha particles, *J. Geophys. Res.,* vol. 72, pp. 5779-5797, 1967.

70. Kuznetsov, E.A., Turitsyn, S.K. Two- and three-dimensional solitons in weakly dispersive media. *Soviet Phys. JETP.* 55, 844-852, 1982.

71. Kuznetsov, E.A. and Musher, S.L. Influence of collapsing acoustic waves on the structure of noncollision shockwaves in magnetized plasma, *Zh. Eksp. Teor. Fiz.*, vol. 91, no.5, pp. 1605-1619, 1986.

72. Litvak, A.G. On one type of self-action of waves in plasma, *Fiz. Plazmy*, vol. 9, no. 3, pp. 495-500, 1983.

73. Liu, Y. and Wang, X.-P. Nonlinear stability of solitary waves of a generalized Kadomtsev-Petviashvili equation, *Comm. Math. Phys.*, vol. 183, pp. 253-266, 1997.

74. Manin, D.Yu. and Petviashvili, V.I. Self-focusing of magnetoacoustic waves across the magnetis field, *Pisma Zh. Eksp. Teor. Fiz.,* vol. 38, no. 9, pp. 427-430, 1983.

75. McKerr, M., Haas, F. and Kourakis, I. Relativistic theory for localized electrostatic excitations in degenerate electron-ion plasmas, *Phys. Rev. E,* vol. 90, no. 3, 033112, 2014.

76. McKerr, M., Haas, F., and Kourakis, I. Ion-acoustic envelope modes in a degenerate relativistic electron-ion plasma, *Phys. Plasmas*, vol. 23, 052120, 2016.

77. Mikhailovskii, A.B., Lakhin, V.P., Mikhailovskaya, L.F., Onishchenko, O.G. On the theory of vortices in a plasma. *Sov. Phys. JETP*, 59, 1198-1205, 1984.

78. Mishin, E.V., Ruzhin, I.I., Telegin, V.A. *Interaction between electron fluxex and ionospheric plasma.* Gidrometeoizdat, Leningrag, 1989. (in Russian).

79. Modi, K.V., Sharma, R.P. Nonlinear interaction of kinetic Alfvén wave with fast magnetosonic wave and turbulent spectrum. *Phys. Plasmas*. 20, 032303, 6 pp., 2013.

80. Nariyuki, Y., Hada, T., Tsubouchi K. Nonlinear dissipation of circularly polarized Alfvén waves due to the beam-induced obliquely propagating waves. *Phys. Plasmas*. 19, 082317, 8 pp., 2012.

81. Nejon, Y. A two-dimensional ion acoustic solitary wave in a weakly relativistic plasma, *J. Plasma Phys.*, vol. 38, pp. 439-444, 1987.

82. Overman, E.A., Zabusky, N.J., Ossakow, S.L. Ionospheric Plasma Cloud Dynamics via Regularized Contour Dynamics. *Technical Report ICMA-82-36*, 1981.

83. Passoni, M., Bertagna, L., and Zani, A. Target normal sheath acceleration: Theory, comparison with experiments and future perspectives, *New J. Phys.*, vol. 12, 0450122, 2010.

84. Pava, J.A. *Nonlinear Dispersive Equations. Existence and Stability of Solitary and Periodic Travelling Wave Solutions*, Providence, Rhode Island: American Mathematical Society, 2009.

85. Petviashvili, V., Pokhotelov, O. *Solitary waves in plasmas and in the atmosphere*. Gordon and Breach, Philadelphia, 1992.

86. Pokhotelov, O.A., Stenflo, L., Shukla, P.K. Alfven solitons in the Earth's ionosphere and magnetosphere. *J. Geophys. Res.* 101, 7913-7915, 1996.

87. Pokhotelov, O.A., Pokhotelov, D.O., Gokhberg, M.B., et al. Alfvén solitons in the Earth's ionosphere and magnetosphere. *J. Geophys. Res.*, 101, A4, 7913-7915. 1996.

88. Pokhotelov, O.A., Stenflo, L., Shukla, P.K. Nonlinear structures in the Earth's magnetosphere and atmosphere. *Plasma Physics Reports*. 22, 10, 852-863, 1996.

89. Popel, S.I., Vladimirov, S.V. and Tsytovich, V.N. Theory of modulational interactions in plasmas in the presence of an external magnetic field, *Phys. Rep.,* no. 6, pp. 327-405, 1995.

90. Rahman, A. and Ali, S. Solitary and rogue waves in Fermi-Dirac plasmas: Relativistic degeneracy effects, *Astrophys. Space Sci.*, vol. 351, no.1, pp.165-172, 2014.

91. Shukla, P.K., Yu, M.Y., and Tsintsadze, N.L. Intense solitary laser pulse propagation in a plasma, *Phys. Fluids*, vol. 27, pp. 327-334, 1984.

92. Shukla, P.K. and Eliasson, B. Nonlinear theory for a quantum diode in a dense Fermi magnetoplasma, *Phys. Rev. Lett.*, vol. 100, 036801, 2008.

93. Taniuti, T. and Wei, C.C. Reductive perturbation method in nonlinear wave propagation, I, *J. Phys. Soc. Jpn.*, vol. 24, pp. 941-946, 1968.

94. Taylor, J.B., McNamara, B. Plasma diffusion in two dimensions. *Phys. Fluids* 14, 1492-1499, 1971.

95. Taylor, J.B. Turbulence in two-dimensional plasmas and fluids. *Plasma Phys. Control. Fusion* 39, A1-A9, 1977.

96. Tsugawa, T., Shiokawa, K., Otsuka, Y. Ogawa, T., Saito, A., Nishioka, M. Geomagnetic conjugate observations of large-scale traveling ionospheric disturbances using GPS networks in Japan and Australia. *JGR.* 111, A02302/1-1, 2006.

97. Tsytovich, V.N. *Lectures on Non-Linear Plasma Kinetics*. Berlin: Springer, 1995.

98. Vaulina O.S., Samarian, A.A., Nefedov, A.P., Fortov, V.E. Self-excited motion of dust particles in a inhomogeneous plasma. *Phys. Lett*. A 289, 240-244, 2001.

99. Vette, J.I. Summary of particle populations in the magnetosphere, *Particles and Fields in the Magnetosphere,* McCormac, B.M., Ed., Dordrecht: Reidel, pp. 305-318, 1970.

100. Washimi, H. and Taniuti, T. Propagation of ion-acoustic solitary waves of small amplitude, *Phys. Rev. Lett.,* vol. 17, no. 17, pp. 966-971, 1966.

101. Zabusky, N.J., Hughes, M.N., Roberts K.V. Contour dynamics for the Euler equations in two dimensions. *J. Comput. Phys*. 135, 220-226, 1979.

102. Zakharov, V.E. and Kuznetsov, E.A. On three-dimensional solitons, *Zh. Eksp. Teor. Fiz.*, vol. 66, no. 2, pp. 594-597, 1974.

103. Zakharov, V.E. Instability and nonlinear oscillations of solitons, *Sov. Phys.: JETP Lett*. 22, 172-173. 1975.

104. Zakharov, V.E., Manakov, S.V., Novikov, S.P., and Pitaevskii, L.P. *Teoriya solitonov: Metod obratnoi zadeachi* (Theory of Solitons: The Method of Inverse Problem), Moscow: Nauka, 1980.

105. Zakharov, V.E. and Kuznetsov, E.A. Solitons and collapses: Two evolution scenarios of nonlinear wave systems, *Phys.-Usp.*, vol. 55, no. 6, pp. 537-556, 2012.

Previous Issues

1. **W.-L. Schulze**. *Pseudo-differential Calculus and Applications to Non-smooth Configurations.* Volume 1, 2000,

2. **S. Camiz.** *Exploratory 2- and 3-way Data Analisys and Applications.* Volume 2, 2001, 44 p.

3. **G. Jaiani**. *Theory of Cusped Euler-Bernoulli Beams and Kirchhoff-Love Plates.* Volume 3, 2002, 129 p.

4. **G. Jaiani, S. Kharibegashvili, D. Natroshvili, W.L. Wendland**. *Hierarchical Models for Cusped Plates and Beams.* Volume 4, 2003, 121 p.

5. **A. Bernardini, G. Bretti, P.E. Ricci.** *Laguerre-type Exponentials, Multidimensional Special Polynomials and Applications.* Volume 5, 2004, 28 p.

6. **Ts. Gabeskiria, G. Jaiani, J. Antidze, G. Datashvili.** *English-Georgian-Russian-German-French-Italian Glossary of Mathematical Terms.* Volume 6, 2005, 228 p.

7. **J. Rogava, M. Tsiklauri**. *High Order Accuracy Decomposition Schemes for Evolution Problem.* Volume 7, 2006, 164 p.

8. Volume 8, 2007 **was dedicated to the Centenary of Ilia Vekua.**

   It contains the following articles:

   - **R.P. Gilbert, G.V. Jaiani.** *Ilia Vekua's Centenary*
   - **H. Begehr, T. Vaitekhovich.** *Complex Partial Differential Equations in a Manner of I.N. Vekua.*pp. 15-26
   - **B.-W. Schulze.** *Operators on Configurations with Singular Geometry.* pp.27-42
   - **V. Kokilashvili, V. Paatashvili.** *On the Riemann-Hilbert Problem in Weighted Classes of Cauchy Type Integrals with Density from $L^{P(\cdot)}(\Gamma)$.* pp. 43-52
   - **Tavkhelidze.** *Classification of a Wide Set of Geometric Figures.* pp. 53-61

9. **N. Chinchaladze**. *On Some Nonclassical Problems for Differential Equations and Their Applications to the Theory of Cusped Prismatic Shells.* Volume 9, 2008,

10. **D. Caratelli, B. Germano, J. Gielis, M.X. He, P. Natalini, P.E. Ricci**. *Fourier Solution of the Dirichlet Problem for the Laplace and Helmholtz Equations in Starlike Domains.* Volume 10, 2009, 64 p.

11. **A. Cialdea.** *The L^P–Dissipativity of Partial Defferential Operators.* Volume 11, 2010, 94 p.

12. **D. Natroshvili.** *Mathematical Problems of Thermo-Electro-Magneto-Elasticity.* Volume 12, 2011, 128 p.

13. **G. Akhalaia, G. Giorgadze, V. Jikia, N. Kaldani, G. Makatsaria, N. Manjavidze.** *Elliptic Systems on Riemann Surface.* Volume 13, 2012, 155 p.

14. **I. Vekua.** *On Metaharmonic Functions.* Volume 14, 2013, 62 p.

15. **Wolfgang H. Müller & Paul Lofink.** *The Movement of the Earth: Modelling the Flattening Parameter.* Volume 15, 2014, 42 p.

16. **W.H. Müller,** E.N. Vilchevskaya, & A.B. Freidin. *Structural Changes in Micro-Materials: Phenomenology, Theory, Applications, and Simulations.* Volume 16, 2015, 74 p.

17. Volume 17, 2016 contains the following articles**:**

   - **Alexander Meskhi.** *Multilinear Integral Operators in Weighted Function Spaces,* pp. 5-18

   - **Alice Fialowski.** *The Moduli Space and Versal Deformations Of Algebraic Structures,* pp. 19-34

   - **Reinhold Kienzler.** *Material Conservation and Balance Laws in Linear Elasticity with Applications,* pp. 35-65

Information for the Authors

1. Papers written in English should be submitted as TeX and PDF files via email to the managing editor

Dr. Natalia Chinchaladze
I.Vekua Institute of Applied Mathematics
of Tbilisi State University,
2, University st.
Tbilisi 0186
Georgia
e-mail: chinchaladze@gmail.com

2. Papers should be prepared in any standard version of TeX (i.e. plain, LaTeX, AMS-(La)TeX)

3. Letter's size and intervals between lines should be 12 pt, with a printed text area of 140mm x 225mm on a page.

4. Manuscripts should be compiled in the following order: title page; abstract; keywords; main text; acknowledgments; appendices (as appropriate); references; table(s) with caption(s) (on individual pages); figure caption(s) (as a list).

5. Abstracts of 100-150 words are required for all papers submitted.

6. Each paper should have 3-6 keywords. In addition to keywords, authors are encouraged to provide 2-6 AMS 2010 Mathematics Subject Classification codes.

7. Section headings should be concise and numbered sequentially, using a decimal system for subsections.

8. All the authors of a paper should include their full names, affiliations, postal addresses, telephone and fax numbers and email addresses on the cover page of the manuscript. One author should be identified as the Corresponding Author.

9. The decision on the acceptance is taken after a peer-reviewing procedure.

10. Authors submit their papers on the condition that they have not been published previously and are not under consideration for publication elsewhere.